

AD-A250 193

PAGE

Form Approved
OMB No. 0704-0188

Public reporting burden
gathering and maintaining
collection of information
Davis Highway, Suite



in response, including the time for reviewing instructions, searching existing data sources,
information. Send comments regarding this burden estimate or any other aspect of this
headquarters Services, Directorate for Information Operations and Reports, 1215 Jefferson
d Budget, Paperwork Reduction Project (0704-0188), Washington, DC 20503

1. AGENCY USE ONLY (Leave blank)		2. REPORT DATE 1991		3. REPORT TYPE AND DATES COVERED THESIS/DISSEMINATION	
4. TITLE AND SUBTITLE Studies in Control For Vibration Suppression of the UWAA 20-Bay Planar Truss				5. FUNDING NUMBERS	
6. AUTHOR(S) Michael J. Shepherd, 2d LT					
7. PERFORMING ORGANIZATION NAME(S) AND ADDRESS(ES) AFIT Student Attending: University of Washinton				8. PERFORMING ORGANIZATION REPORT NUMBER AFIT/CI/CIA- 91-133	
9. SPONSORING/MONITORING AGENCY NAME(S) AND ADDRESS(ES) AFIT/CI Wright-Patterson AFB OH 45433-6583				10. SPONSORING/MONITORING AGENCY REPORT NUMBER	
11. SUPPLEMENTARY NOTES					
12a. DISTRIBUTION/AVAILABILITY STATEMENT Approved for Public Release IAW 190-1 Distributed Unlimited ERNEST A. HAYGOOD, Captain, USAF Executive Officer				12b. DISTRIBUTION CODE	
13. ABSTRACT (Maximum 200 words)					
14. SUBJECT TERMS				15. NUMBER OF PAGES 97	
				16. PRICE CODE	
17. SECURITY CLASSIFICATION OF REPORT		18. SECURITY CLASSIFICATION OF THIS PAGE		19. SECURITY CLASSIFICATION OF ABSTRACT	
				20. LIMITATION OF ABSTRACT	

DTIC
S ELECTE D
MAY 7 1992
C

University of Washington

1991
Abstract

Studies in Control for Vibration Suppression of the UWAA 20-Bay Planar Truss

by Michael J. Shepherd, 2Lt, USAF

Master of Science in Aeronautics and Astronautics 97 pages

Chairperson of Supervisory Committee: Prof. Juris Vagners

Dept. of Aeronautics and Astronautics

This thesis is based on research conducted at the newly constructed Aeronautics and Astronautics Control Sciences Laboratory at the University of Washington. The set up of the UWAA 20-bay planar truss is described, and is based upon a similar experimental test bed at the United States Air Force Academy. Validation of existing open loop finite element models of the truss in the cantilevered configuration was conducted for this research. The formulation of non-linear and approximate linear models for the two primary means of structurally-borne actuation, the air jet thrusters and the reaction mass actuators, is also explored. Computer non-linear simulation and experimental testing of classical analog controllers to actively suppress vibration of the planar bending modes of the truss using the air jet thruster and reaction mass actuators independently and jointly for hybrid linear/non-linear actuation is reported in this thesis. The design of an optimal controller for the reaction mass actuators utilizing linear quadratic Gaussian techniques is reported, and includes non-linear simulation of hybrid actuation utilizing the optimal reaction mass actuator controllers and the classical air jet thruster controllers. Recommendations for future study based upon both the hardware implementation and the computer simulation are suggested in the conclusions section of this thesis.

Key Sources:

Hallauer, W.L. and Lamberson, S.E. Experimental Active Vibration Damping of a Plane Truss Using Hybrid Actuation. AIAA Paper 89-1169, 30th Structures, Structural Dynamics and Materials Conference, Mobile AL, April 3-5, 1989.

Inman, D.J. Control/Structure Interaction: Effects of Actuator Dynamics. Mechanics and Control of Large Flexible Structures. ed Junkins, J.L., AIAA Inc, vol.129, 1990

92-11976



92 5 01 012





Studies in Control for Vibration Suppression of the UWAA 20-Bay Planar Truss

by

Michael J. Shepherd

A thesis submitted in partial fulfillment
of the requirements for the degree of

Master of Science in Aeronautics and Astronautics

University of Washington

1991

Approved by _____

(Chairperson of Supervisory Committee)

Program Authorized

to Offer Degree _____

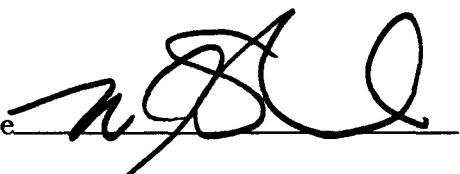
Department of Aeronautics & Astronautics

Date _____

December 18, 1991

Accession For	
NTIS GR&I	<input checked="" type="checkbox"/>
DTIC TAB	<input type="checkbox"/>
Unannounced	<input type="checkbox"/>
Justification	
By _____	
Distribution/	
Availability Codes	
Dist	Avail and/or Special
A-1	

In presenting this thesis in partial fulfillment of the requirements for the Master's degree at the University of Washington, I agree that the Library shall make its copies freely available for inspection. I further agree that extensive copying of this thesis is allowable only for scholarly purposes, consistent with "fair use" as prescribed in the U. S. Copyright Law. Any other reproduction for any purposes or by any means shall not be allowed without my written permission.

Signature 

Date 18 DEC 91

TABLE OF CONTENTS

List of Figures	v
List of Tables	vii
Chapter 1 Introduction	1
1.1 Background	1
1.2 Problem Definition	2
1.3 System Configuration	3
1.3.1 Truss	3
1.3.2 Air Jet Thrusters	6
1.3.3 Accelerometers	6
1.3.4 Reaction Mass Actuators	6
1.3.5 Analog Computers	7
1.3.6 Dynamic Signal Analyzer	8
1.3.7 Force Gage	8
1.3.8 Linear/Non-Linear Analysis and Dynamic Simulation Package	8
1.4 Thesis Outline	9
Chapter 2 System Modeling	10
2.1 Overview	10
2.2 Air Jet Thruster Modeling	10
2.2.1 Theoretical Development of the AJTs	10
2.2.2 Experimental Data	15
2.2.3 Linear Model of the AJT	17
2.3 Reaction Mass Actuators	18
2.3.1 Theoretical Development of the RMA model	18
2.3.2 RMA Experimental Testing and Linear Model Approximation	24
2.4 Truss Modeling	27
2.4.1 Truss Theory	28

2.4.2	Truss Linear Model	29
2.5	Open Loop Truss Model Validation	31
2.5.1	Mode Shapes	31
2.5.2	Free Decay of Bending Modes	32
2.5.3	Open loop frequency response	37
Chapter 3	Classical Control Techniques for Vibration Suppression	39
3.1	Overview	39
3.2	Velocity Feedback to the AJTs	39
3.2.1	The Theory of Velocity Feedback	39
3.2.2	Approximate Integrator for Velocity Feedback	40
3.2.3	AJT Control: Non-Linear Simulation and Experimental Results	43
3.3	RMAs for Vibration Suppression	47
3.3.1	RMA as a Passive Damper	48
3.3.2	Straight Velocity Feedback	50
3.3.3	Relative Velocity Feedback	52
3.3.4	Separate Velocity Feedback using RMA and Truss Inertial Velocities	56
3.4	Hybrid Control: AJTs and RMAs Working Together to Suppress Vibration	60
3.5	Experimental Results	63
3.5.1	Open Loop Testing of the RMA-Augmented Truss	63
3.5.2	Experimental Closed Loop Testing of the RMA Controllers	64
3.5.3	Experimental Hybrid Control	67
3.6	Classical Control Summary	68
Chapter 4	Optimal Control Strategies	71
4.1	Overview	71
4.2	LQG Design Problem	71
4.2.1	Optimal Controller Design	72
4.3	Performance of the Linear Optimal RMA Controller through Simulation	76
4.3.1	Linear Frequency Response	76

4.3.2	Non-linear Simulation of Modal Time Responses	76
4.4	Non-Linear Simulation of the Hybrid Classical-AJT/Optimal-RMA Controller	77
4.5	Optimal Control Conclusions	80
Chapter 5	Conclusions and Recommendations	82
5.1	Overview	82
5.2	Conclusions	82
5.3	Recommendations For Future Research on the UWAA Planar Truss .	83
Bibliography		86
Appendix A	Truss Linear State Space Models	89
A.1	Open Loop Truss Model Without Actuators Attached	89
A.2	Open Loop Truss Model with RMAs Attached at Midpoint and Tip .	91
Appendix B	Full State Feedback Gain	94
B.1	Optimal Control Gain K_c	94
Appendix C	Equipment List	95
C.1	Truss Hardware	95
C.2	Custom Fabricated Truss Hardware	95
C.3	Air Jet Thruster Hardware	96
C.4	Custom Fabricated Air Jet Thruster Hardware	96
C.5	Reaction Mass Actuator Hardware	96
C.6	Custom Fabricated Reaction Mass Actuator Hardware	97
C.7	Instrumentation and Electronics	97

LIST OF FIGURES

1.1	Truss set up	4
1.2	Truss hardware in cantilever configuration	5
1.3	Actuators on board the truss tip	7
1.4	Force gage predicted frequency response	9
2.1	AJT signals	12
2.2	AJT non-linear block diagram	14
2.3	AJT in test stand	15
2.4	Normalized magnitude and phase plots for the AJT	16
2.5	RMA schematic	19
2.6	RMA simplified system	20
2.7	Typical RMA 'stand alone' frequency response	22
2.8	RMA aboard truss station	23
2.9	RMA in the 'stand alone' experimental test configuration	25
2.10	Tip RMA frequency response	26
2.11	Midpoint RMA frequency response	27
2.12	RMA block diagram	28
2.13	Normalized bending mode shape for the UWAA planar truss	32
2.14	Logarithmic decrement	33
2.15	Tip free decay:modes 1 and 2	35
2.16	Tip free decay:modes 3 and 4	36
2.17	Open loop frequency response	38
3.1	Approximate integrator theoretical frequency response	41
3.2	Approximate integrator analog computer implementation	42
3.3	Non-linear simulation truss tip responses. AJT velocity feedback	44
3.4	Non-linear/hardware block diagram for AJT velocity feedback control	45
3.5	Experimental truss tip responses: AJT velocity feedback	46
3.6	Comparison of root loci: $k_t = k_m = 0.0:0.1:10$	50

3.7	Relative velocity feedback to the RMAs	53
3.8	Linear model frequency response for mode-2 suppression	54
3.9	Experimental frequency response for mode-2 suppression	55
3.10	Root locus for separate feedback gains on inertial velocities	57
3.11	Time responses for second mode: separate inertial velocity feedback .	58
3.12	Non-linear simulation of hybrid control:truss tip responses	61
3.13	Non-linear block diagram for hybrid actuation simulation	62
3.14	Experimental open loop RMA-augmented truss tip responses	63
3.15	RMA actuator/instrumentation instability	65
3.16	Experimental RMA-relative velocity feedback only-time responses . .	66
3.17	Experimental hybrid control truss tip time responses	68
3.18	Hardware block diagram for hybrid actuation	70
4.1	Linear simulation of the optimal-RMA controller for vibration suppression	77
4.2	Non-linear simulation modal time responses: RMA optimal controller	78
4.3	Modal time responses hybrid classical-AJT/optimal-RMA controller	79
4.4	Non-linear block diagram for hybrid classical-AJT/optimal-RMA Controller	81

LIST OF TABLES

2.1 Experimentally determined values for RMA models	28
2.2 Planar truss bending mode frequencies	31
2.3 Experimentally determined damping ratios ζ	34
3.1 Non-linear simulation closed loop modal data: AJT velocity feedback	43
3.2 Experimental closed loop modal data: truss velocity feedback to AJTs	47
3.3 Open loop linear model modal data: RMAs as passive dampers . . .	49
3.4 Feedback gains on truss velocities	51
3.5 Closed loop linear model modal data: truss velocity feedback	52
3.6 Feedback gains on relative velocities	56
3.7 Closed loop linear model modal data: relative velocity feedback . . .	56
3.8 Feedback gains on proof mass and truss velocities	59
3.9 Closed loop linear model modal data: separate inertial velocity feed- back	59
3.10 Non-linear simulation closed loop modal data: hybrid actuation . . .	60
3.11 Experimental open loop modal data: RMA-augmented truss	64
3.12 Experimental closed loop modal data: relative velocity feedback to RMAs	67
3.13 Experimental closed loop modal data: hybrid actuation	69
4.1 Penalty weights on the states	75
4.2 Penalty weights on the control inputs	75
4.3 Linear model modal data: optimal RMA controller	76
4.4 Closed loop modal data: hybrid classical/optimal controller	80

ACKNOWLEDGMENTS

I would like to say thanks to the following people who, without their ideas and contributions, this work would not have been possible. Jim Smith and Major Steve Webb at the United States Air Force Academy offered the solutions to the endless questions that I had regarding their research. The two machinists in our lab, Otto and Bill, deserve the real credit for the final design and assembly of the space truss. Bob Blair, our resident electronics technician, was a great help with the maze of wiring that accompanied the truss assembly. Captain Mark Arnold, Wayne Yuen, and Mike Parin of the Flight Dynamics Lab at Wright-Patterson Air Force Base provided many ideas, drawings, and test articles incorporated in this report. Thanks also to professors R.N. Clark and Uy-Loi Ly for their advice on the academic considerations of this thesis. Thanks to Major Ken Barker and the rest of my Air Force compatriates who encouraged me along the way.

Special thanks go out to 2Lt Marcus Schulthess, who spent as much time helping me with my research as he did on his own work. Also, I would like to say a sincere thank you to Professor Juris Vagners, who initiated my coming to the University of Washington, procured funding for my research, and provided insight for this thesis. Finally, thanks to Mom, Dad, and my kid brother Don, all of whom never had any doubts about me despite whatever I told them.

To my favorite girl, Jules

Chapter 1

INTRODUCTION

1.1 Background

The control of flexible space structures is of paramount importance in several high visibility space programs today, including the Hubble telescope, Space Station Freedom, and the Strategic Defense Initiative. All of these systems require stable platforms from which high precision optical systems may be employed. Weight restrictions of establishing orbit dictate the use of lightweight, rigid, flexible structures as basic building blocks for these space platforms.

Several methods have been proposed to deal with the low inherent damping in large space structures. Passive damping through the use of viscoelastic support members in the lattice work of the structure [6], and incorporation of shock absorbing isolators [22] are perhaps the most efficient answers to the control problems, but lack the performance of active control. Increasing the mass of a structure helps to reduce the amplitude of disturbances and lowers the frequency of structural modes, but runs contrary to mission requirements of light weight for orbital deployment. Active control of beam steering mirrors and optical lenses onboard these stations [1, 17] sidesteps the problem of low structural damping in the supporting space structure. However, sometimes low frequency structural resonance effects may be uncontrollable by the high frequency, high precision mirror and optics controllers. Therefore, we realize that some degree of structural stability is desirable.

Space realizable actuation (SRA) is an additional constraint imposed on the control of space-based systems. Control of everything from airplanes to assembly line robots incorporates one simple basic premise for operation—there is a sufficient reacting medium to operate against for control purposes. The airplane control surfaces act against the surrounding air, the robot is securely mounted to ground in an assembly line. In space, the luxury of a reacting medium is lost, so all energy created must be dispensed with by onboard systems. SRA is of two main forms. The first

is a non-renewable type realized through thrusters and rockets capable of translating the structure in space. The second type is momentum exchange equipment realized through linear reaction mass or rotary reaction wheel actuators. While not capable of translating the body through space, these types of SRA may be electrically driven and thus, using power supplies such as solar cells or nuclear fission, may be used without worry of depleting a finite quantity of fuel.

Research at the United States Air Force Academy (USAFA) [8] points towards a unique solution incorporating both air jet thrusters (AJTs) and structurally borne reaction mass actuators (RMAs). The AJTs have advantages at low frequencies, high amplitude disturbances typical of rigid body slewing problems. The RMAs enjoy a higher operating bandwidth than the AJTs and therefore suggest using the two methods of actuation in conjunction with one another. Hybrid actuation was the terminology coined by the USAFA team when researching these two controllers working in unison.

My research was the first to be conducted on the newly constructed planar truss testbed at the University of Washington, Department of Aeronautics and Astronautics Control Sciences Laboratory, which duplicates the USAFA research planar truss. The goal of the work reported in this thesis was to re-examine the previous work on the USAFA truss to include both modeling and control aspects, establish a base-line controller for the UWAA planar truss, and to investigate classical multiple input, multiple output and optimal design techniques in hybrid actuation.

1.2 Problem Definition

This thesis reports the set up, modeling, and control of a lightly damped planar truss in the cantilever configuration. Two methods of actuation were available to control the structure: the air jet thrusters and the structurally borne reaction mass actuators. Both AJTs and RMAs were located at the midpoint and the tip (free end) of the truss and were configured to control lateral motion. The location of the actuators was chosen to best damp the second bending mode of the truss, and duplicated the original USAFA configuration. The accelerometers were also located at the tip and midpoint of the truss and sense lateral motions, and thus provide colocated sensor-actuator pairings.

The goal of this thesis was to improve upon the open loop stability of the truss through the implementation of classical and optimal controllers. A performance goal of 10 % modal damping is suggested by Miller and Crawley [15] as a minimum level of damping in future space structures. Modal damping and time responses to modal excitement were the primary means of measuring success in attaining this goal.

Measurement of all frequencies reported in this thesis is in radians per second (rad/sec). Hertz is the choice of structural engineers desiring to report modal frequencies, and has merit when describing the response of structures to the mechanical engineering community. However, from strictly a control systems design standpoint, frequencies reported in rad/sec are much more desirable. For instance, the conversion of frequency responses (Bode plots) to easily recognizable transfer functions is easier when results are reported in rad/sec. As this thesis is directed towards the controls community, the rad/sec frequency convention will be used throughout.

1.3 System Configuration

In this section, the hardware and analysis equipment used in the UWAA planar truss control experiment is described. Computer modeling of the truss and actuators will be discussed in the chapter two. An appendix is also included which describes some of the idiosyncracies and special considerations of the equipment. It is intended to provide aid to future students working with this particular hardware but is not essential to the academic understanding of this thesis.

1.3.1 Truss

Figure 1.1 show the experimental set up of the truss. The planar truss is 23.2 feet long, containing 20 square bays of equal size with alternating diagonal members to increase stiffness. The cantilevered end of the truss is bolted to a rigid steel table which is in turn anchored into the concrete floor. The truss rides on steel ball bearings to minimize the friction with the supporting table. The lateral members of the truss are affixed to rigid steel batans to increase the mass and hence lower the natural frequencies associated with the lateral bending modes [1].

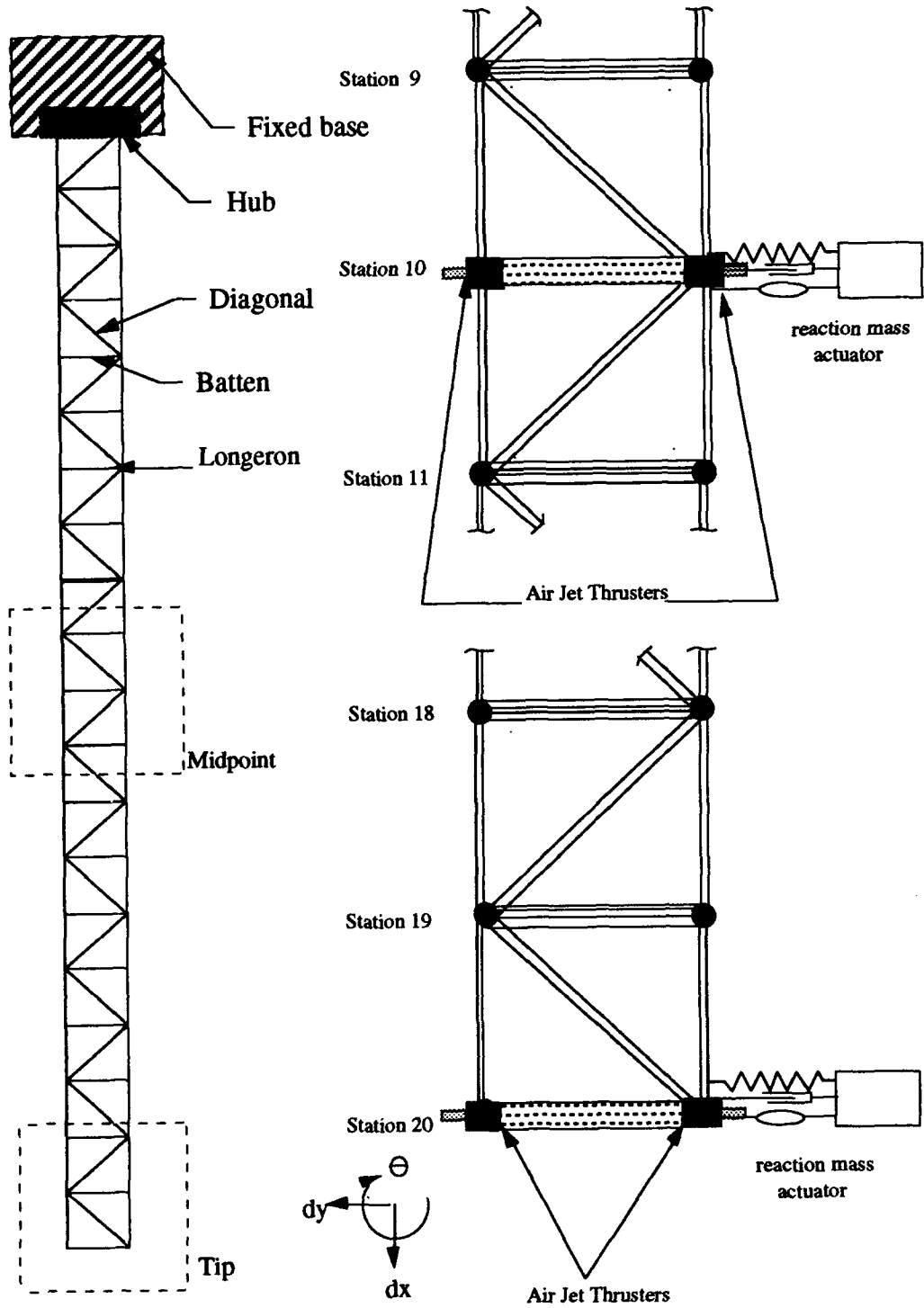


Figure 1.1: Truss set up

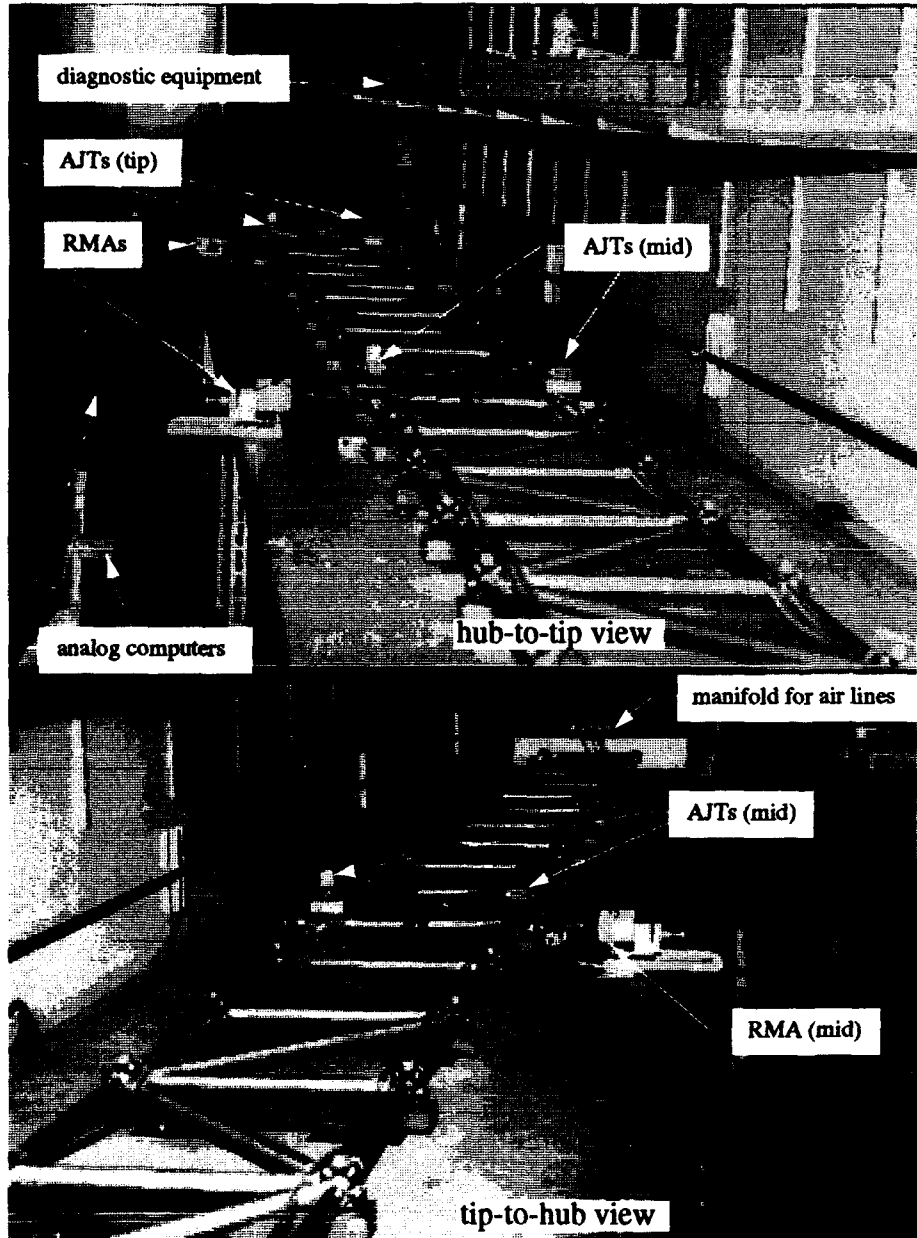


Figure 1.2: Truss hardware in cantilever configuration

The first four bending modes of the truss were experimentally determined to occur at 9.30, 55.8, 146.52, and 262.32 rad/sec. The 1/4 point (station 5), midpoint (station 10), 3/4 point (station 15), and truss free-end tip (station 20) were the locations kept for the formation of finite element models of the truss, and will be referred to in the thesis by either their location or station number interchangeably.

1.3.2 Air Jet Thrusters

Two pairs of air jet thrusters are mounted on the truss, the first pair at the tip, the second at the midpoint. The pairs work together, firing transversely in opposite directions: a positive voltage from a control signal fires one of the pair, a negative signal fires its opposite twin. A regulated high pressure supply of air enters a manifold located near the base of the truss, which is then routed up to the four AJTs via separate polyvinyl tubes. A solenoid valve manufactured by MAC valves, model 113B-551BA, in each of the AJT's releases air from the source tubes through the AJT's nozzles, providing thrust which may be used alternately to excite or control the transverse bending modes of the truss.

As previously noted, the AJTs' locations were chosen primarily to control second mode disturbances. Other locations are possible and warrant investigation.

1.3.3 Accelerometers

Two high-precision, low-noise Sundstrand PA700 accelerometers are mounted to measure transverse motion at the tip and midpoint of the truss. Their location is colocated with the actuators' locations. The scale factor of these accelerometers is 9.70 inches per second squared per volt. The accelerometers have a useful range of plus or minus 15 volts. Two additional accelerometers are mounted on the reaction masses of the RMAs.

1.3.4 Reaction Mass Actuators

Two structurally-borne reaction mass actuators are attached to the truss at the tip and midpoint lateral degrees of freedom. The RMAs are Ling Dynamics V102 Shakers mounted on a base of aluminum construction and ride on ball bearings similar to those for the planar truss. The shaker DC motor is connected to the truss node via

a stinger which allows for slight misalignment of RMA and truss node. The power supplies for the RMAs are variable gain Ling Dynamics signal amplifiers, model PA-35. An accelerometer is rigidly mounted to the RMA aluminum housing to sense lateral motion as noted in section 1.3.3, and provided for measurement of RMA lateral motion relative to the truss relative motion at the corresponding connection node.

A photograph which shows the AJT and RMA at the tip of the planar truss is shown in figure 1.3.

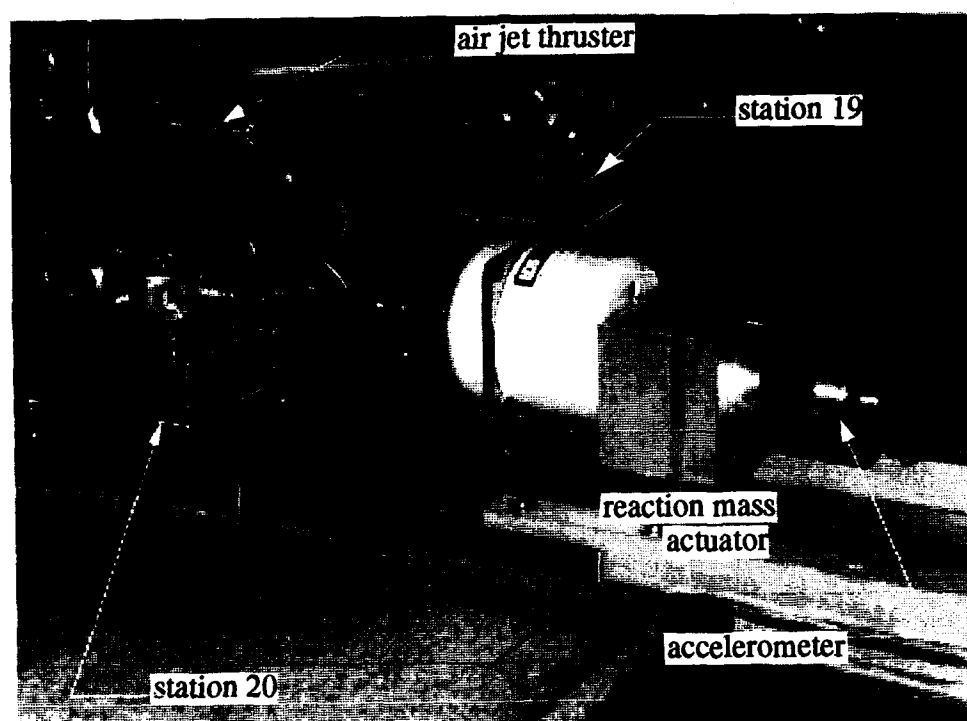


Figure 1.3: Actuators on board the truss tip

1.3.5 Analog Computers

Two types of analog computers were used to implement control laws in this experiment. They were the Electronic Associates, Inc. EAI TR-20 computer built in 1966 and the more recent Comdyna GP-6 analog computer. Despite the age difference of the two computers, their operation and performance is similar. No attempt was

made to differentiate between the two computers when analog control circuitry was implemented.

1.3.6 Dynamic Signal Analyzer

Data acquisition and signal analysis was performed on the Hewlett Packard HP 35665A Dynamic Signal Analyzer. It is a two-channel FFT spectrum/network analyzer with an extended frequency range well beyond our requirements. The HP 35665A is primarily a frequency domain analyzer, but was also used for time domain measurements. The analyzer was equipped to perform both random noise and swept sine device characterization.

1.3.7 Force Gage

Although not used in the implementation of control laws in this thesis, a Transducer Techniques force gage, model MDB-10, was used extensively in the device characterization of the AJTs and the RMAs. The force gage has a linear range of -10 to 10 lbs, and is calibrated in compression only. The readings in tension were not calibrated from the factory, but are sufficient for device characterization. The force gage TM-2 amplifier is equipped with a $10 \mu f$ filter capacitor for noise suppression, resulting in a linear response for signals less than 100 rad/sec. The frequency response for the force gage, assuming the 100 rad/sec bandwidth, is calculated and shown in figure 1.4.

1.3.8 Linear/Non-Linear Analysis and Dynamic Simulation Package

Computer analysis and simulation was performed using SIMULAB/MATLAB software by Mathworks, Inc. [19] run upon DEC workstations equipped with X-windows. For non-linear simulation the "linear" numerical option was used. The simulation package was designed to work for systems containing many linear blocks with a few non-linear blocks, which is typical of the hybrid systems simulated for this thesis. The algorithm is based upon the work presented by Frederick and Rimer [5].

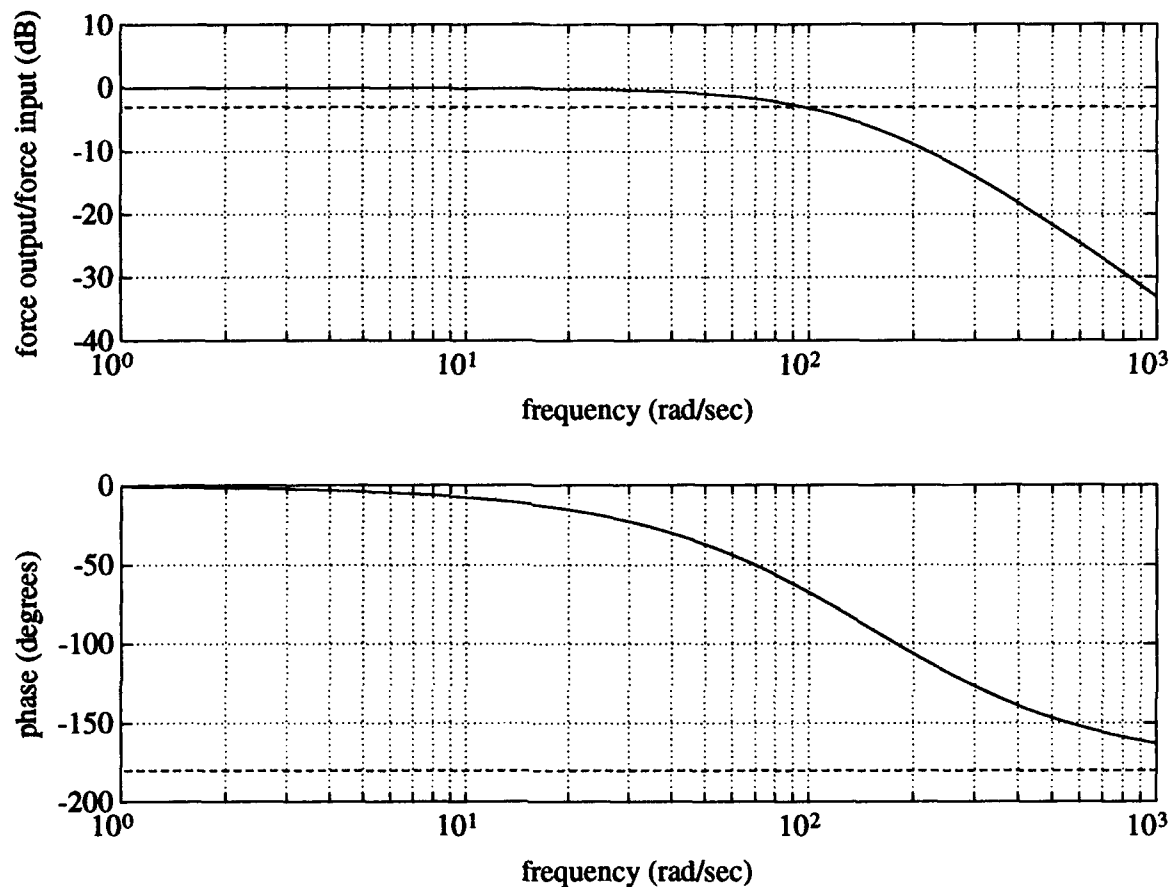


Figure 1.4: Force gage predicted frequency response

1.4 Thesis Outline

Theoretical development and experimental verification of the AJT, the RMA, and the UWAA planar truss models are reported in chapter 2. The use of classical control techniques to increase eigenvalue damping is discussed in chapter 3. Both linear model evaluation and experimental results are presented in chapter 3. Chapter 4 presents an optimal controller for the RMAs. Conclusions and recommendations for future study are stated in chapter 5.

Chapter 2

SYSTEM MODELING

2.1 Overview

Before designing a controller for the planar truss, a viable model must be formulated. An existing model for the planar truss in the cantilever configuration had already been developed using finite element methods [8, 17] ,and requires validation for this application. Likewise, the controllers had been previously explored [2, 8], but lacked the experimental implementation that forces one to rethink the theoretical models. This chapter re-explores the theoretical development of the models used in this thesis and compares them with the actual experimental data. Changes are made to theoretical models to better reflect the experimental data.

2.2 Air Jet Thruster Modeling

Before examining the truss model it is necessary to develop models for the AJTs, the primary means of excitation and control. The models of the air jet thrusters may be mistakenly overlooked when examining the frequency characteristics of truss. This error may be extremely serious considering the inherent non-linearities and the limited bandwidth of the AJTs.

2.2.1 Theoretical Development of the AJTs

The AJTs work through the actuation of a solenoid valve which may be either open or closed. Resulting output force is the full-on or full-off thrust characteristic of AJTs, resulting in their nickname of "bang-bang" controllers. The AJTs used in this thesis are connected to a source of pressurized air at 65 psig, and each develop a steady state thrust of 0.6 lbs when opened. Ideal on-off control is not possible, however, due to the dynamics of the air flow in the jet and the lags of the solenoid valve. The relationship between the output thrust $f(t)$ for an ideal AJT with a uniform solenoid

valve time delay τ_d and a steady state output force F_{ss} to a control signal $e(t)$ is given by Hallauer to be [8]:

$$f(t) = \frac{1}{2}F_{ss}[1 + \text{sgn}(e(t - \tau_d))] \quad (2.1)$$

where

$$\begin{aligned} \text{sgn}[e(t)] &= 1, e(t) > e_d \\ \text{sgn}[e(t)] &= 0, |e(t)| < e_d \\ \text{sgn}[e(t)] &= -1, e(t) \leq -e_d \end{aligned}$$

and e_d is a small 'dead band' voltage which prevents the AJTs from firing for small biases and noises in the control signal.

Equation 2.1 is valid assuming the AJT develops full thrust immediately after the solenoid opens the valve. This is an unrealistic assumption, however, as a rise time delay will occur after the valve is opened as the AJT thrust builds to its steady state value. The lag is caused not by the time it takes for the valve to open, but by the time it takes for the force output of the AJT to rise to its steady state value once the valve opens. The valve opening may therefore be considered to happen instantaneously with the application of a control signal commanding it to open. The rise time of the AJT force may then be modeled by a second order critically damped system with natural frequency ω_n . The natural frequency of a critically damped second order system is equal to [16]:

$$\omega_n = \frac{6}{t_r} \quad (2.2)$$

where t_r is the time it takes the system to reach 95 percent of its steady state value when subjected to a step input. By modeling an AJT 'back to back' pair acting in opposite directions, and writing the time domain step response of a second order system, the following equation results:

$$f(t) = F_{ss}\text{sgn}[e(t)][1 - \exp(-\omega_n(t - sw(t)))(1 + \omega_n(t - sw(t)))] \quad (2.3)$$

where the function $sw(t)$ is defined as:

$$sw(t) = t, \text{ when } e(t) = 0 \quad (2.4)$$

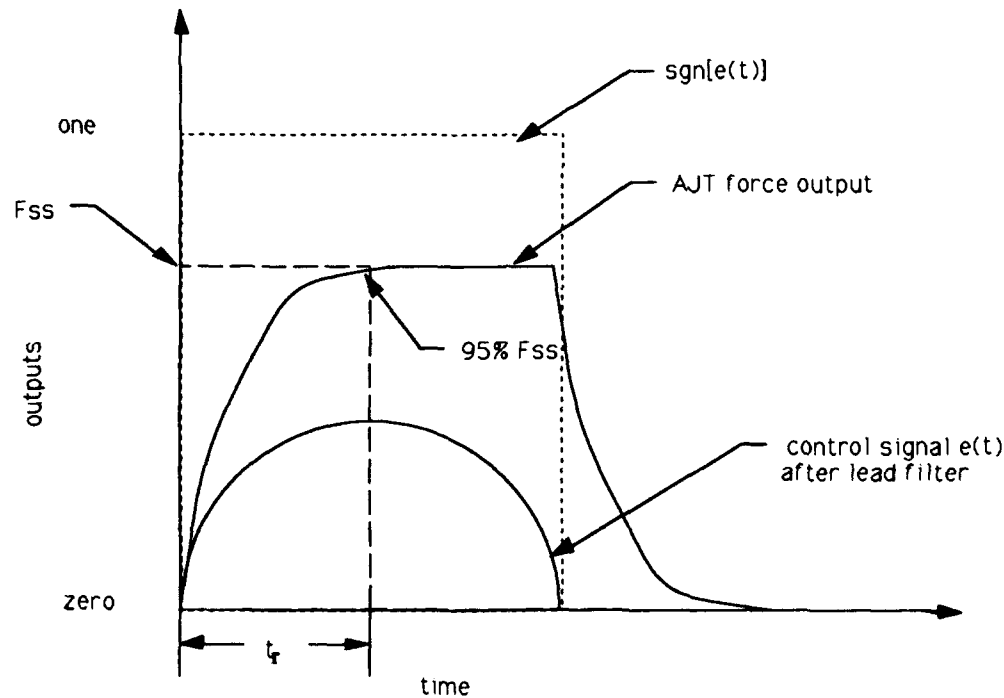


Figure 2.1: AJT signals

Thus, a new AJT force pulse is initiated whenever the control signal passes through a zero reference. The force will be positive when the control signal is positive, and negative when the control signal is negative. A picture illustrating the operation of an AJT with a control signal $e(t)$, a switching signal $sgn[e(t)]$, and AJT force output $f(t)$ is presented in figure 2.1. This switching is realized in the hardware by applying a positive voltage to the transistor of the AJT to be opened. The transistor then closes the power signal circuit to the AJT solenoid which opens the valve and allows pressurized air out through the nozzle. Likewise, a negative voltage command signal to the AJT transistor will open, and shut off, the power signal to the AJT solenoid and allow the valve to close. The AJTs are set up to work in opposing pairs. The opposite AJT operates by applying its force when a negative voltage is applied to its

switching transistor, and shutting off the force with a positive voltage.

Equation 2.3 is a simple equation for the magnitude of the output force of the AJTs. However, due to the non-linear nature of the AJTs, it is important to note that it is impossible to relate the force of the output signal to the magnitude of the input control signal $e(t)$. Theoretically, a sinusoidal input control signal of 0.1 volt magnitude will have the same magnitude output force as a 10 volt input signal. This limitation is caused by the fact that the transistors in the AJT circuitry close the power circuit for all voltages above a small threshold value. Despite this limitation, an arbitrary linear input/output relationship is assigned for the design problem. This relationship will be discussed shortly.

The phase of the AJT is fortunately easier to describe and verify. As proposed by Hallauer [8], the phase lag ϕ of the AJT due to the time delay of the AJT solenoid is simply:

$$\phi_d = -\omega\tau_d \quad (2.5)$$

The phase lag in our model is instead better described by a second order system transfer function. Substituting $s = j\omega$ into the second order transfer function [16]:

$$G(j\omega) = \left. \frac{F_{ss}\omega_n^2}{(s + \omega_n)^2} \right|_{s = j\omega} = \frac{F_{ss}\omega_n^2}{(j\omega + \omega_n)^2} \quad (2.6)$$

where the phase angle is therefore:

$$\phi_r = \angle \frac{F_{ss}\omega_n^2}{(j\omega + \omega_n)^2} \quad (2.7)$$

There is one additional factor that affects the phase lag of the AJTs that is not the result of the actual mechanical operation of the AJTs. A lead filter precedes the transistors in the solenoid switching circuit. This lead filter circuit is modeled by the transfer function [17]:

$$G(s) = \frac{\frac{1}{2}s}{s + \frac{1}{\tau_l}} \quad (2.8)$$

with phase angle

$$\phi_l = \angle \frac{j\omega}{j\omega + \frac{1}{\tau_l}} \quad (2.9)$$

Adding the phase effects due to the lead filter and force rise time yields:

$$\phi = \phi_l + \phi_r \quad (2.10)$$

One additional point should be made here. Because some linear matrix algebra packages work best when all the roots of a system are ordered, it is convenient to depart slightly from the critically damped case for the AJT force output and allow a variable damping ratio which may be adjusted to be close to one (critically damped) yet just under to allow for oscillatory (unique-non-repeated) roots. In order to do so equation 2.6 may take the following form:

$$G(s) = \frac{F_{ss}\omega_n^2}{s^2 + 2\zeta\omega_n s + \omega_n^2} \quad (2.11)$$

where it is recognized the the damping ratio ζ will be just under one. The results of this section are shown in a frequency response in figure 2.4. In section 2.2.2 an explanation is presented as to how the scaling on the magnitude plot was determined. The non-linear block diagram for this system suitable for simulation is shown in figure 2.2:

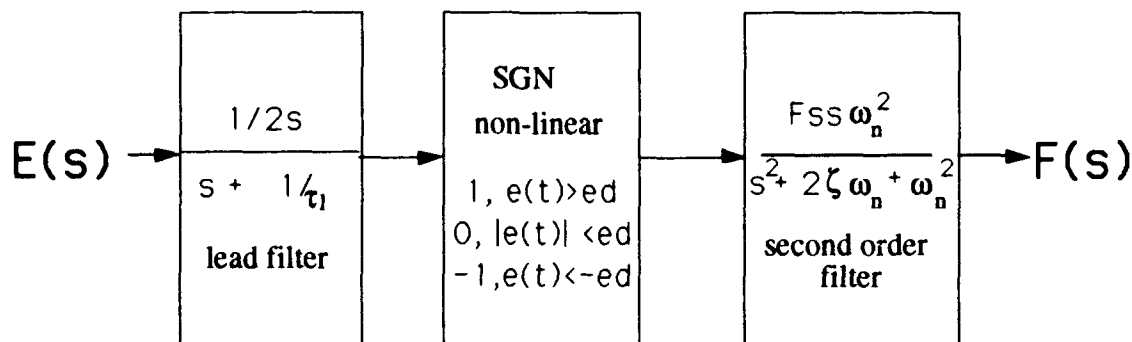


Figure 2.2: AJT non-linear block diagram

2.2.2 Experimental Data

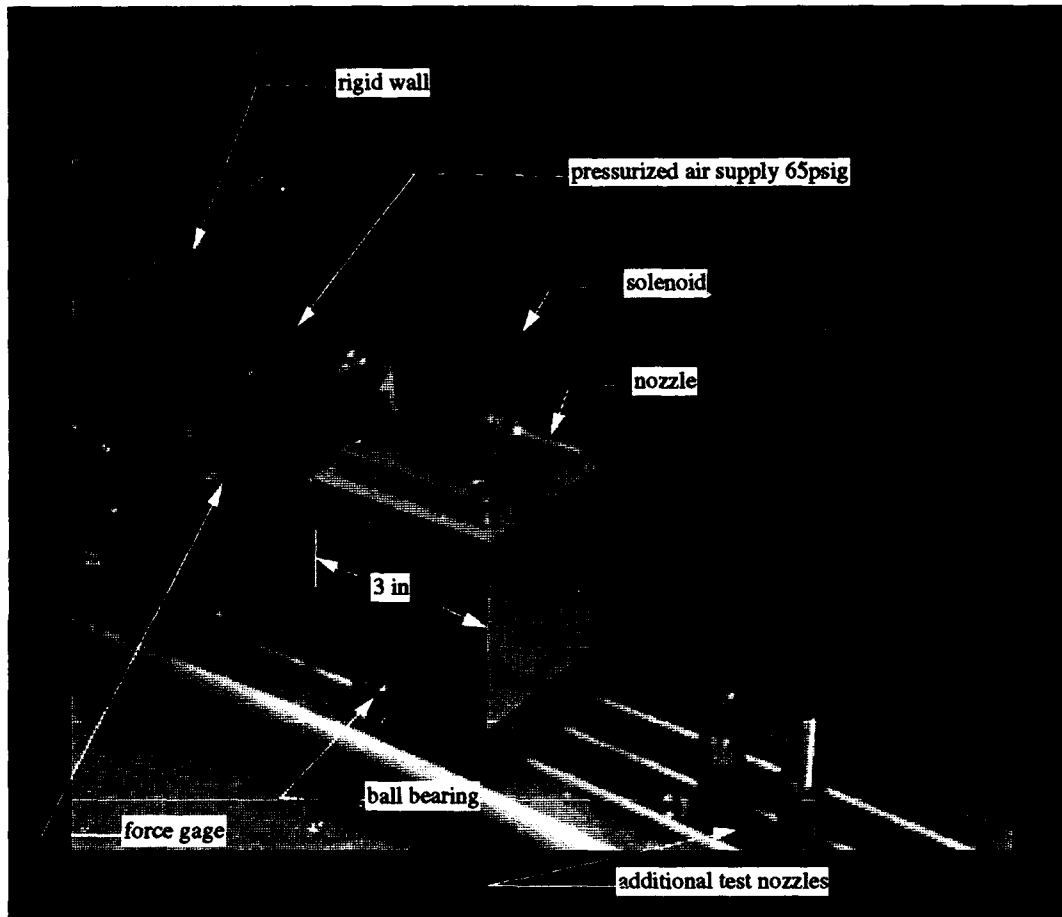


Figure 2.3: AJT in test stand

The AJT was placed into a test jig shown in figure 2.3. The configuration allows for the measurement of AJT output thrust when the solenoid valves are opened by an electronic control signal $e(t)$. The rise time t_r of the AJT was measured by comparing the output thrust time response to the square wave power signal to the solenoids. The rise time constant t_r for the AJTs averages about 30 ms, and was found by measuring the length of time the AJT required to produce 95 percent of the steady state output force after the solenoid opened. A natural frequency for the second order rise time was then found to be $\omega_n = 200ms$ using equation 2.2.

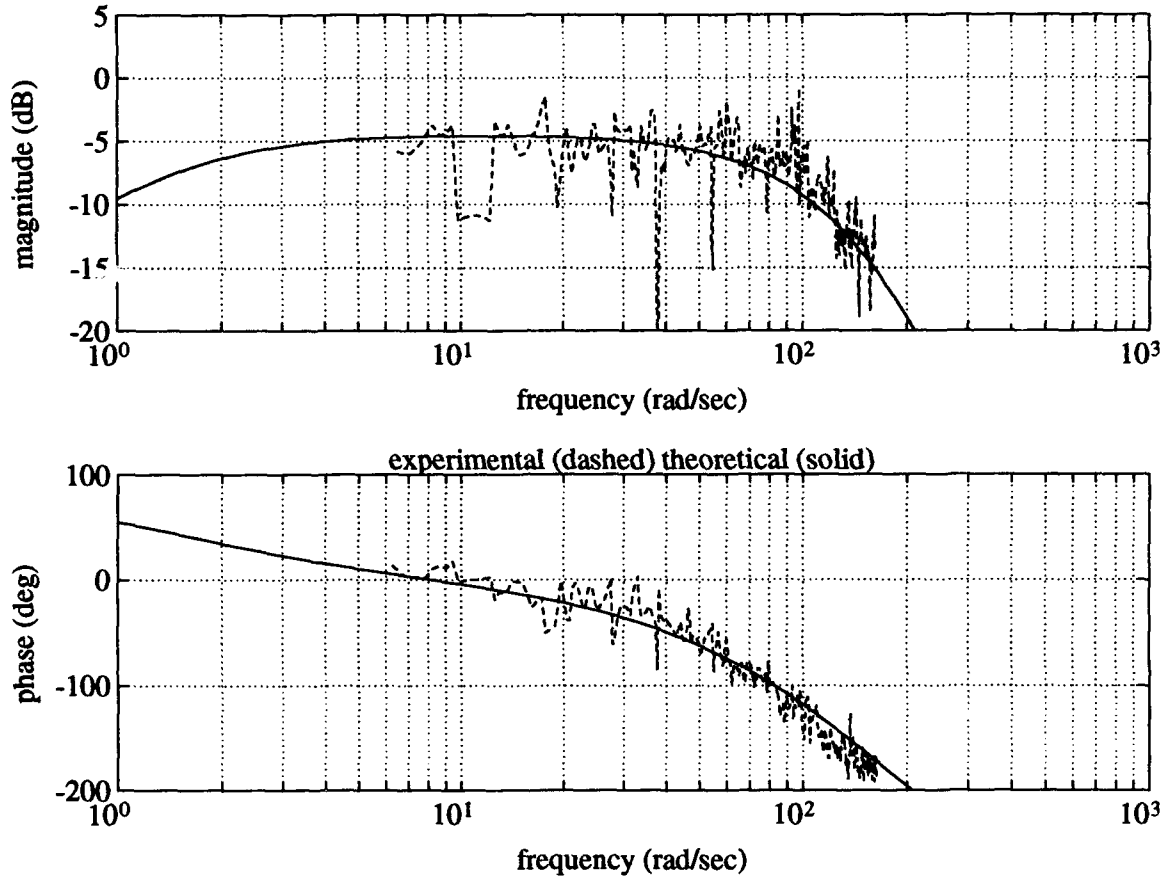


Figure 2.4: Normalized magnitude and phase plots for the AJT

The AJT frequency response was obtained by exciting the input transistor switching circuit with a random noise source from the dynamic signal analyzer from the range of 1 to 50 hz, or 6.28 to 157.0 rad/sec and taking the Fast Fourier Transform of the output. The magnitude portion of the frequency response was scaled so that a one volt input would equal a 0.6 lbf output. This is an *arbitrary* scaling as the theoretical development (see section 2.2.1) shows the independence of the force output from the control signal input. It is useful to assign an input/output relationship to the magnitude plot in order to make a linear model of the AJT while realizing there will be error in the linear model. Thus, the experimental data appears to have less resolution than was actually attained. Furthermore, a swept sine capability was later

added to the dynamic signal analyzer software package which would give better experimental frequency information than the random noise excitation used on the AJT. In figure 2.4 the experimental data is represented by a dashed line, the theoretical linearized model is shown as a solid line.

The shape of the magnitude plot (figure 2.4) confirms the validity of the modeling performed in section 2.2.1. It is important to note that the second order behavior of the force gage filter is reflected in the experimental data, and is likewise added to the theoretical linear model so that a valid comparison may be made. The experimentally determined response closely matches the theoretical values below 30 rad/sec and remains within 3 dB at 56 rad/sec, the frequency of the second bending mode of the truss. The force of the AJTs drops off significantly in the regions of the third and fourth bending modes of the truss at rates of 40 db/decade (figure 2.4 shows a more extreme drop off rate of 80 dB per decade due to the force gage filter effects), illustrating the problem of using AJTs alone to control the higher modes.

The phase plot of the AJTs (figure 2.4) is free of the problems of the lack of a relationship between the magnitude of the input signal and the magnitude of the output force. The AJT phase relationship was clear in equation 2.10, and the experimental data confirms the phase relationship. Again, it is important to note that the theoretical linear phase information has been run through a second order filter representative of the force gage to match the experimental data.

2.2.3 Linear Model of the AJT

The AJTs are modeled with a third order linear model to produce the plot shown in figure 2.4. A third order model was chosen to reflect the theoretical development in section 2.2.1. The third order model maintains the lead filter in the AJT circuit as well as the second order critically damped force output of the AJTs. The AJT model is given the arbitrary magnitude scaling of 0.6lbf/volt. Defining a linear model for the AJTs does not allow one to design controllers using linear techniques—the results would be misleading and most probably not realizable in the hardware. However, by defining a linear model for the AJT it may be used in the linear model packages for assessing the performance of other controllers implemented on the UWAA planar truss. Specifically, vibration suppression may be measured in the magnitude portion

of a frequency response with a input to the AJTs and output measured at a truss location. Experimental open loop data may be scaled against the open loop responses of the linear model, and then closed loop responses may be compared using the same scaling. This method is used extensively in chapter three. Furthermore, the validation of the open loop model may be performed by comparing open loop linear responses against scaled experimental frequency responses as is done in section 2.5.3. In all of this testing, phase information is not affected by the nonlinearities of the AJT and may be compared directly between experimental results and linear model results. The linear model transfer function is given by the AJT equation

$$G(s) = \frac{40000s + 0.004}{s^3 + 381.5s^2 + 40570s + 60000} \quad (2.12)$$

2.3 Reaction Mass Actuators

Another means of space realizable actuation for vibration suppression is implemented in the truss control problem by the use of reaction mass actuators. The RMAs in this test configuration act laterally at the end and midpoint of the truss, although any lateral location along the twenty bays of the truss could have been chosen. Accelerometers are mounted onboard the reaction mass in order to measure the relative acceleration between the truss bay and the reaction mass using the difference between the truss bay acceleration signal and the RMA acceleration signal.

2.3.1 Theoretical Development of the RMA model

The RMA consists of a moveable reaction (or proof) mass, a colocated accelerometer sensor on board the proof mass, a fixed coil to which a current is applied via a power amplifier, and a magnet inside of the coil to which the structure to be controlled is attached, and a supporting flexible suspension system which suspends the magnet in the coil and connects the magnets to the reaction mass.

The theoretical development of a reaction mass actuator model was investigated by Zimmerman, Horner, and Inman [23]. However, their reaction mass actuators were much more complex than the type implemented here, for they had provisions to feedback velocity and position signals to the power signal to the coil and hence create artificial damping and stiffness constants. The RMA here is of a much simpler con-

struction and may be modeled by a constant coefficient spring-mass-damper system. A schematic of the RMA is shown in figure 2.5.

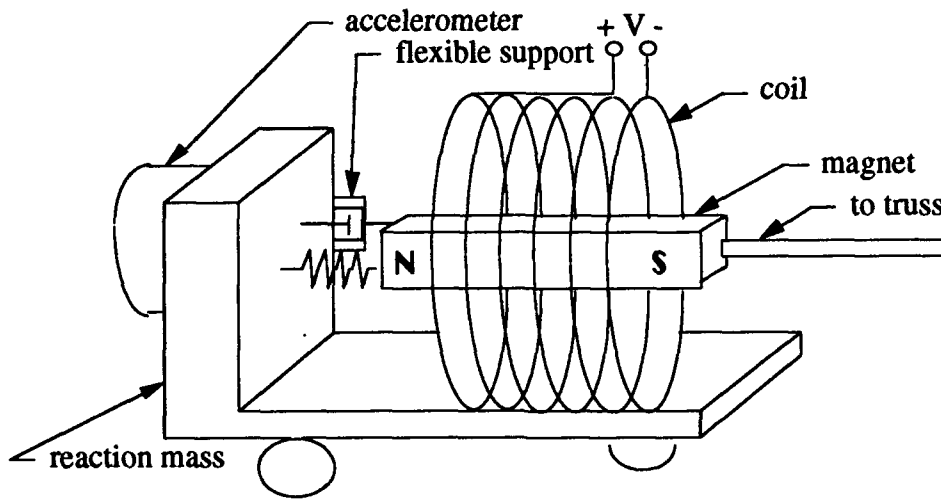


Figure 2.5: RMA schematic

The force produced by the energized coil is proportional to the input current:

$$f_b(t) = BLi(t) \quad (2.13)$$

where B is the magnetic flux density of the magnet which is cut by the coil and L is the length of the wire in the coil as a function of coil diameter and number of turns per unit of coil length. The product of B and L is specific to each RMA and may be defined as the constant G_1 with the units of lbs/amp. The current supplied to the coil is proportional to the input voltage by another constant, G_2 , with the units of volts/amp. Using equation 2.13 and the definitions of the constants G_1 and G_2 the force produced by the coil is given by [23]:

$$f_b(t) = G_1 G_2 v(t) \quad (2.14)$$

where $v(t)$ is the total voltage applied across the coil. If back emf damping is neglected and there is no equilibrium position restoring voltage, then the total voltage across the coil is simply the command voltage $e(t)$. Equation 2.14 becomes:

$$f_b(t) = G_1 G_2 e(t) \quad (2.15)$$

The assumption that back emf is negligible for the RMAs in this paper is valid because the flexible suspension system provides for much greater factor of damping than back emf is capable of generating. However, for an actuator with velocity feedback on the proof mass, back emf would be essential for modeling purposes.

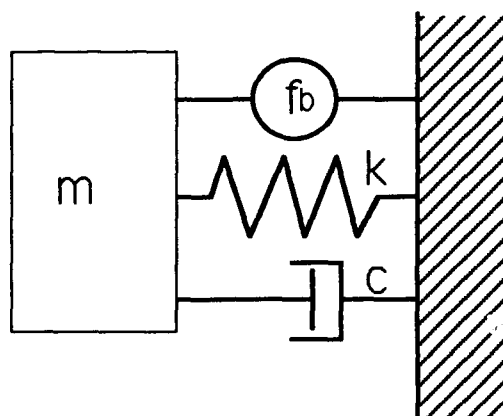


Figure 2.6: RMA simplified system

A spring-mass-damper system representative of the RMA in the test configuration (mounted to a rigid support structure) is shown in figure 2.6. The damping of the flexible support structure may be approximated by a viscous damping constant c . The stiffness of the support structure may likewise be approximated by the linear spring constant k . Summing the forces acting on the reaction mass and applying Newton's second law yields the following relationship:

$$\sum_{mass} F(t) = F_b(t) - c\dot{x}(t) - kx(t) = m\ddot{x}(t) \quad (2.16)$$

Taking the Laplace transform of equation 2.16 (assuming no initial conditions) and applying the results of equation 2.15 results in:

$$F(s) = G_1 G_2 E(s) - csX(s) - kX(s) = ms^2 X(s) \quad (2.17)$$

Equation 2.17 may be rearranged to provide a relationship between input voltage and the output position of the reaction mass:

$$\frac{X(s)}{E(s)} = \frac{G_1 G_2}{ms^2 + cs + k} \quad (2.18)$$

Since $F(s) = ms^2 X(s)$, equation 2.18 may be rewritten to provide a transfer function relating output force to input command voltage. This transfer function is important to test and calibrate the RMA and is well recognized in the literature as the "stand alone" transfer function for a reaction mass actuator [8, 23, 2]. A typical frequency response is shown in figure 2.7.

$$\frac{F(s)}{E(s)} = \frac{G_1 G_2 m s^2}{ms^2 + cs + k} \quad (2.19)$$

When the RMAs are attached to the truss midpoint and endpoint the lateral dynamics of the system must be re-derived to include the dynamics of the truss. This was performed by Barker in his dissertation on control structure interaction [2], and is repeated here from first principles. A diagram of the RMA on a truss lateral attachment node is shown in figure 2.8. The mass of the RMA magnet is assumed to be small and is neglected. For simplicity the truss is modeled as a spring-mass-damper system as well, realizing that from this form it is simple to implement into the MAPMODES finite element code. The MAPMODES code is a finite element model developed by Professor W.L. Hallauer of Virginia Polytechnic Institute and is formally titled *Matrix Algebra Package/Structural MODES*. It is used to model the planar truss in section 2.4.

To realize the equations of motion, a Lagrangian approach is used [14]. The variables are defined in figure 2.8:

$$\mathcal{L} = T - V = \frac{1}{2} m_a \dot{x}_a^2 + \frac{1}{2} m_s \dot{x}_s^2 - \frac{1}{2} k_a (x_a - x_s)^2 - \frac{1}{2} k_s x_s^2 \quad (2.20)$$

For the coordinate x_s :

$$\begin{aligned} \frac{\partial \mathcal{L}}{\partial x_s} &= k_a (x_a - x_s) - k_s x_s \\ \frac{\partial \mathcal{L}}{\partial \dot{x}_s} &= m_s \dot{x}_s \end{aligned}$$

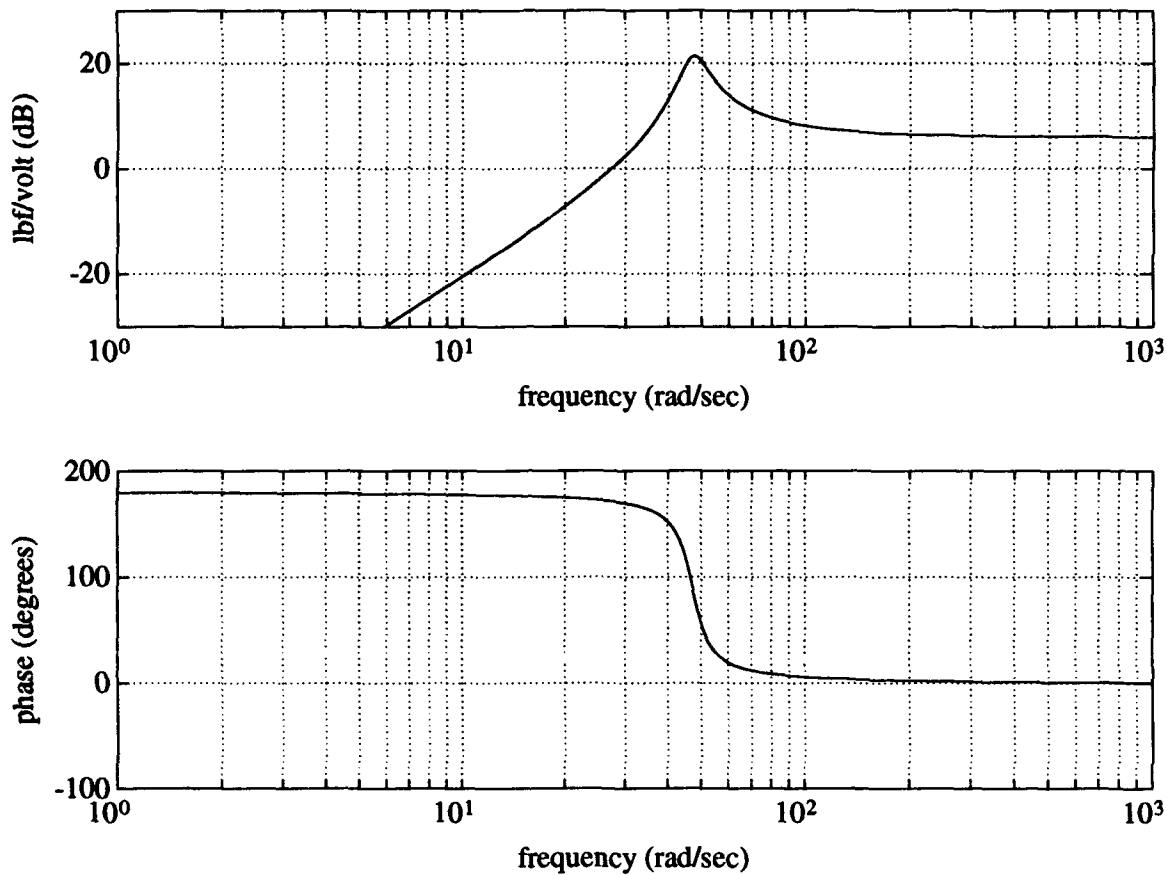


Figure 2.7: Typical RMA 'stand alone' frequency response

$$\begin{aligned} \frac{d}{dt} \frac{\partial \mathcal{L}}{\partial \dot{x}_a} &= m_s \ddot{x}_s \\ Q_{x_s, n.c.} &= -c_s \dot{x}_s + c_a (\dot{x}_a - \dot{x}_s) + f_b(t) \end{aligned}$$

For the coordinate x_a :

$$\begin{aligned} \frac{\partial \mathcal{L}}{\partial x_a} &= -k_a (x_a - x_s) \\ \frac{\partial \mathcal{L}}{\partial \dot{x}_a} &= m_a \dot{x}_a \end{aligned}$$

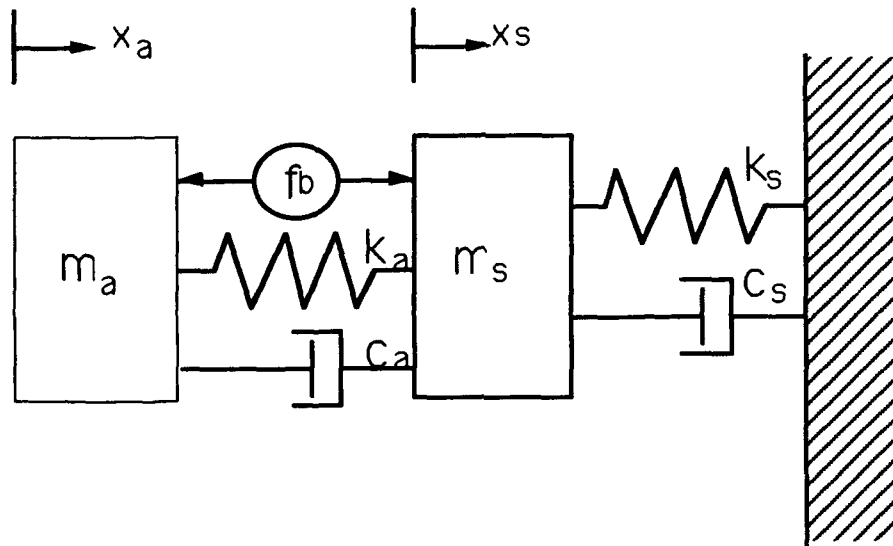


Figure 2.8: RMA aboard truss station

$$\frac{d}{dt} \frac{\partial \mathcal{L}}{\partial \dot{x}_a} = m_a \ddot{x}_a$$

$$Q_{x_a n.c} = -c_a(\dot{x}_a - \dot{x}_s) - f_b(t)$$

The resulting equations of motion are:

$$\frac{d}{dt} \frac{\partial \mathcal{L}}{\partial \dot{q}_r} - \frac{\partial \mathcal{L}}{\partial q_r} = Q_{r n.c.} \quad (2.21)$$

$$m_s \ddot{x}_s - k_a(x_a - x_s) + k_s x_s = -c_s \dot{x}_s + c_a(\dot{x}_a - \dot{x}_s) + f_b(t) \quad (2.22)$$

$$m_a \ddot{x}_a + k_a(x_a - x_s) = -c_a(\dot{x}_a - \dot{x}_s) - f_b(t) \quad (2.23)$$

The equations of motions may be rewritten as:

$$m_s \ddot{x}_s + c_s \dot{x}_s - c_a(\dot{x}_a - \dot{x}_s) - k_a(x_a - x_s) + k_s x_s = +f_b(t) \quad (2.24)$$

$$m_a \ddot{x}_a + c_a(\dot{x}_a - \dot{x}_s) + k_a(x_a - x_s) = -f_b(t) \quad (2.25)$$

Which lend themselves to the matrix form first shown by Barker [2]:

$$\begin{bmatrix} m_s & 0 \\ 0 & m_a \end{bmatrix} \begin{bmatrix} \ddot{x}_s \\ \ddot{x}_a \end{bmatrix} + \begin{bmatrix} c_s + c_a & -c_a \\ -c_a & c_a \end{bmatrix} \begin{bmatrix} \dot{x}_s \\ \dot{x}_a \end{bmatrix} + \begin{bmatrix} k_s + k_a & -k_a \\ -k_a & k_a \end{bmatrix} \begin{bmatrix} x_s \\ x_a \end{bmatrix} = \begin{bmatrix} 1 \\ -1 \end{bmatrix} f_b \quad (2.26)$$

In order to implement the above matrix equation into the MAPMODES finite element program it is necessary to first designate a relative coordinate $x_{as} = x_a - x_s$. This coordinate transformation removes the dynamic coupling in equation 2.26 in favor of an inertially coupled mass matrix. There are two advantages to presenting the system in this manner. One is the ability to easily incorporate the matrices into the finite element code. Secondly, the eigenvalue damping appears in the diagonal damping matrix. This gives us the hint that the relative velocity between the reaction mass and the structure will be an important element of our control strategies. Equation 2.26 written in terms of the relative coordinate x_{as} is:

$$\begin{bmatrix} m_s + m_a & m_a \\ m_a & m_a \end{bmatrix} \begin{bmatrix} \ddot{x}_s \\ \ddot{x}_{as} \end{bmatrix} + \begin{bmatrix} c_s & 0 \\ 0 & c_a \end{bmatrix} \begin{bmatrix} \dot{x}_s \\ \dot{x}_{as} \end{bmatrix} + \begin{bmatrix} k_s & 0 \\ 0 & k_a \end{bmatrix} \begin{bmatrix} x_s \\ x_{as} \end{bmatrix} = \begin{bmatrix} 0 \\ -1 \end{bmatrix} f_b \quad (2.27)$$

Using equation 2.27 the RMA theoretical model may be implemented directly into the finite element code. Verification of the model is the next task.

2.3.2 RMA Experimental Testing and Linear Model Approximation

The RMAs to be connected to the truss tip and midpoint were individually characterized in the specially fabricated test stand shown in figure 2.9. The RMA is in the 'stand alone' configuration. The RMA to be calibrated is attached via a metal stinger to a force gage which is affixed to a rigid wall, and rides upon the ball bearings it would normally ride upon when attached to the structure. The ball bearings reside in machined grooves to preserve RMA alignment. The stinger is attached to the RMA's magnet (which is suspended in the coil by the flexible suspension system), connecting

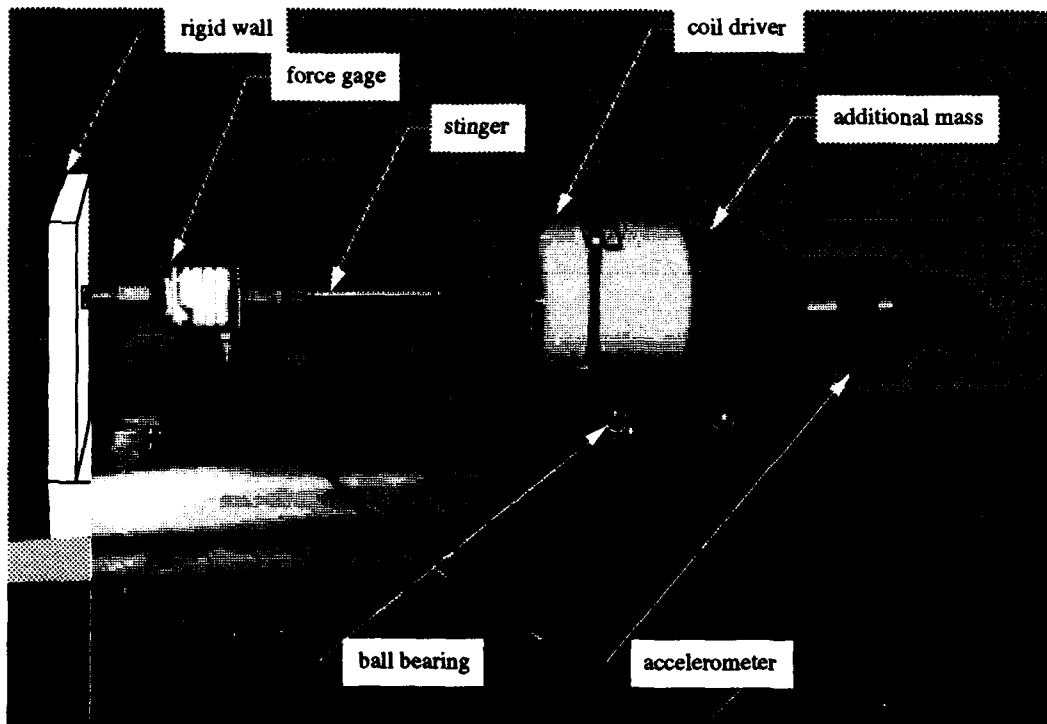


Figure 2.9: RMA in the 'stand alone' experimental test configuration

the magnet to a force gage designed to measure axial force. The stinger is equipped with a ball socket joint at each end to insure that the axial alignment of the RMA on its ball bearings is not affected by small rotary effects of the truss station. Although not necessary on the test stand, the stingers are considered to be an integral part of the RMA and are included in the characterization. Using the dynamic signal analyzer, a swept sine characterization was performed utilizing the signal input to the RMA amplifiers while the force gage measured the output. The amplifier was set to a gain of 2. The swept sine program adjusted the signal input to maintain an output force level of approximately 0.5 lbf over the entire frequency range of the test without exceeding 2 lbf to ensure accurate measurement without overstraining the force gage.

Figures 2.10 and 2.11 show the magnitude and phase plots of the tip RMA and midpoint RMA, respectively. On the plots are the experimental frequency responses as well as the theoretical models for the RMAs. The theoretical models are augmented

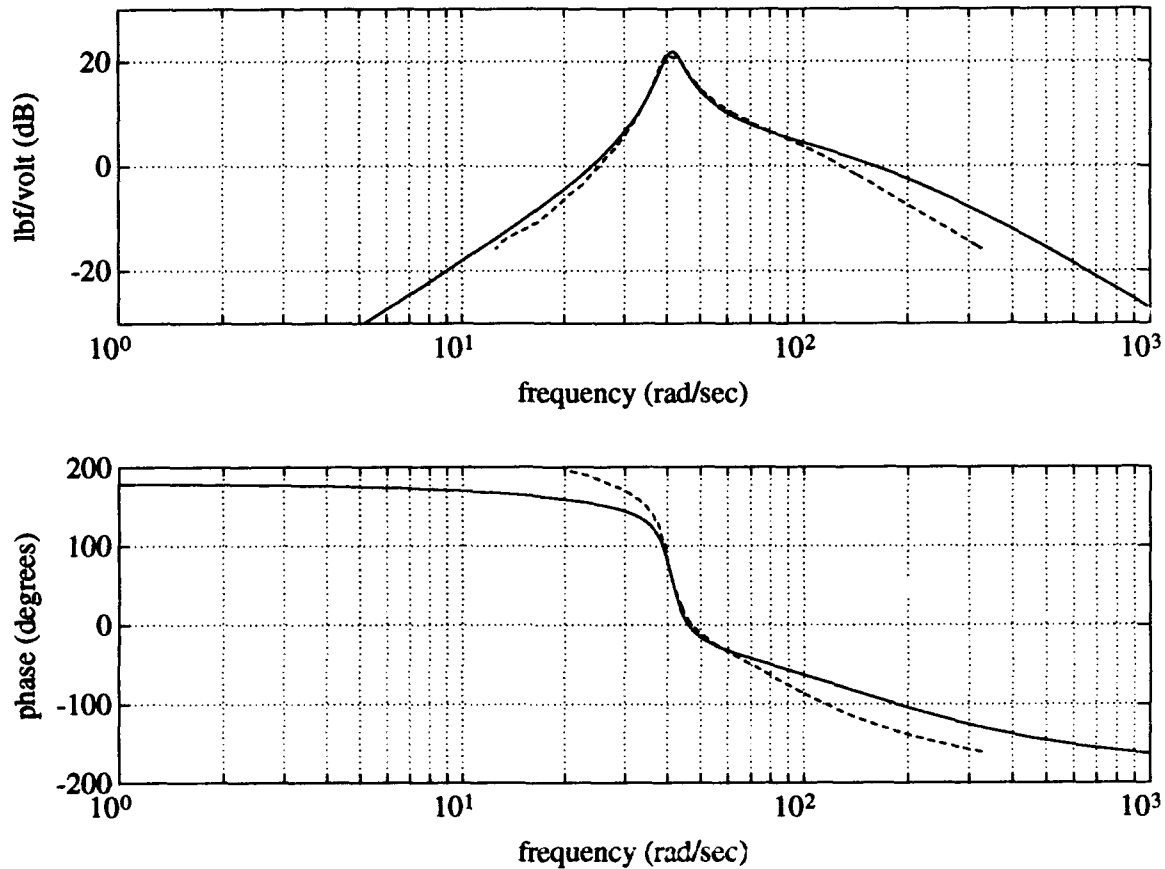


Figure 2.10: Tip RMA: theoretical (dashed), experimental (solid)

with a second order filter representative of the force gage in section 1.3.7. Values for the mass, damping, and stiffness coefficients in the theoretical models are chosen to reflect the experimental data. Close agreement between the RMA models and the experimental frequency responses is achieved below 100 rad/sec, the bandwidth of the force gage used in the device characterization. This validates the assumptions and modeling of section 2.3.1 of the RMA in the stand alone configuration. The final block diagram is shown in figure 2.12. The experimentally determined coefficients are listed in table 2.1.

With an accurate RMA model now defined, attention may be turned to the plant for this experiment, the 20-bay planar truss.

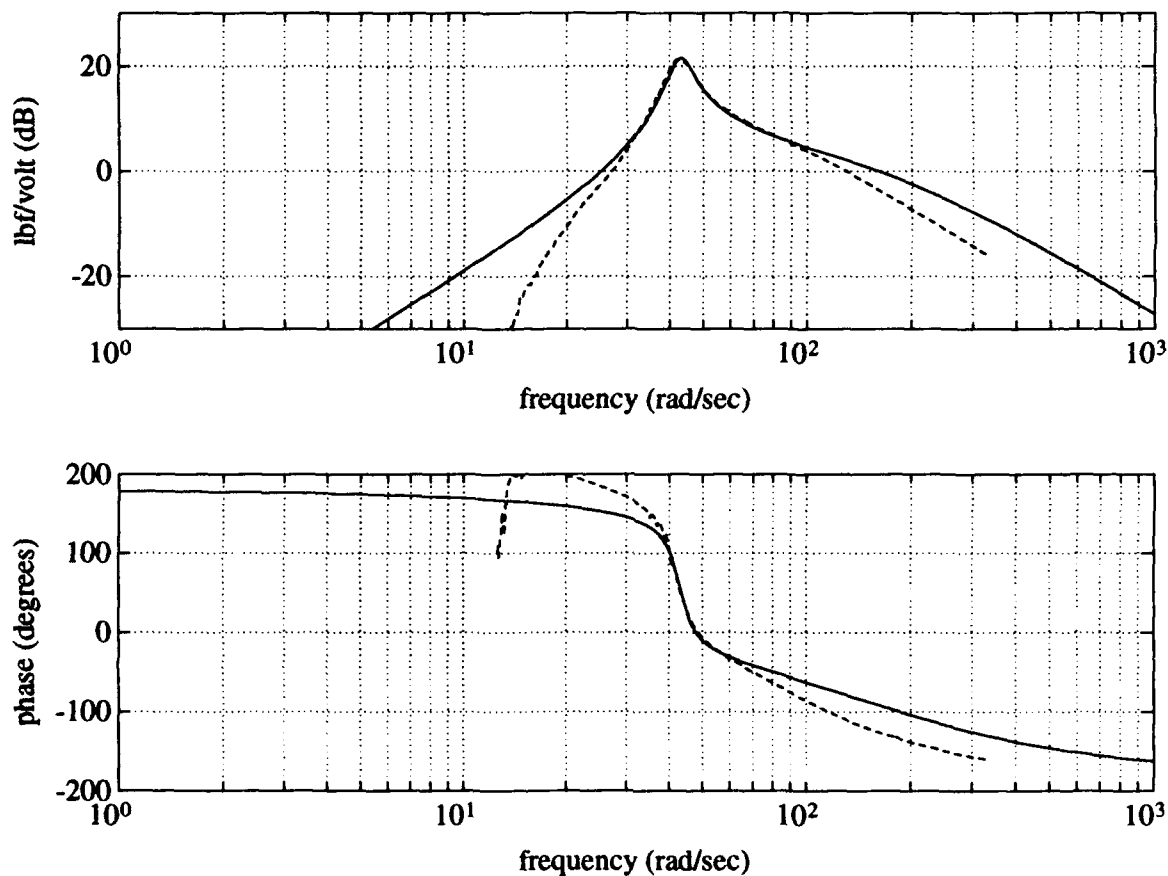


Figure 2.11: Midpoint RMA: theoretical (dashed), experimental (solid)

2.4 Truss Modeling

The dynamics of truss structures are well understood [14], and this experiment utilizes the MAPMODES finite element code to define a linear state space model for the truss developed at USAFA [8] and modified by Barker and Schulthess [2, 17]. In his master's thesis, Schulthess reports the theoretical and experimental validation of the finite element model for the UWAA planar truss used in this controls experiment.

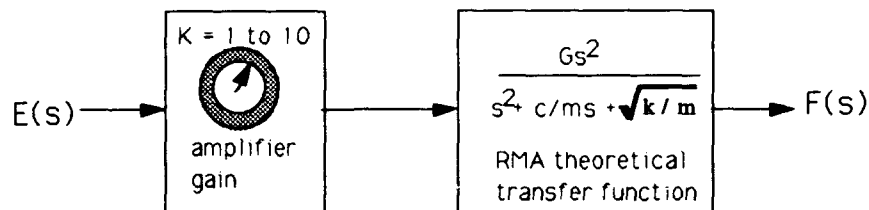


Figure 2.12: RMA block diagram

Table 2.1: Experimentally determined values for RMA models

constant	RMA tip	RMA midpoint
G	1 lbf/volt	1 lbf/volt
m	0.0097255 lbf $\frac{sec^2}{in}$	0.0097542 lbf $\frac{sec^2}{in}$
c	0.060 lbf sec/in	0.065 lbf sec/in
k	16.5 lbf/in	18.0 lbf/in
ω_n	41.12 rad/sec	42.96 rad/sec
ζ	0.0750	0.0776

2.4.1 Truss Theory

The planar truss may be modeled as a simple cantilevered Euler-Bernoulli beam to provide an upper limit on the natural frequencies of the truss and the approximate shapes of the bending modes. Assuming constant bending stiffness EI and constant mass per unit length m the resulting differential equation is [14, 17]:

$$\frac{\partial^4 y(x, t)}{\partial x^4} + \frac{m}{EI} \frac{\partial^2 y(x, t)}{\partial t^2} = 0 \quad (2.28)$$

This equation assumes plane sections remain planar, thus neglecting shear and rotary effects, as is the case for the planar truss testbed where analysis is limited to only the first four lateral bending modes. Limiting the truss analysis to the first four bending modes is not arbitrary, but a result of the use of the low-bandwidth AJTs

to excite the structure. Assuming a separable solution and applying the geometric and natural boundary conditions for the cantilevered Euler-Bernoulli beam yields the modeshape equations:

$$Y_n(x) = A_n[(\sin k\sqrt{w_n}L - \sinh k\sqrt{w_n}L)(\sin k\sqrt{w_n}x - \sinh k\sqrt{w_n}x) + (\cos k\sqrt{w_n}L + \cosh k\sqrt{w_n}L)(\cos k\sqrt{w_n}x - \cos k\sqrt{w_n}x)]$$

$$n = 1, 2, \dots, \infty \quad (2.29)$$

where

$$k^4 = \frac{m}{EI} \quad (2.30)$$

and $Y_n(x)$ is the modeshape of arbitrary amplitude A_n for a beam of length L with natural frequencies defined by the equation:

$$\cosh(w_n^2 kL) \cos(w_n^2 kL) = -1 \quad (2.31)$$

2.4.2 Truss Linear Model

A low order linear model for the truss was obtained by using the MAPMODES program and the model reduction technique highlighted by Schulthess in his master's thesis [17]. A brief outline of the procedure is included here for completeness.

The MAPMODES program solves the generalized 63 degree of freedom FEM free vibration problem

$$[M]\ddot{q} + [K]q = 0 \quad (2.32)$$

yielding the eigenvalues of the full order system. Since only the first four bending modes of the truss system were required for this system (as they are the only lateral modes of the system within the frequency range of the primary means of truss disturbance, the AJTs), modal truncation was applied and a damping coefficient was assigned for each mode (the damping coefficients' experimentally determined values are reported in section 2.5.2). The final reduced order system model including viscous damping (assuming no cross-coupling in the damping matrix) is [17]

$$[M_r]\ddot{q}_r + [C_r]\dot{q}_r + [K_r]q_r = f_r \quad (2.33)$$

Defining a state space model is possible by recognizing that equation 2.33 may be rewritten as:

$$\ddot{q}_r = -M_r^{-1}C_r\dot{q}_r - M_r^{-1}K_rq_r + M_r^{-1}f_r \quad (2.34)$$

The state space model is therefore of the form (with I_4 the 4 x 4 identity matrix and O_4 the 4 x 4 null matrix):

$$\frac{d}{dt} \begin{bmatrix} \dot{q}_r \\ q_r \end{bmatrix} = \begin{bmatrix} -M_r^{-1}C_r & -M_r^{-1}K_r \\ I_4 & 0_4 \end{bmatrix} \begin{bmatrix} \dot{q}_r \\ q_r \end{bmatrix} + \begin{bmatrix} M_r^{-1} \\ O_4 \end{bmatrix} f_r \quad (2.35)$$

Where q_r was chosen, in the case of the model with the four retained bending modes, simply the displacement of the tip, 3/4 point, mid point, and 1/4 point, such that the states were defined as

$$x = \begin{pmatrix} x_1 \\ x_2 \\ x_3 \\ x_4 \\ x_5 \\ x_6 \\ x_7 \\ x_8 \end{pmatrix} = \begin{pmatrix} \dot{q}_{tip} \\ \dot{q}_{3/4} \\ \dot{q}_{mid} \\ \dot{q}_{1/4} \\ q_{tip} \\ q_{3/4} \\ q_{mid} \\ q_{1/4} \end{pmatrix} \quad (2.36)$$

and the inputs chosen only to include the force input at the truss tip and midpoint locations such that

$$u = \begin{pmatrix} u_1 \\ u_2 \end{pmatrix} = \begin{pmatrix} f_{tip} \\ f_{mid} \end{pmatrix} \quad (2.37)$$

The state space equation then has the form of

$$\dot{x} = A_8x + B_8u \quad (2.38)$$

The C and D matrices may then be chosen by the user to output the truss acceleration, velocity, and displacement at the chosen truss locations. The numerical values which constitute the A and B matrix for the open loop truss model are presented in section A.1.

Table 2.2: Planar truss bending mode frequencies

Mode	Modal Frequencies (rad/sec)		
	Beam Theory	FEM	Truss Hardware
1	9.60	9.48	9.30
2	60.44	5.59	55.80
3	169.14	146.40	146.52
4	331.19	260.12	262.32

2.5 Open Loop Truss Model Validation

Open loop testing of the planar truss serves several purposes. First, it shows the agreement between the both theoretical and finite element models to the existing hardware, thus verifying the modeling techniques. Second, it serves as a basis to fine tune the linear truss model to reflect the discrepancies between the theoretical calculations and hardware test results. Finally, there is no analytical method for determining the modal damping of the truss so modal damping coefficients had to be determined experimentally. The truss underwent three series of tests used to confirm the modeling validity and help with the tuning of the model. The tests were open loop acquisition of the mode shapes, open loop modal free decay time responses, and frequency responses of mid and tip accelerations to tip excitation via the AJTs.

2.5.1 Mode Shapes

Mode shapes were taken by driving the truss at its first three bending modes using the tip mounted AJTs and measuring the lateral displacement at each of the twenty truss bays. The fourth mode created displacements below the threshold of the test equipment, consequently it was not measured for mode shape verification. The natural frequencies for the truss bending modes¹ are shown in table 2.2. The mode shapes were normalized to the point of greatest displacement and graphed along with the

¹ The experimentally determined natural frequencies for the first four bending modes of the USAFA planar truss were reported to be 9.80, 62.8, 155.2, and 270.1 rad/sec, slightly higher than the experimental values shown in table 2.2 [8].

theoretical beam theory and finite element model predictions. Stiffness constants in the finite element/linear truss model were changed to better reflect the experimental data natural frequencies, consequently only the final finite element model results are shown. The results are depicted in figure 2.13 for the first four modes shapes in relation to the twenty stations of the planar truss.

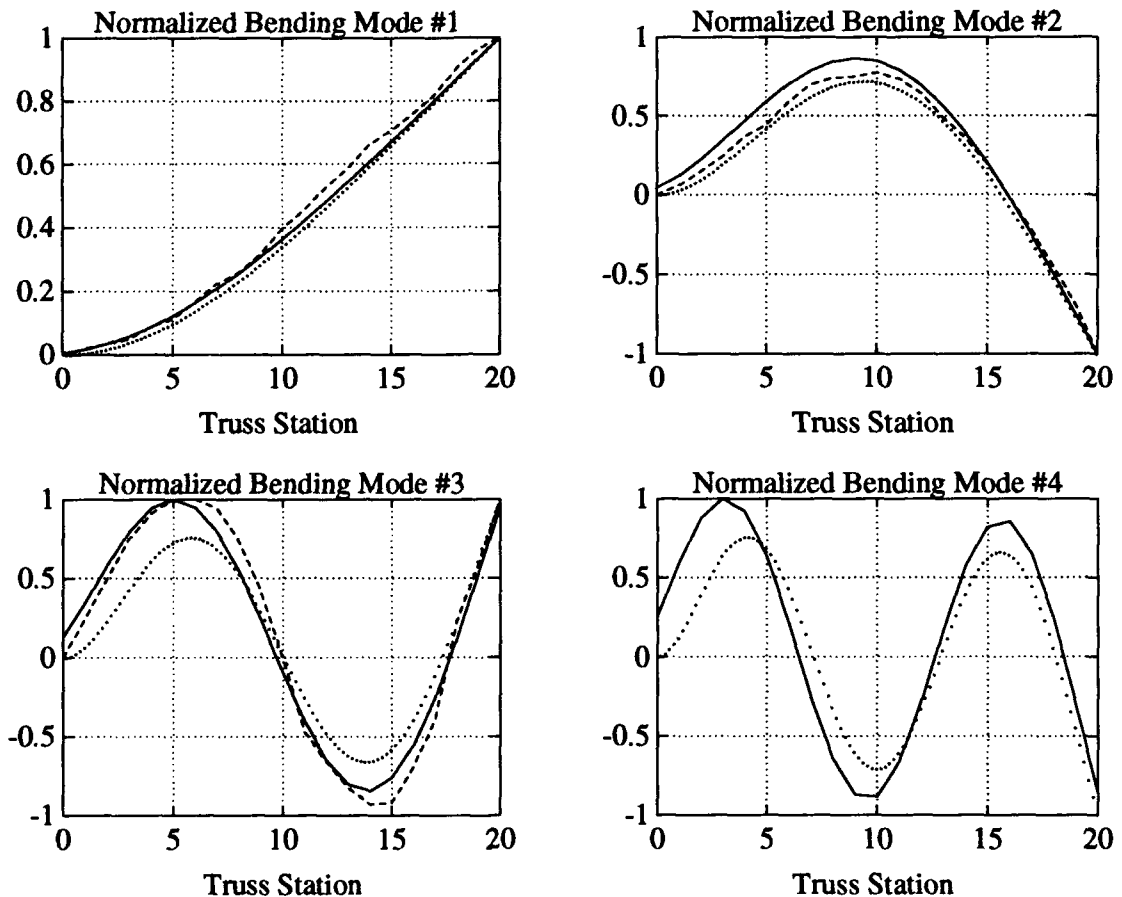


Figure 2.13: Normalized bending mode shapes: beam theory (dotted), experimental (dashed), and FEM (solid)

2.5.2 Free Decay of Bending Modes

After the mode shapes were recorded, the next step was to determine the equivalent viscous damping coefficient for each mode. A logarithmic decrement procedure was

applied to obtain the viscous damping coefficients. The method is described by Thompson [20] and used to obtain damping coefficients for the USAFA truss [18]. It is outlined here for completeness.

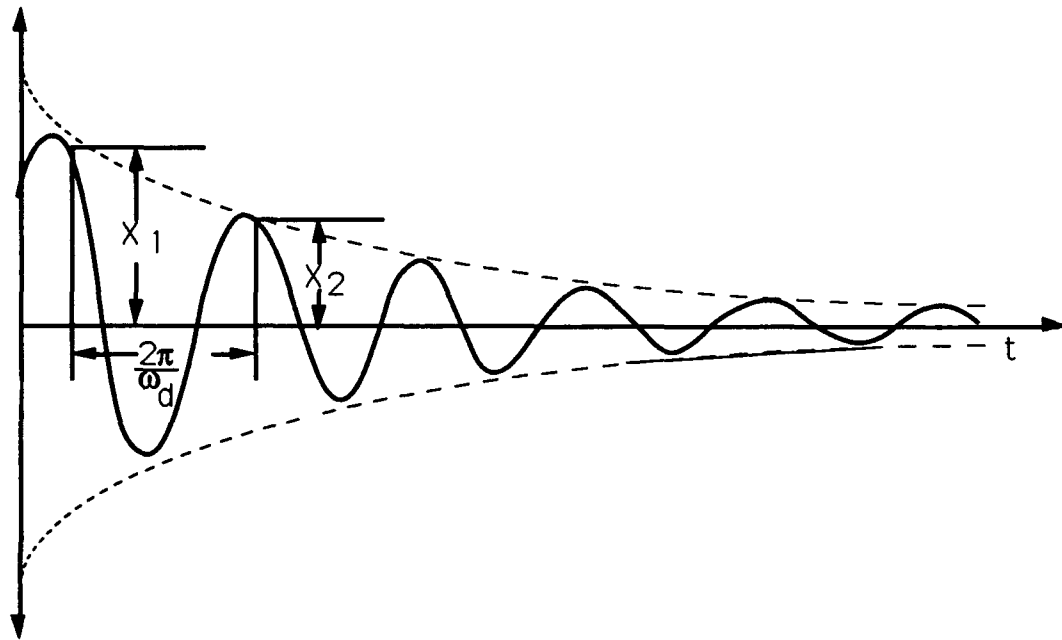


Figure 2.14: Logarithmic decrement

A viscously damped second order free vibration is shown in figure 2.14 and has a solution of the form:

$$x(t) = A \exp^{-\zeta \omega_n t} \sin(\sqrt{1 - \zeta^2} \omega_n t + \phi) \quad (2.39)$$

The logarithmic decrement δ is defined as the natural logarithm of the ratio of any two successive amplitudes [20]. It is formally expressed as:

$$\delta = \ln \frac{x_1}{x_2} = \ln \frac{\exp^{-\zeta \omega_n t_1} \sin(\sqrt{1 - \zeta^2} \omega_n t_1 + \phi)}{\exp^{-\zeta \omega_n (t_1 + \frac{2\pi}{\omega_d})} \sin(\sqrt{1 - \zeta^2} \omega_n (t_1 + \frac{2\pi}{\omega_d}) + \phi)} \quad (2.40)$$

The sine terms are equal for multiples of $\frac{2\pi}{\omega_d}$, therefore equation 2.40 reduces to:

$$\delta = \ln \frac{\exp^{-\zeta \omega_n t_1}}{\exp^{-\zeta \omega_n (t_1 + \frac{2\pi}{\omega_d})}} \quad (2.41)$$

Table 2.3: Experimentally determined damping ratios ζ

Mode	(ζ_r)
1	0.0068
2	0.0042
3	0.0090
4	0.0160

which may be simplified to yield:

$$\delta = \ln \exp^{\zeta \omega_n \frac{2\pi}{\omega_d}} = \zeta \omega_n \frac{2\pi}{\omega_d} \quad (2.42)$$

Given that the damped natural frequency ω_d is equal to $\omega_n \sqrt{1 - \zeta^2}$ [16], equation 2.42 becomes

$$\delta = \frac{2\pi\zeta}{\sqrt{1 - \zeta^2}} \quad (2.43)$$

The damping ratio may then be explicitly defined as

$$\zeta = \frac{\delta}{\sqrt{4\pi^2 + \delta^2}} \quad (2.44)$$

For lightly damped structures the logarithmic decrement between peaks will be small and the expression

$$\zeta = \frac{\delta}{2\pi} \quad (2.45)$$

may be used with little loss of accuracy. A similar approach for peaks separated by n cycles will show that the logarithmic decrement may be expressed as [18]:

$$\delta = \frac{1}{n} \ln \frac{x_1}{x_{n+1}} \quad (2.46)$$

The logarithmic decrement for each mode is determined experimentally by driving the planar truss at its resonant bending frequencies with the AJTs until a full range of motion is recorded. Then, the AJTs are shut off and the truss is allowed to free decay until no motion is present. For the first mode the truss endpoint was

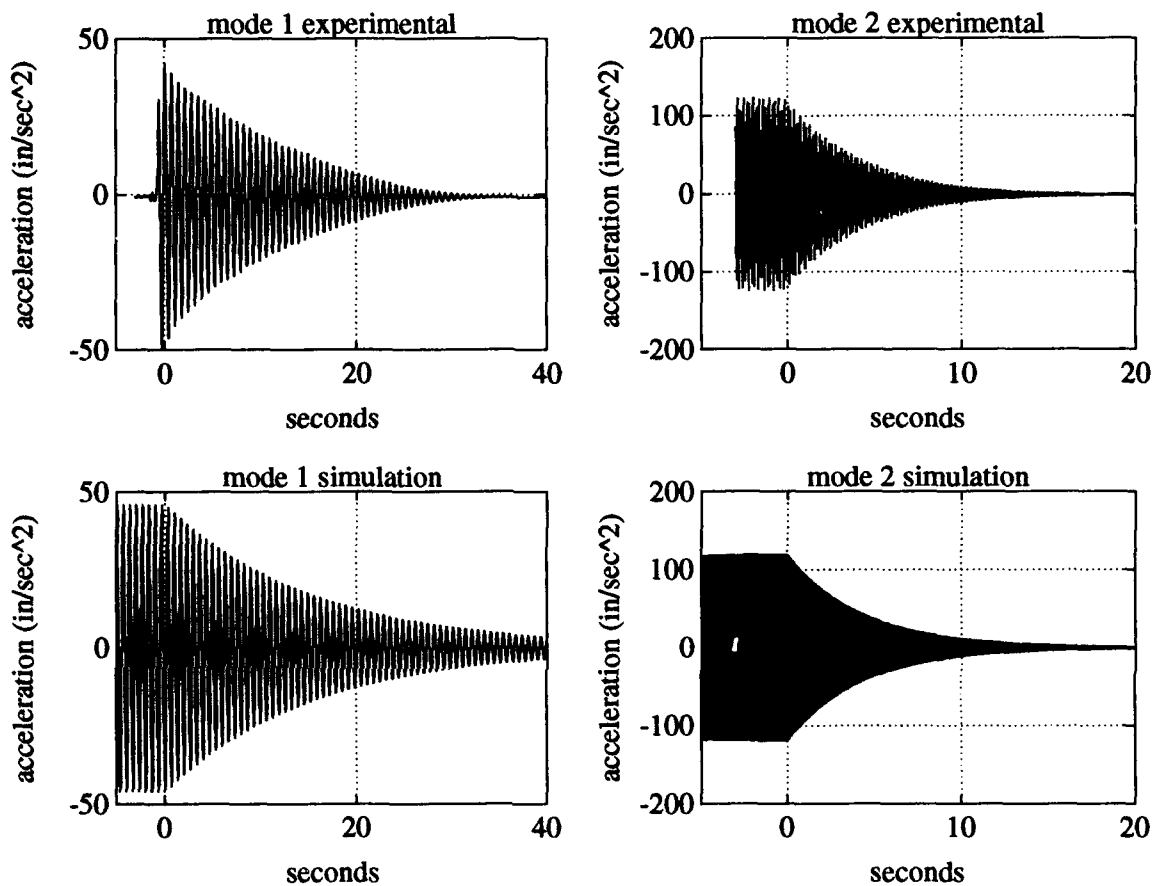


Figure 2.15: Tip free decay: actual (top), linear model (bottom)

displaced laterally .5 inches and released since full displacement of the first mode by the AJTs could cause the truss to shake off of its ball bearing supports. The acceleration at the truss tip and midpoint is measured during the decay cycle. Although the damping coefficient ζ was derived for the displacement signal, the acceleration signal will decay in the same logarithmic proportion as the displacement signal for low frequency, lightly damped modal vibrations and thus is sufficient for determining approximate damping ratios for the truss modes. To realize an average logarithmic decrement δ the peaks measured are at 90 percent and 10 percent of full displacement amplitude and formula 2.46 is applied where n cycles are counted between the two measurement points. The truss midpoint and tip values are averaged as well for all

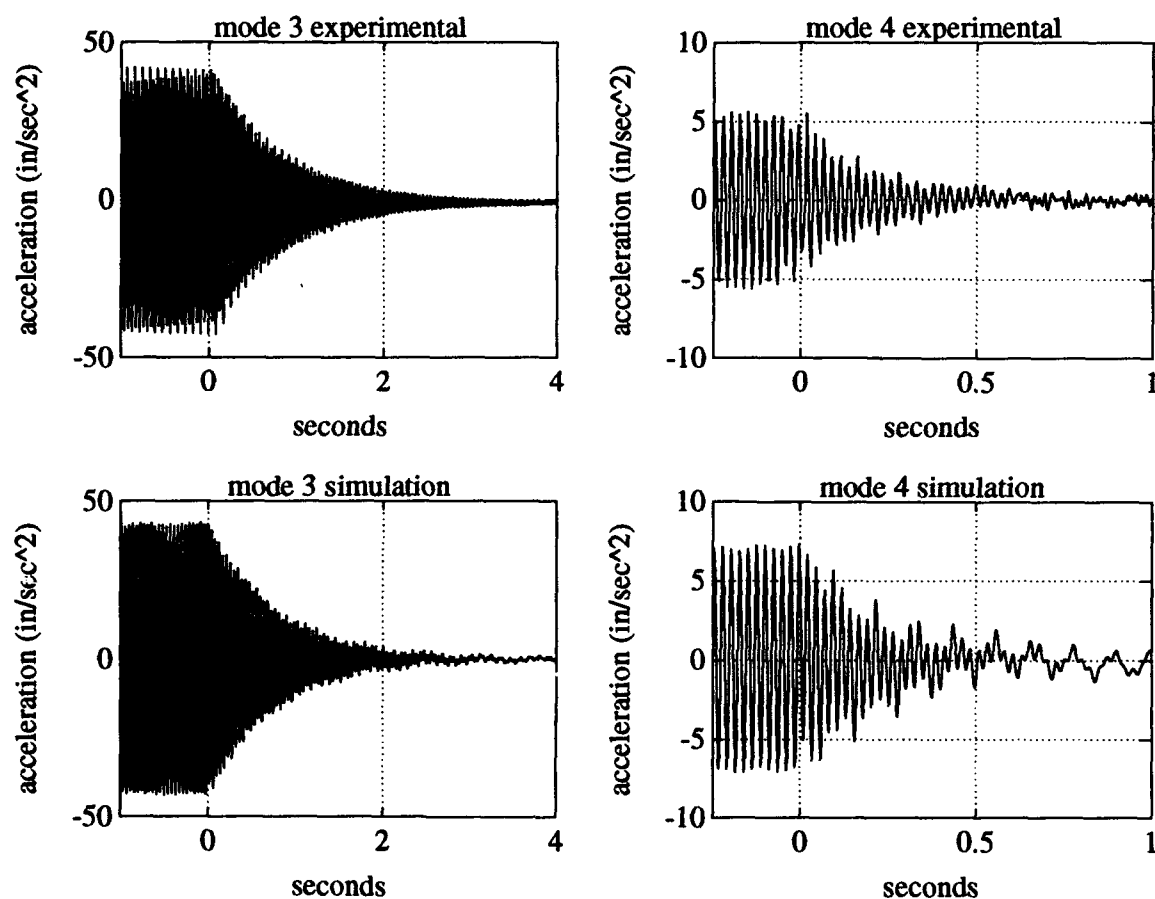


Figure 2.16: Tip free decay: actual (top), linear model (bottom)

modes except the third where the midpoint lies on a nodal point (see figure 2.13). The results incorporated into the model² are shown in table 2.3. The free decay

² The damping ratios of the USAFA truss for the first four modes were determined to be 0.011, 0.0022, 0.00278, and 0.00632 [18]. The modal damping of the USAFA truss was lower for all modes except the first mode, which is about 60% higher for the USAFA truss compared to the UWAA truss. The damping ratios for the UWAA truss were calculated before the final test instrumentation and hardware was placed upon the truss so that theoretical calculations and design could be performed. Later testing of the truss indicates that a value of damping in the first mode is closer to 0.012, which closely reflects the Academy data. Although 0.0068 is the value used throughout this paper, special mention will be made to compare the damping to the more recent data acquisition. The experimental data in figure 2.15 has been changed to reflect the more

plots of the experiment data and the linear FEM are shown in figures 2.15 and 2.16. It is important to note that this development assumes only linear viscous damping, and therefore is subject to errors caused by non-linear Coulomb (dry-friction) damping and structural (hysteretic) damping which comprise the main energy dissipation features of the planar truss.

2.5.3 Open loop frequency response

The open loop frequency response of the truss model is obtained using the tip mounted AJTs to excite the structure. The swept sine dynamic signal analyzer package is used with an input voltage of plus and minus one volt. The acceleration signal at the tip of the truss is measured. A frequency response of the linear model of the truss augmented with the linear AJT models is also calculated for comparison. The results are shown in figure 2.17. The results show a very close agreement in the overall shape of the magnitude plot, especially as to the locations of the poles and zeros. This further confirms our assumptions made when adding damping to the model. The phase of the linear model drops more quickly than the experimental data—this is due to the model of the AJTs and is not a problem with the linear truss FEM. The bandwidth of the AJTs may be clearly seen, as the phase and magnitude of the truss plummet at 120 rad/sec in the experimental data, a phenomenon reflected by the linear model which rolls off at about 40 dB/decade and seeks 360 degrees of phase lag.

With the truss and actuator models thus rigorously verified, we may now turn our attention to the control problem of vibration suppression and expect good agreement between theoretical design and actual experimental results.

recent data. That explains the discrepancy between the simulation and the experimental results.

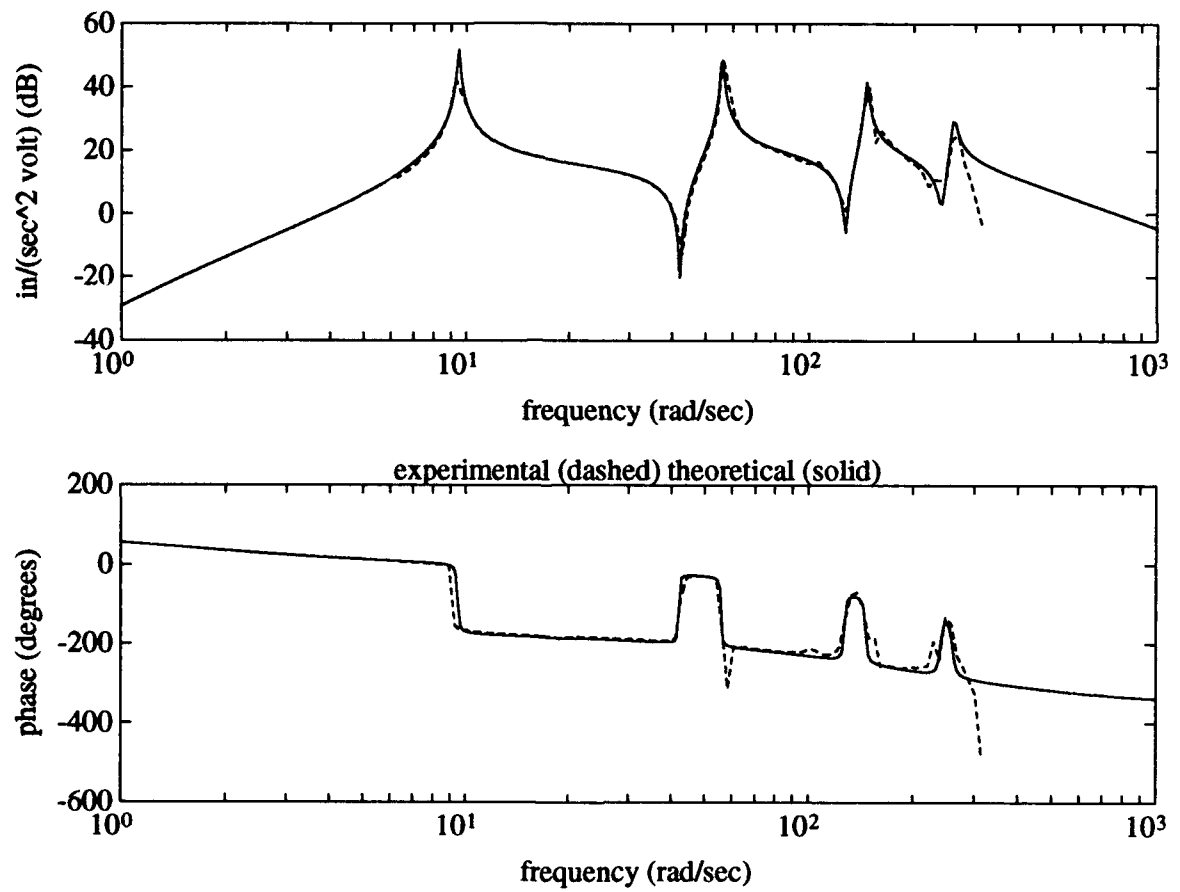


Figure 2.17: Open loop frequency response

Chapter 3

CLASSICAL CONTROL TECHNIQUES FOR VIBRATION SUPPRESSION

3.1 Overview

Design of a classical controller using the available means of actuation to control structural vibration was the primary goal of this thesis. Velocity feedback controllers of the type used at the Air Force Academy are presented here, complete with discussions of the theoretical basis of using velocity control.

3.2 Velocity Feedback to the AJTs

Velocity feedback for vibration suppression has long been recognized as a primary means of achieving higher damping ratios in lightly damped systems. Zimmerman applied velocity feedback to damp the transverse (bending) modes of a 0.654m cantilever beam with a reaction mass actuator [23]. The USAFA truss was controlled using velocity feedback to both RMAs and AJTs [8]. It is worthwhile to explore some of the guarantees and shortcomings of velocity feedback, and to report test results performed on the UWAA planar truss.

3.2.1 The Theory of Velocity Feedback

Consider a spring-mass-damper system with an available forcing function such as the reaction mass actuator in figure 2.5. The system has been shown to be modeled by the differential equation:

$$m_a \ddot{x} + c_a \dot{x} + k_a x = f_b(t) \quad (3.1)$$

Control of the mass is easily achieved if the velocity signal is present for feedback to the force generator (in the case of the RMA, feedback to the coil's amplifier). As shown by Inman and others [10], the feedback is of the form of $-KG\dot{x}$ where G is the

gain constant of the RMA and K is the amplifier gain. Dropping the subscripts from equation 3.1 and letting $KG = g$ the differential equation for the system undergoing feedback is:

$$m\ddot{x} + c\dot{x} + kx = -g\dot{x} \quad (3.2)$$

Rewriting equation 3.2 in standard second order form [10]:

$$\ddot{x} + \frac{2\zeta\omega_n}{m}\dot{x} + \omega_n^2 x = 0 \quad (3.3)$$

Equation 3.2 may be rewritten as:

$$\ddot{x} + \frac{c+g}{m}\dot{x} + \frac{k}{m}x = 0 \quad (3.4)$$

where the natural frequency is $\omega_n = \sqrt{k/m}$ and the damping ratio is $\zeta = (c + g)/2\sqrt{k/m}$. We see that for any amplifier gain $KG = g$ negative velocity feedback will result in a stable system since k , c , and m are all positive values.

Although this is a simple example, it illustrates the advantage of velocity feedback. For a reaction-less actuator without any lag in its application of force, any velocity feedback gain will serve to increase the stability of the system to which it is applied. This is the main impetus behind using velocity feedback to the AJTs for vibration suppression.

3.2.2 Approximate Integrator for Velocity Feedback

To achieve velocity feedback, a velocity signal is obviously required. On the UW planar truss in the current configuration the accelerometers are colocated with the AJTs at the truss tip and midpoints. These sensors measure the lateral acceleration of the truss at their respective locations. To achieve a velocity signal, the first guess would be to try to integrate the acceleration signal directly. There are problems with this set-up as any slight bias in the system while the planar truss is in the unexcited, resting state would be integrated until a sufficient level of voltage is built up, tripping the switching transistor circuit of the AJTs and forcing an unwarranted, destabilizing firing of the AJT associated with the runaway bias signal. Therefore, some feedback is desirable to keep unwanted bias from triggering the system at rest.

The USAFA research team used an approximate integrator of the type used by the Martin Marietta Astronautics Group [8]. The approximate integrator is modeled by the differential equation:

$$\ddot{e}_{vi} + \Omega \dot{e}_{vi} + \Omega^2 e_{vi} = \frac{1}{RC} e_{ai} \quad (3.5)$$

where e_{ai} is the accelerometer signal, e_{vi} is the velocity signal, Ω is a user constant, and RC is a user specified time constant. Taking the Laplace transform of equation 3.5

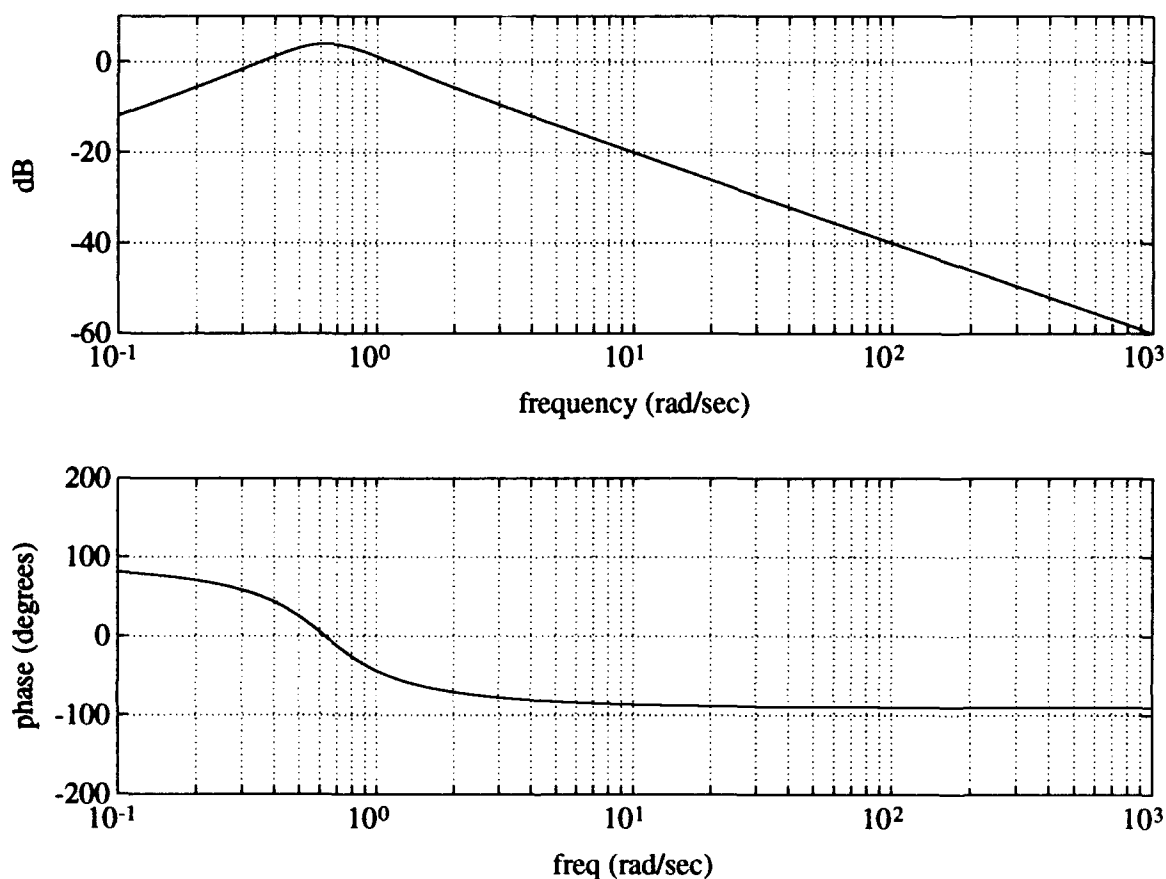


Figure 3.1: Approximate integrator theoretical frequency response

yields

$$s^2 E(s)_{vi} + s\Omega E(s)_{vi} + \Omega^2 E(s)_{vi} = s \frac{1}{RC} E(s)_{ai} \quad (3.6)$$

which may be put into the transfer function form:

$$G(s) = \frac{E(s)_{vi}}{E(s)_{ai}} = \frac{s/RC}{s^2 + \Omega s + \Omega^2} \quad (3.7)$$

The frequency response of the transfer function $G(s)$ is shown in figure 3.1 for constants of $RC = 1$ and $\Omega = 0.628$. The resulting frequency response is very close to that of an ideal integrator's frequency response for frequencies above 10 rad/sec.

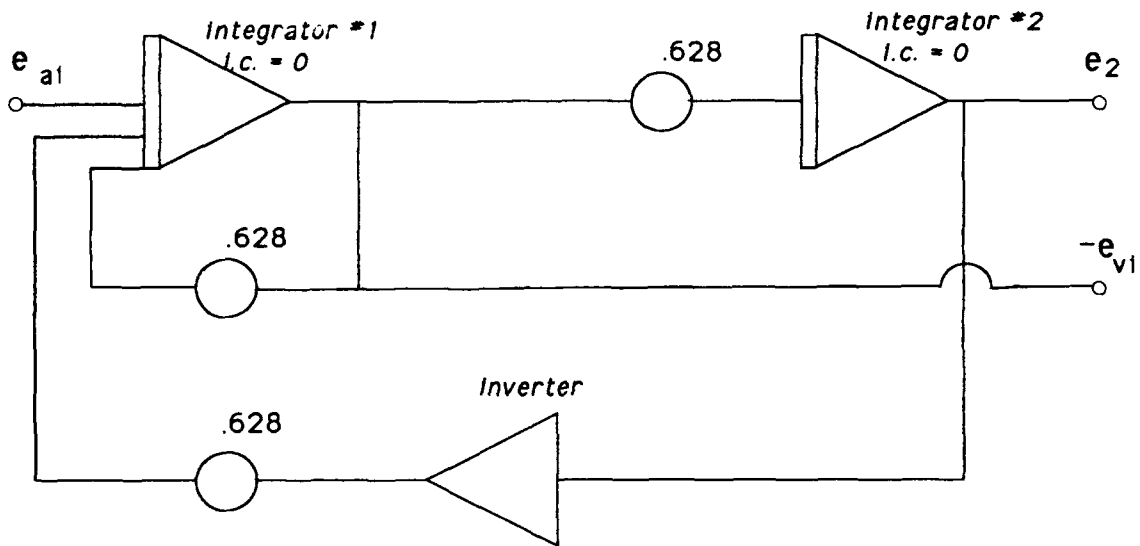


Figure 3.2: Approximate integrator analog computer implementation

To implement equation 3.5 a state space representation is more convenient to use. The states may be defined by the following equations [8]:

$$\begin{aligned} \dot{e}_1 &= -\Omega e_1 + \Omega + \frac{1}{RC} e_{ai} \\ \text{where } \dot{e}_2 &= -\Omega e_2 \\ \text{or } e_2 &= -\Omega \int e_1 dt + i.c. \end{aligned} \quad (3.8)$$

The state space equations which result are:

$$\begin{bmatrix} \dot{e}_1 \\ \dot{e}_2 \end{bmatrix} = \begin{bmatrix} -\Omega & \Omega \\ -\Omega & 0 \end{bmatrix} \begin{bmatrix} e_1 \\ e_2 \end{bmatrix} + \begin{bmatrix} \frac{1}{RC} \\ 0 \end{bmatrix} [e_{ai}]$$

$$y = \begin{bmatrix} 1 & 0 \end{bmatrix} \begin{bmatrix} ev_i \\ e_2 \end{bmatrix} + \begin{bmatrix} 0 \end{bmatrix} \begin{bmatrix} ea_i \end{bmatrix} \quad (3.9)$$

Figure 3.2 in an analog computer diagram of equation 3.9 which is suitable for programming the GP-6 and EAI-20. The values for Ω again equals 0.628 and the constant RC again has the value of one. It is important to note that the integrators and summers of an analog computer invert the incoming signal. Figure 3.2 shows a negative (inverted) velocity signal as the system output rather than the positive velocity signal derived in the state space equations. This is because it is convenient to allow the velocity signal to remain negative for feedback purposes. If a positive signal was desired, an inverter would need to be added at the output.

3.2.3 AJT Control: Non-Linear Simulation and Experimental Results

The classical controller for the AJT control circuit is simply velocity feedback to the AJT control circuitry. As mentioned in section 3.2.1, negative velocity feedback will always stabilize a system when there is no appreciable lag in the feedback loop. Unfortunately, there is significant phase lag in the AJTs. However, for the low frequency bending modes, the AJTs still provide a significant increase in damping.

Table 3.1: Non-linear simulation closed loop modal data: AJT velocity feedback

	frequency (rad/sec)	damping ratio	$\log \left[\frac{\zeta}{\zeta_{openloop}} \right]$
mode 1	9.30	0.06	0.945
mode 2	55.80	0.0345	0.915
mode 3	146.52	0.009	0.000
mode 4	262.32	0.009	-0.250

Using non-linear simulation with the theoretical non-linear AJT model acting upon the truss tip and midpoint lateral DOF the time response in figure 3.3 were obtained. The truss was driven in same manner as the experimental data, a sinusoidal wave was input to the AJT circuit at the different modal frequencies of the linear model. However, instead of allowing the truss to reach steady state excitation as is the case

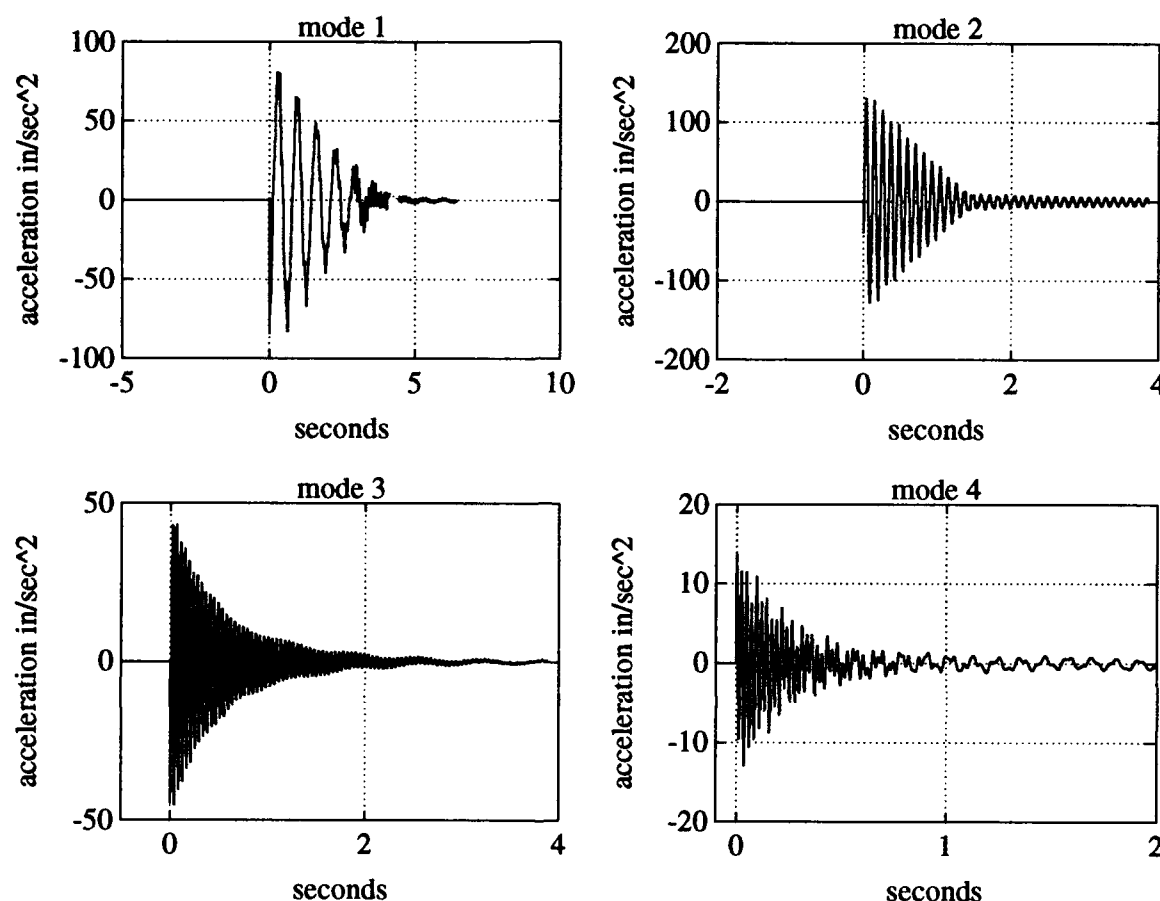


Figure 3.3: Non-linear simulation truss tip responses. AJT velocity feedback

with the experimental data, the sine signal was switched to the control signal when the modal excitation of the linear model was approximately the same value as obtained in the experimental testing. The modal decay is seen to occur at a much faster rate for modes one and two than in the open loop case presented in figure 2.15. This is expected due to the AJT's lack of phase lag at the lower modes. A small oscillation is still apparent in the second mode plot as the AJTs stop firing when the control signal drops into the deadband voltage cut-off level. Modes three and four are not visibly affected by the addition of the AJT controllers.

To help to quantify the effects of the controller, damping ratios were calculated for each mode utilizing the logarithmic decrement method of section 2.5.2 and are

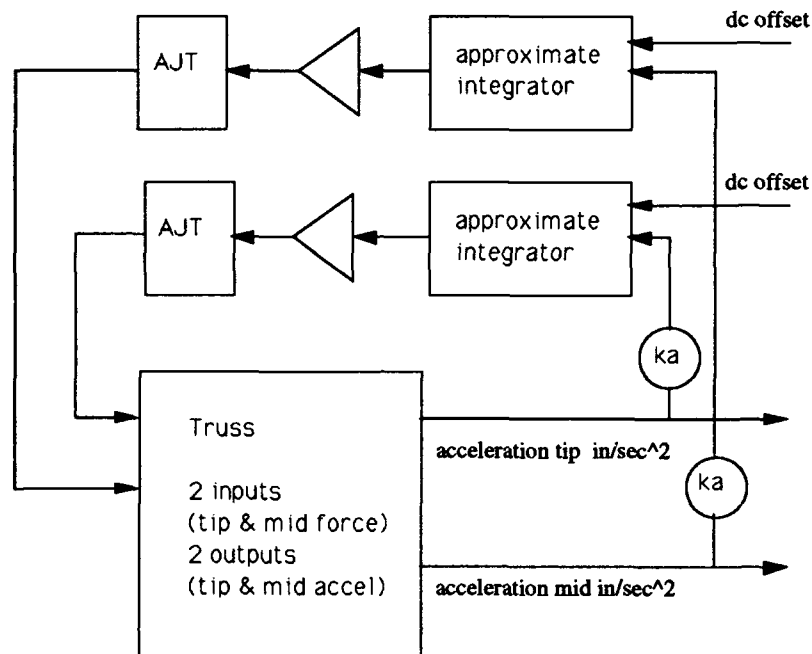


Figure 3.4: Non-linear/hardware block diagram for AJT velocity feedback control

displayed in table 3.1. It is realized that no linear method imposed on a non-linear system can fully quantify the damping as all damping is assumed to be viscous, but it is still valuable for comparison to the open loop system. The \log_{10} of the ratio of the closed loop to the open loop value is displayed in table 3.1 in favor of percentages because of the large increases in damping achieved (nearly a factor of 10 for both the first and second modes in non-linear simulation). The damping of the third and fourth modes is not positively affected, in fact the damping decreases slightly in the fourth mode compared to the open loop system.

The experimental truss tip responses are presented in figure 3.5, and show a slightly different story than predicted by the non-linear simulation of AJT velocity feedback performance. The third and fourth mode have AJT misfires which are destabilizing, indicating that the AJT velocity feedback controller is detrimental at higher frequencies, not of little effect as predicted by the non-linear simulation. The first and second

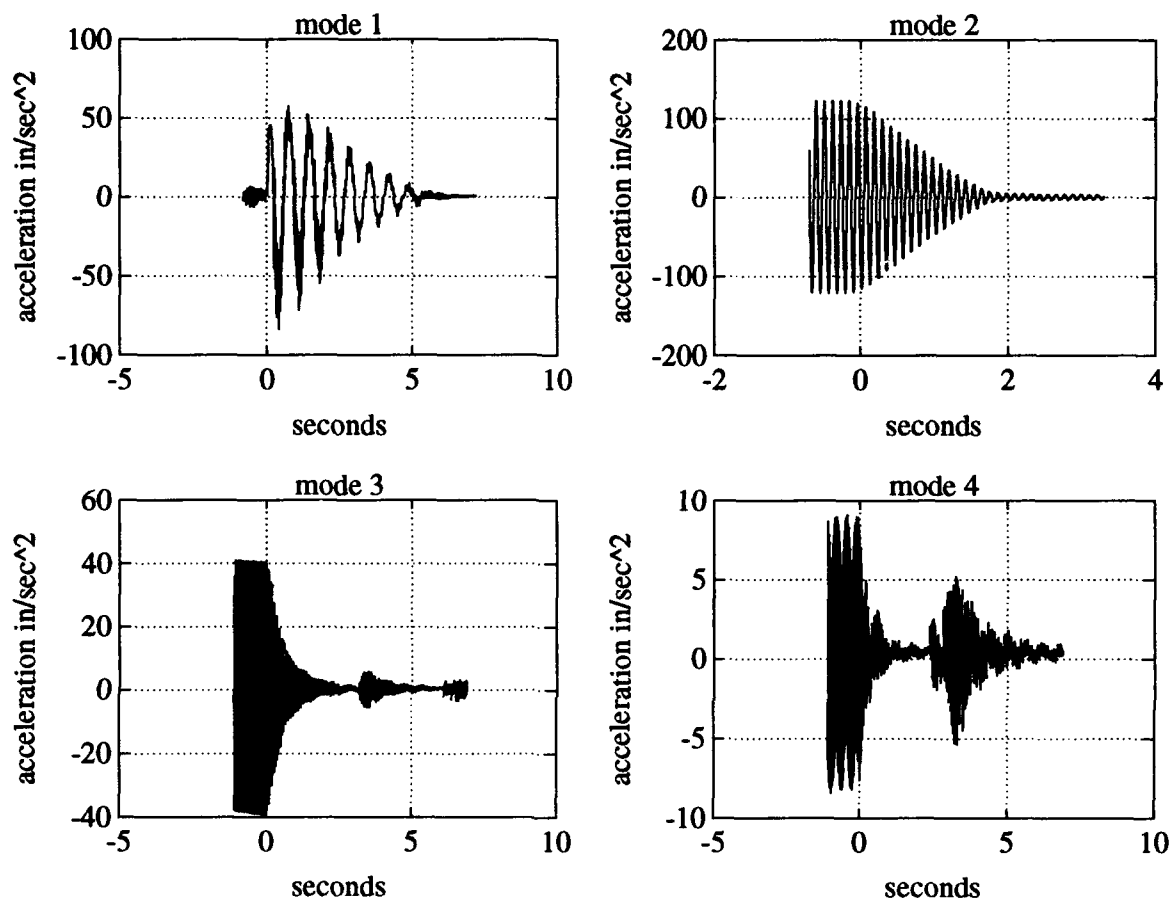


Figure 3.5: Experimental truss tip responses: AJT velocity feedback

modes behave similarly to the non-linear simulation predicted results, including the small oscillation of the second mode when the control signal is within the AJT dead-band. The second mode oscillation was noticed in the USAFA truss experiments, but specific mention was made that the AJTs never destabilized a mode [8]. It seems that either slightly greater lags in our AJTs or slightly more noise in our control circuitry must have been present. As seen in table 3.2, significant damping increases were reported for first and second mode damping ratios, although slightly below the performance achieved in non-linear simulation. The first and second mode damping increases were in the same relative proportion at about 7/10ths of a factor of ten, just as in non-linear simulation the increases were in the same relative proportion at

9/10ths of a factor of 10

Table 3.2: Experimental closed loop modal data: truss velocity feedback to AJTs

	frequency (rad/sec)	damping ratio	$\log \left[\frac{\zeta}{\zeta_{openloop}} \right]$
mode 1	9.30	0.035	0.712
mode 2	55.80	0.025	0.775
mode 3	146.52	AJT misfires	na
mode 4	262.32	AJT misfires	na

Overall, it was demonstrated that the AJTs were effective in controlling low frequency first and second mode disturbances. However, the failure to effectively dampen the vibrations of the third and fourth modes, and possibly excite them, indicates that the use of velocity feedback to the AJTs alone is an inadequate solution to the vibration suppression problem.

3.3 RMAs for Vibration Suppression

The reaction mass actuators are linear, space-realizable forms of actuation ideally suited to control lateral vibration modes of the planar truss. Unlike the AJT thrusters, only electrical energy is necessary to power these actuators, not the expulsion of a finite supply of gas as is the case with the AJTs. However, the amount of force the RMAs may exert is somewhat limited, and they are limited in effectiveness by their non-tuneable natural frequencies as we shall see. The RMAs are located at the truss midpoint and tip, locations which might be adjusted later to suppress different modes. As the RMAs are set up in the current configuration, the midpoint RMA is at an anti-node of the third lateral truss bending mode, which limits its effectiveness to control that particular mode.

A discussion of the different levels of classical control is given in this section. The use of the RMAs in the open loop system as passive dampers is described in section 3.3.1. Feedback of only the truss' velocity signals as performed by Zimmerman [23] is discussed in section 3.3.2. The use of relative velocities between the truss' inertial velocities and the RMAs' proof mass inertial velocities is presented in

section 3.3.3 and builds upon the separate works of Hallauer [8], Miller and Crawley [15], and Inman [10]. Finally, an approach proposed by Inman which utilizes separate gains on the proof mass velocities and the truss velocities is applied to yield a very attractive classical velocity control feedback system. These results are reported in section 3.3.4.

3.3.1 RMA as a Passive Damper

The use of reaction mass actuators as vibration absorbers is not a new concept. The simplicity of merely adding a spring-mass-damper to a dynamic system to reduce vibrations is very attractive, and the problem has been thoroughly explored. Applications to large space structures, such as the optimal design of a vibration absorbers for multi-degree of freedom (MDOF) systems such as beams and trusses, have been the subject of recent literature [11, 15]. The results give general guidelines for the application of vibration absorbers to systems similar to the UWAA planar truss. Although Miller and Crawley [15] used quadratic optimization techniques to arrive at a closed form solution to the passive damping problem, their results may be summarized as follows. A vibration absorber may be added to a MDOF system to reduce the response of structural modes. Tuning the vibration absorber to control the vibration of a system is performed by selecting the lowest frequency mode of interest and matching the natural frequency of the absorber to that natural frequency. The vibration absorber is placed at point of maximum modal excitation for best results. The frequency of the vibration absorber will have to be slightly lessened as its mass approaches the equivalent modal mass for the structural mode of interest. The damping ratio of the vibration absorber is then increased until the desired structural modal damping is achieved. Many vibration absorbers may be individually tuned and placed strategically along the structure to attenuate multiple modal responses, realizing that slight residual damping will occur in the modes above the tuned frequency, while modes below the tuned frequency will be slightly adversely affected.

For the UWAA planar truss with the RMAs acting at the lateral truss tip and endpoint degrees of freedom, the results of Miller and Crawley may be used to predict the effect of the passive damping of the RMAs on the planar truss. The RMAs are

Table 3.3: Open loop linear model modal data: RMAs as passive dampers

	frequency (rad/sec)	damping ratio	$\log \left[\frac{\zeta}{\zeta_{openloop}} \right]$
mode 1	9.19	0.0067	-.006
mode 2	57.95	0.0190	0.656
mode 3	146.58	0.0098	0.037
mode 4	260.30	0.0164	0.011
RMA	40.64	0.0635	-0.073
RMA	43.19	0.0776	0.000

acting on positions of maximum displacement for the second mode (see figure 2.13). Furthermore, the natural frequencies of the RMAs occur at 41.12 rad/sec for the tip RMA and 42.96 rad/sec for the midpoint RMA, both of which are about 10 rad/sec below the second mode but well above the first bending mode. Therefore, we expect the RMAs will add significant damping to the second bending mode of the truss but below their true attainable capability if they were to have their natural frequencies lowered by the addition of some more mass (since the spring constants of the RMAs are fixed). Since the hardware is already assembled, the masses will not be changed for this experiment, but leaves room for a study to be performed where the mass of the RMAs is varied.

The linear model for the RMA system is formed using the methods of sections 2.3.1 and 2.4.2. It is a twelfth order system of the form

$$\dot{x} = A_{12}x + B_{12}u \quad (3.10)$$

The numerical values which constitute A_{12} and B_{12} are listed in section A.2.

As we see in table 3.3, the predictions that the damping ratio of the second mode would significantly increase are correct as a 0.656 factor of ten increase in second mode damping occurred in the linear model. The goal of 10% damping in each structural mode is not achieved with the addition of passive damping alone, although damping of the second mode is increased substantially. The next step is to add active control to supplement the passive damping.

3.3.2 Straight Velocity Feedback

This section begins the discussions on classical control of the truss through the use of the RMAs. All feedback gains in this and following sections assume the use of the a scaled accelerometer output equal to 38.8 volts per g, or approximately 0.1 volts per $1 \frac{\text{in}}{\text{sec}^2}$. This is easily achieved in the hardware as the amplifier gain on the RMA amplifier is marked in units ranging from 0 to 10. Additionally, negative feedback is assumed unless a negative gain is specified, which indicates positive feedback.

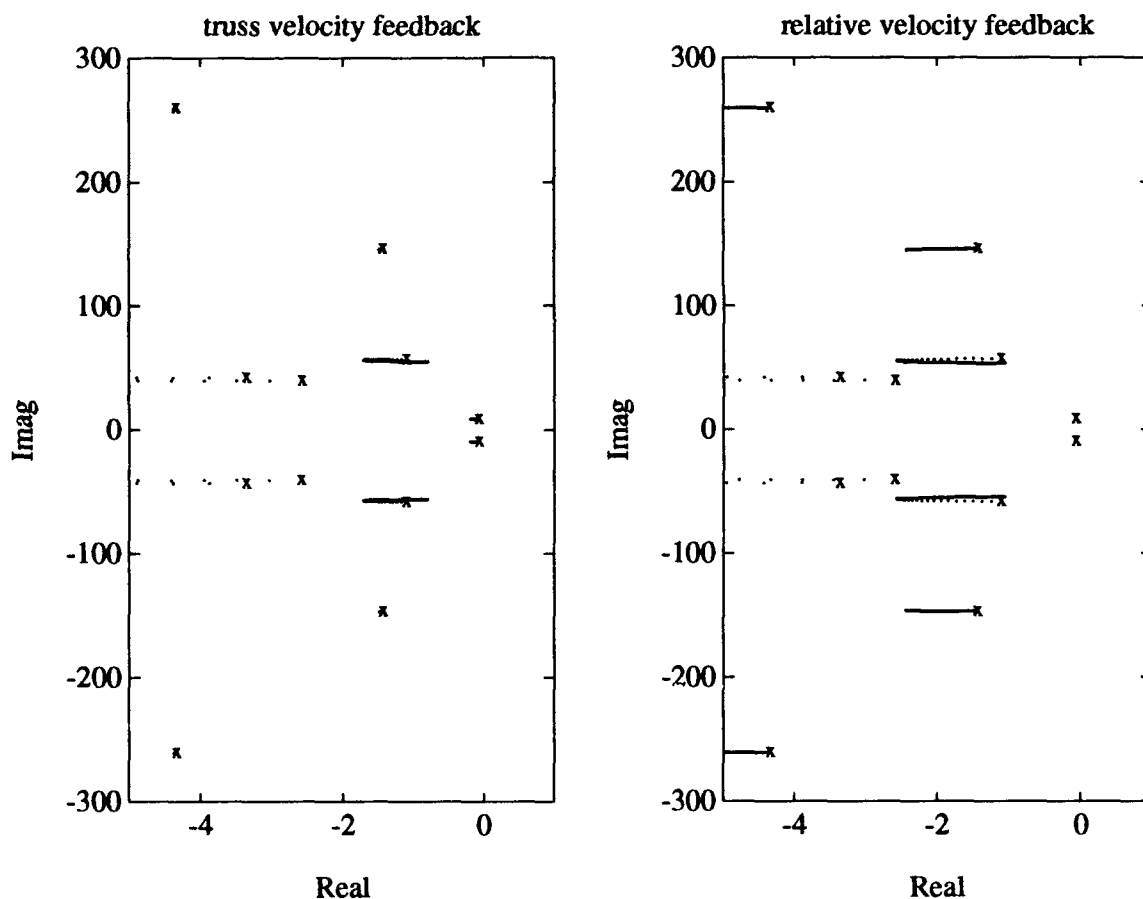


Figure 3.6: Comparison of root loci: $kt = km = 0.0:0.1:10$

The use of velocity feedback from the truss stations without regard to the inertial or relative velocities of the RMA proof mass is similar to the work of Zimmerman [23] where control of a cantilever beam was performed using an RMA tuned to the first

bending mode of the beam. Simple proportional feedback of the beam tip velocity to the RMA amplifier yields a feedback law of the form:

$$f_{b(tip)} = -k_t \dot{q}_t \quad (3.11)$$

The beam was then only excited at the first mode at amplitudes well within the stroke limits of the RMA. Two problems were apparent. First, there was no way to predict how different feedback gains would affect the throw of the proof mass since actuator dynamics were ignored in the modeling as well as in the implementation. Second, small levels of vibration persisted well after the most of the modal energy was dissipated. Although it was felt that the D/A converters were responsible for the problem, the fact that straight velocity feedback is risky and assumes a well behaved system to begin with may have well compounded the D/A problem.

Table 3.4: Feedback gains on truss velocities

velocity	feedback gain	value
\dot{q}_t	k_t	2.0
\dot{q}_m	k_m	2.0

Figure 3.6 illustrates the disadvantage of the using straight truss station velocity feedback when compared to feedback which takes into account the dynamics of the proof mass on board the RMA. The feedback control law was of the form

$$\begin{aligned} f_{b(tip)} &= -k_t \dot{q}_t \\ f_{b(mid)} &= -k_m \dot{q}_t \end{aligned} \quad (3.12)$$

The root locus for feedback gains of 0 to 10 on the truss tip and midpoint velocities only indicates that the implementation of the feedback law results in significant stabilization of only the second mode. The gains in table 3.4 are chosen where the second mode damping is the highest. Although the damping of mode 1 is also improved, the trade off versus relative velocity feedback is the complete lack of authority over the higher modes of the system.

Table 3.5: Closed loop linear model modal data: truss velocity feedback

	frequency (rad/sec)	damping ratio	$\log \left[\frac{\zeta}{\zeta_{openloop}} \right]$
mode 1	9.19	0.0100	0.167
mode 2	56.85	0.0298	0.850
mode 3	146.57	0.0098	0.037
mode 4	260.28	0.0167	0.019
RMA	41.43	0.2972	0.598
RMA	43.19	0.31466	0.608

The use of straight velocity feedback does have one very significant advantage: ease of application. The number of sensors required is one-half the number required for relative velocity feedback. However, given that the UWAA planar truss is representative of a high performance requirement large space structure, that advantage does not outweigh the disadvantage of overall poor performance. It was decided not to implement the velocity controller in the hardware because of the difficulty in determining a performance increase over the passively damped system of section 3.3.1.

3.3.3 Relative Velocity Feedback

The use of relative velocity feedback was used effectively by Hallauer to suppress bending mode vibrations [8]. The feedback control law is of the form

$$\begin{aligned} f_{b(tip)} &= -k_t \dot{q}_{ta} \\ f_{b(mid)} &= -k_m \dot{q}_{ma} \end{aligned} \quad (3.13)$$

where q_{ta} and q_{ma} are the relative velocities between the tip actuator mass and tip truss station and the mid actuator mass and mid truss station, respectively.

As seen in figure 3.6 the feedback of relative velocities to the RMAs has a much greater effect on the closed loop eigenvalues of the truss than does the straight velocity feedback of the previous section. The feedback gains for the truss and midpoint RMAs were adjusted in equal increments to provide the levels of damping which are shown graphically in figure 3.7. The first, third, and fourth bending modes

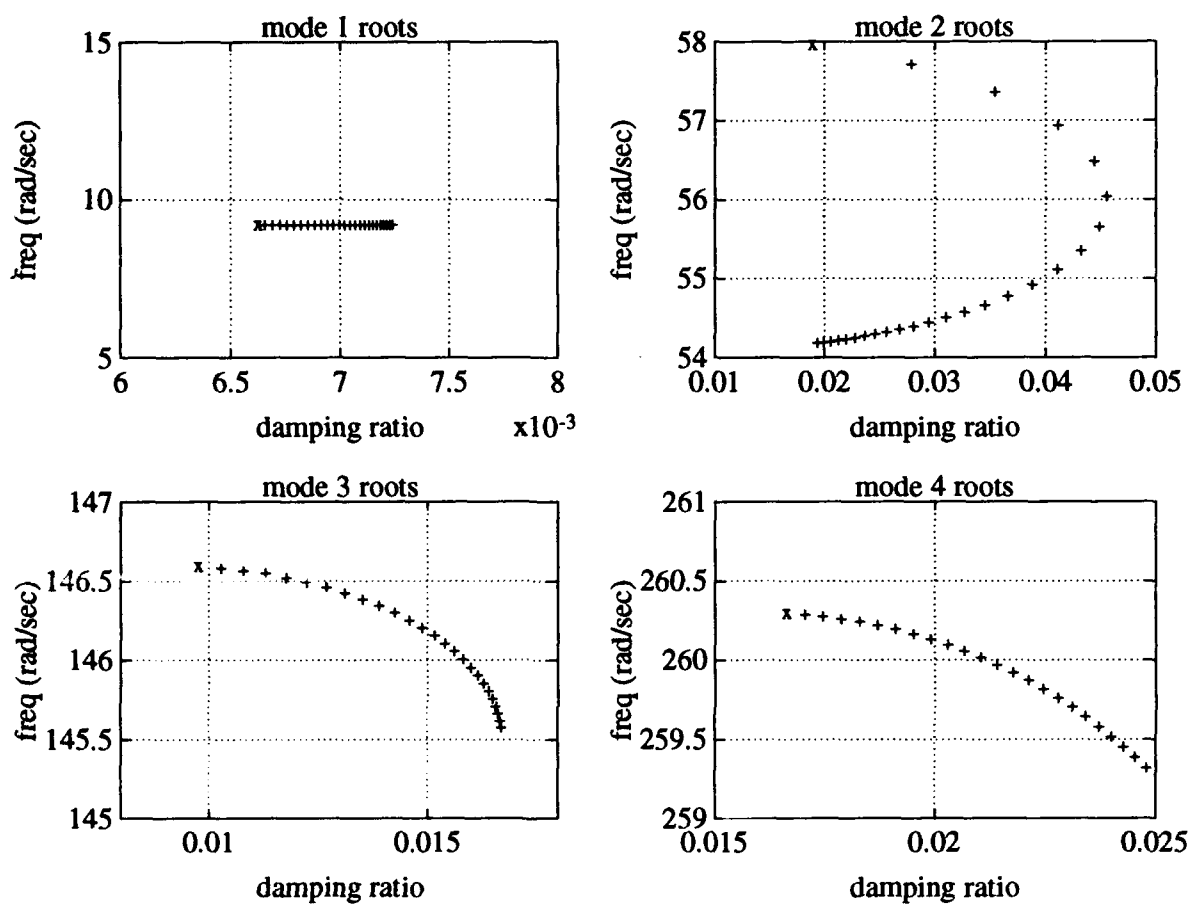


Figure 3.7: Relative velocity feedback to the RMAs: $k_t = k_m = 0:0.4:10$

all respond favorably to increases in feedback gain within the range of the RMA amplifiers. Increases in gain beyond the range of the amplifiers would easily be obtained by adding additional gains in the feedback loops using the analog computers, but high gain systems are generally undesirable due to the penalty of increased noise in the feedback loop and were not considered here. For the second mode, however, increasing the gain adversely affected stability after a value of 0.2 was reached. Similar behavior occurs for the third and fourth modes at higher levels of gain avoided here. This led Hallauer to correctly state that the best performance using relative velocity feedback would be obtained if the gains were implemented using band-pass filters which would allow for the best possible gain individually selected for each mode [8].

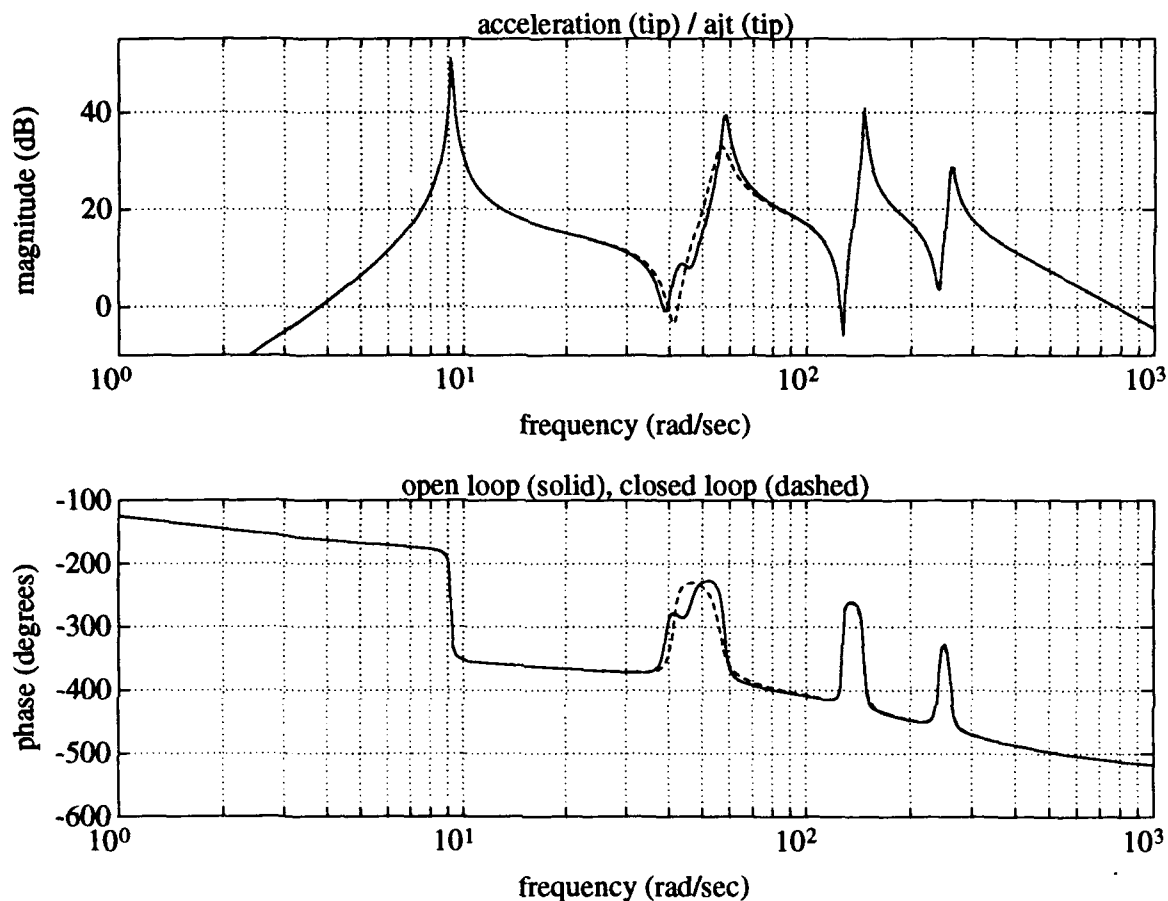


Figure 3.8: Linear model frequency response for mode-2 suppression: $k_t = k_m = 2.0$

This approach, however, is very difficult to implement in the hardware.

The ability of the RMAs to suppress vibration when gains are chosen for a specific mode is shown in the frequency responses of figure 3.8 and figure 3.9. The data in figure 3.8 was obtained by using the linear model of the AJTs to input force to the RMA-augmented truss model with the feedback gains on the relative velocities set to 2.0 in the closed loop case. Comparison of the open and closed loop responses shows 6.3 dB of vibration suppression occurred at the second mode. A similar approach was applied in the case of the experimental hardware results shown in figure 3.9 where suppression of the second mode due to AJT tip excitation is 8.58 dB. The closed loop gains for the experimental case were found by exciting the truss at the second mode

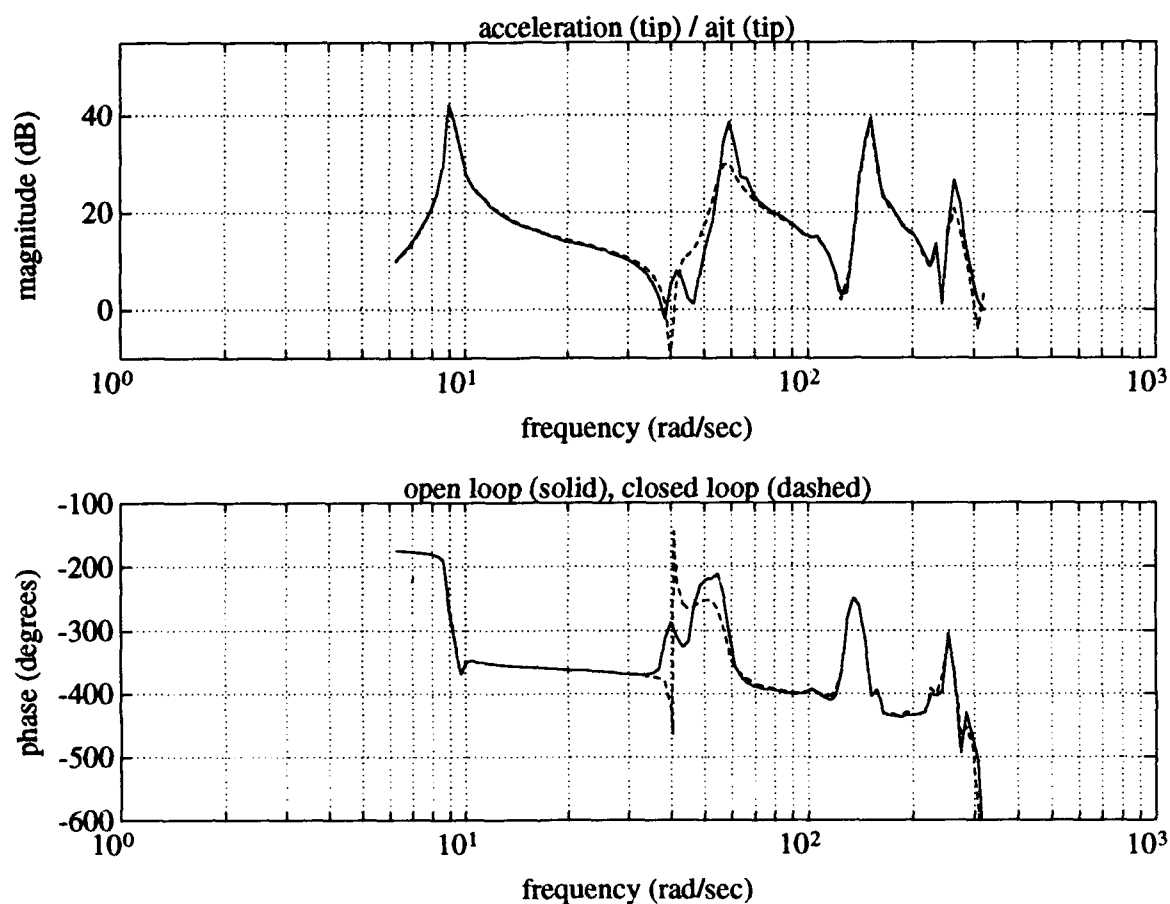


Figure 3.9: Experimental frequency response for mode-2 suppression: $kt = km = 3.5$

frequency with the AJTs and then adjusting the amplifier gains and measuring the real-time acceleration output of the truss tip and midpoint accelerations until the accelerations were at a minimum. The experimental data confirms the linear model's utility in predicting second mode vibration suppression.

As previously stated, to design a band-pass filter for individual modes makes a difficult task for hardware implementation. Instead, it is desirable to have one set of gains which may be implemented which might realize most of the performance of the band-pass filter designs. Taking the approach that the midpoint-mounted RMA has little effect on the third bending mode of the truss due to its location at a third mode node, the relative velocity feedback gain was set to a value to dampen the second

Table 3.6: Feedback gains on relative velocities

velocity	feedback gain	value
$\dot{q}_a - \dot{q}_t$	k_t	6.0
$\dot{q}_a - \dot{q}_m$	k_m	1.9

mode of the truss. Then, to increase the damping of the third and fourth modes, the tip-mounted RMA had its gain increased to values more in line with damping the higher modes. The final gains chosen are shown in table 3.6. The modal damping is shown in table 3.7 for the linear model results.

Table 3.7: Closed loop linear model modal data: relative velocity feedback

	frequency (rad/sec)	damping ratio	$\log \left[\frac{\zeta}{\zeta_{openloop}} \right]$
mode 1	9.20	0.0070	0.013
mode 2	55.12	0.0368	0.943
mode 3	146.04	0.0156	0.239
mode 4	260.00	0.0205	0.108
RMA	43.04	0.2904	0.586
RMA	43.08	0.7764	1.000

This is a suitable compromise as the damping is significantly increased for modes 2, 3, and 4. The damping of the second mode is still nearly a factor of ten greater than the open loop case, while the damping of the third and fourth modes are increased by a smaller factor. This makes sense as the third and fourth modal frequencies are 'further' away from the ideal controlling frequency of the RMAs which is just below the natural frequency of the second mode.

3.3.4 Separate Velocity Feedback using RMA and Truss Inertial Velocities

Inman stated in the conclusions of his paper on control/structure interaction [10], that a better approach for using the reaction mass actuator would be to use a separate

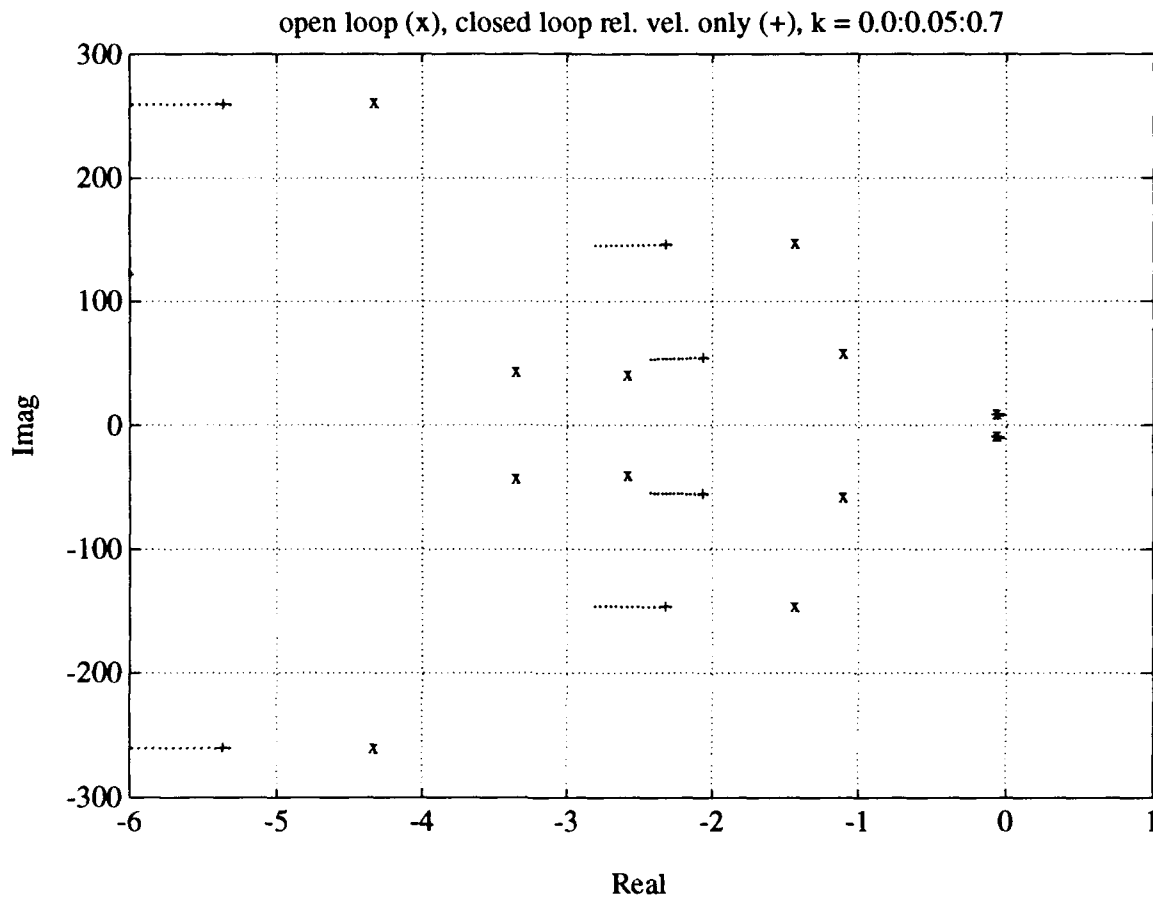


Figure 3.10: Root locus for separate feedback gains on inertial velocities

feedback path for the inertial velocities of the proof mass and the corresponding truss station. The feedback law for the truss tip would take the form of:

$$f_b = -k_{tt}\dot{q}_t - k_t\dot{q}_a \quad (3.14)$$

where \dot{q}_t is the truss tip inertial velocity and \dot{q}_a and proof mass inertial velocity. A root locus of showing the effects of separating the feedback paths is shown in figure 3.10. The root locus is obtained by beginning with the closed loop system using relative velocity feedback as presented in section 3.3.3 (marked as '+'). Then, the inertial truss velocity is added to the relative velocity as the root locus gain is increased: $\dot{q}_a - k\dot{q}_t$. The first mode is destabilized by this type of feedback, so a limit of 0.7 was

chosen for k to preserve the stability of the first mode. Since the ultimate goal of this research was to improve damping using both the RMAs and AJTs, the increase in the higher mode damping where the AJTs are ineffective is seen as a worthwhile trade-off for the decrease in the first mode damping where the AJT performance is most effective.

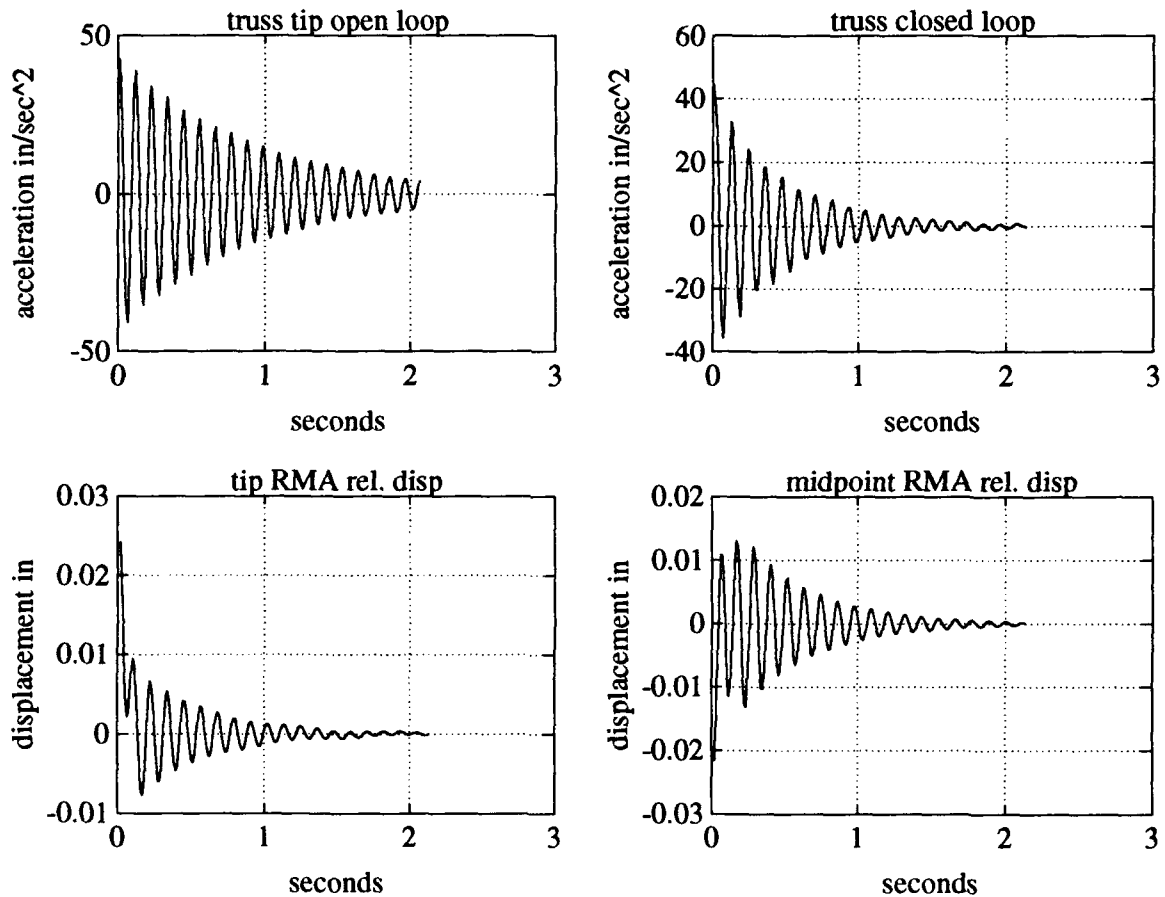


Figure 3.11: Time responses for second mode: separate inertial velocity feedback

The feedback gains on the inertial velocities chosen for the final design are presented in table 3.8. The resulting modal damping from the linear model is shown in table 3.9. The damping of the second, third, and fourth modes is approximately 50 % better than the damping achieved through the use of relative velocity feedback alone (compare to table 3.7). A time response for the linear model second mode

Table 3.8: Feedback gains on proof mass and truss velocities

velocity	feedback gain	value
$\dot{q}_a(tip)$	k_t	6.0
\dot{q}_t	k_{tt}	-1.2
$\dot{q}_a(mid)$	k_m	1.9
\dot{q}_m	k_{mt}	-0.57

Table 3.9: Closed loop linear model modal data: separate inertial velocity feedback

	frequency (rad/sec)	damping ratio	$\log \left[\frac{\zeta}{\zeta_{openloop}} \right]$
mode 1	9.18	0.00146	-0.668
mode 2	54.24	0.0446	1.026
mode 3	145.72	0.0192	0.329
mode 4	259.82	0.0230	0.158
RMA	43.29	0.2882	0.585
RMA	43.76	0.8856	1.057

vibration suppression is shown in figure 3.11. The figure shows the open loop free decay and the closed loop time response for the truss tip acceleration. It also shows the reaction mass relative displacement for the tip and midpoint RMAs. These plots show that the reaction masses are both well within their limited throw excursions of ± 0.1 in. In fact, it would take second mode vibrations well in excess of $100 \frac{in}{sec^2}$ to cause the reaction masses to travel beyond their throw limitations. The second mode plot was included because the amplitude of travel of the reaction mass was greater at this mode than the higher frequency third and fourth modes. The first mode is not examined because the RMAs do not aid the damping of that mode, although the tip RMA will reach the limits of its throw excursion for first mode vibrations in excess of $50 \frac{in}{sec^2}$ measured at the tip accelerometer.

3.4 Hybrid Control: AJTs and RMAs Working Together to Suppress Vibration

Hybrid actuation was the term used by Hallauer [8] to describe the use of both the AJTs and the RMAs to suppress vibration of the planar truss bending modes. To employ the two different actuators in the non-linear simulation and experimental hardware, it is first necessary to note that both of the controllers were designed to work independently of each other. No effort was made to make the controllers work together except the reasoning in that the AJTs would dampen the low frequency vibrations while the RMAs would suppress the high frequency vibrations. This control effectively 'piggy-backs' the non-linear AJT controllers on top of the RMA-augmented linear closed loop system. Effectiveness of this system will allow the design of an optimal controller for the linear RMA-augmented truss without regard to the AJTs, which then may be piggy-backed on board the optimally controlled truss.

Table 3.10: Non-linear simulation closed loop modal data: hybrid actuation

	frequency (rad/sec)	damping ratio	$\log \left[\frac{\zeta}{\zeta_{openloop}} \right]$
mode 1	9.18	0.0904	1.12
mode 2	54.24	0.0914	1.33
mode 3	145.72	0.0170	0.276
mode 4	259.82	0.0212	0.122

The non-linear simulation conducted to test the effectiveness of hybrid actuation was performed by using the AJT velocity controller discussed in section 3.2.3 and the RMA controller from section 3.3.4. Figure 3.13 shows the set up put into the non-linear simulation program. The RMA-controlled truss was driven with the AJTs at the natural frequencies until a level of excitation which was representative of the experimental excitations was reached, and then the AJTs control circuit was switched on. This allowed both the AJTs and the RMAs to work together to control the truss model. The non-linear simulation of the truss tip acceleration time responses for the four bending modes is presented in figure 3.12.

From the data presented in figure 3.12, logarithmic decrements were measured and damping ratios calculated. These values are presented in table 3.10. The damping of

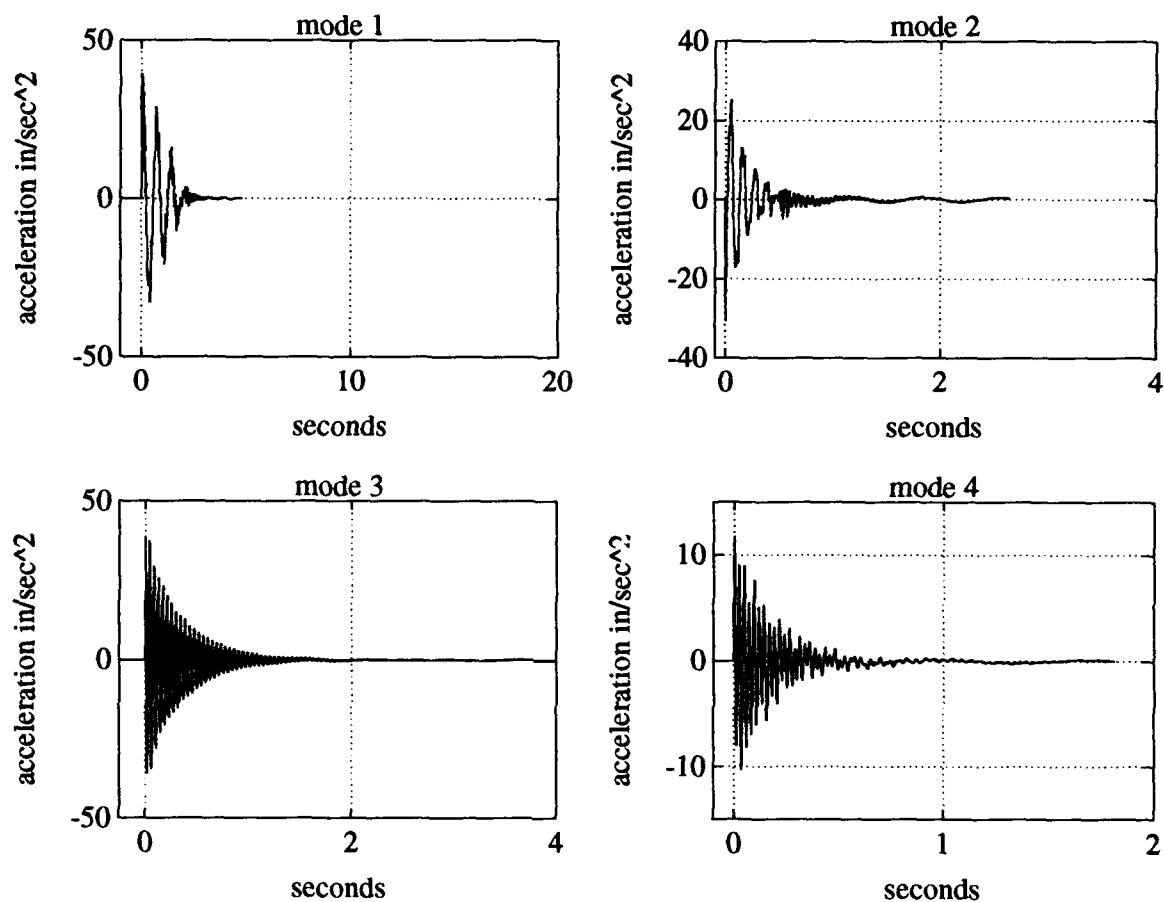


Figure 3.12: Non-linear simulation of hybrid control:truss tip responses

the modes increases as is expected. In general, the second, third, and fourth modes had levels of damping comparable to the RMA-only controlled system in section 3.3.4, while the first mode damping was clearly more influenced by the AJTs. The level of damping appears to increase significantly over the AJT-only control of section 3.2.3, but this may in part be due to the lower amplitudes of the hybrid testing. The damping in the first two modes nearly meets the goal of ten percent damping in future large space structures. The next step is to perform the experimental tests.

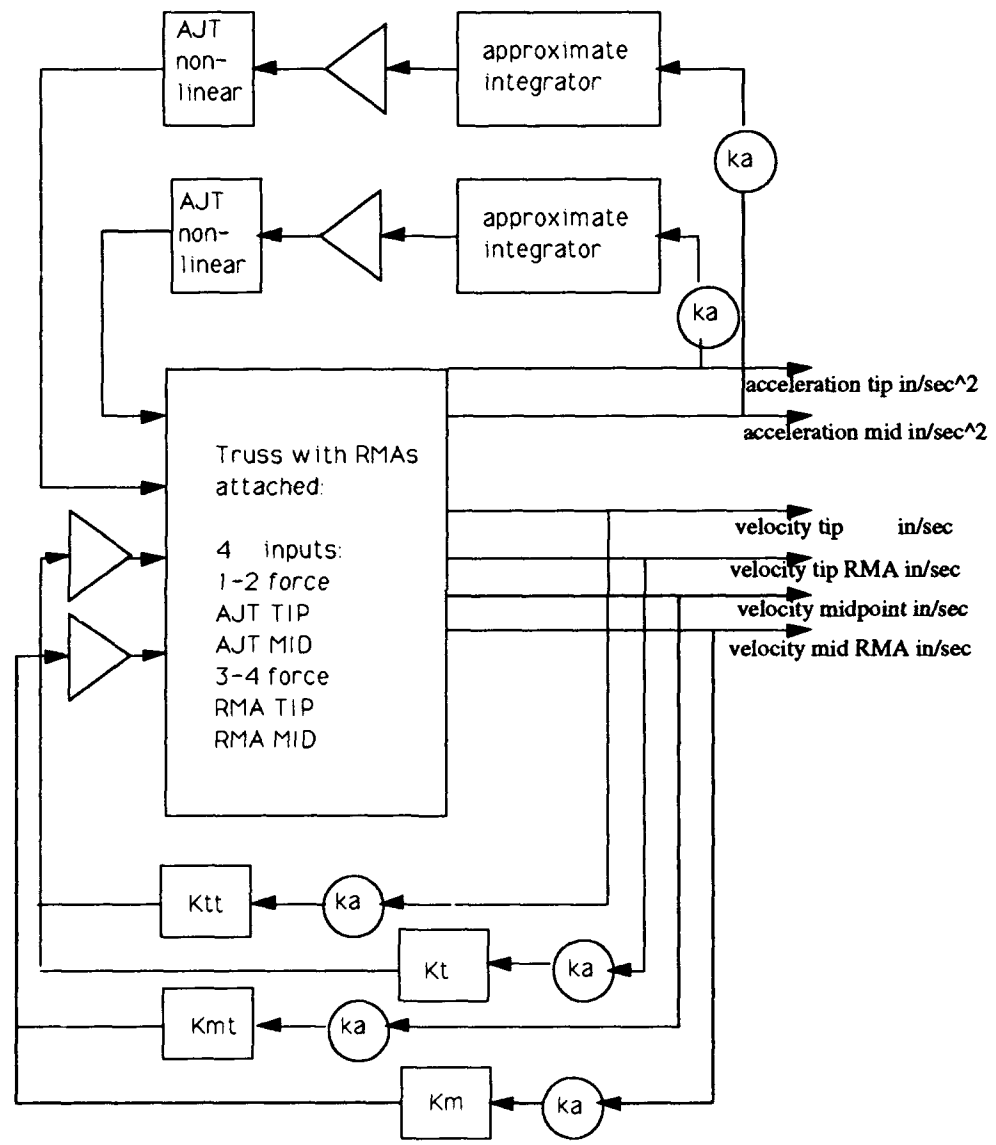


Figure 3.13: Non-linear block diagram for hybrid actuation simulation

3.5 Experimental Results

3.5.1 Experimental Open Loop Testing of the RMA-Augmented Truss

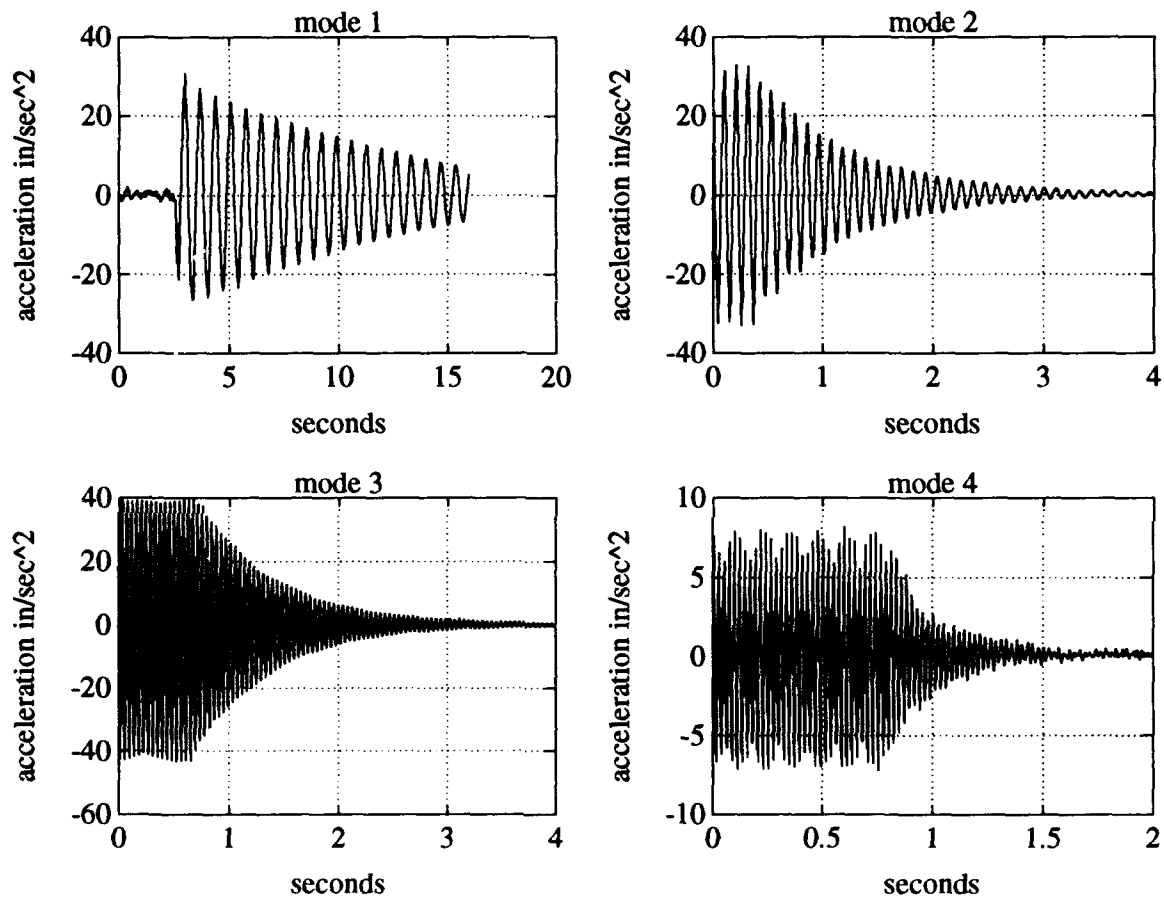


Figure 3.14: Experimental open loop RMA-augmented truss tip responses

The experimental testing was conducted close to the same manner as the non-linear simulation, but the RMA-augmented truss was excited with the AJTs without any of the RMA control circuitry on. Open loop RMA-augmented truss plots are included from the day of the experimental testing to give a basis of comparison between the passive damping effects of the RMAs and the closed loop time responses. The RMA-augmented open loop plots are presented in figure 3.14. The displacement differences

between the open loop time responses in figures 2.15 and 2.16 are due to two reasons. One, the RMAs prevent the full level of truss excitement due to their passive damping effects. Two, the testing environmental conditions differed between the two test days. It was cooler in temperature when the RMA tests were conducted compared to the open loop tests of chapter two.

Table 3.11: Experimental open loop modal data: RMA-augmented truss

	frequency (rad/sec)	damping ratio	$\log \left[\frac{\zeta}{\zeta_{openloop}} \right]$
mode 1	9.18	0.0120	0.246
mode 2	54.24	0.0156	0.570
mode 3	145.72	0.0085	-0.025
mode 4	259.82	0.0128	-0.097

The damping ratio of the open loop RMA-augmented truss increase at the second mode of the truss as expected. The increase in damping of the first mode is not substantial when one takes into consideration the change in damping that occurred when the truss was retested as noted in section 2.5.2. The damping in mode one is identical to later tests on that mode made after the baseline open loop damping was established. Therefore, the truss behaves as expected for the first mode with the addition of the RMA passive dampers. The change in damping of the third and fourth mode is slight as predicted by the modeling performed in section 3.3.1.

3.5.2 Experimental Closed Loop Testing of the RMA Controllers

The next step in the experimental testing was to conduct a test of the RMA controller acting independently. A problem surfaced when amplifier gains were set at levels above 7.0. Although this problem surfaced when the feedback loops were connected, open loop tests confirmed that this problem was isolated to the amplifier circuitry. In figure 3.15, a time response of the tip actuator operating at the second mode of the truss is displayed. The figure shows the RMA acceleration compared to the truss tip acceleration. For the first second, the system is open-loop with the gain set to zero. At about one second, the RMA's amplifier is switched on to a gain of seven acting on the

relative velocity between the actuator mass and the truss station. Normal attenuation is recorded. At about two seconds on the plot, the AJTs providing the second mode disturbance to the truss are switched off. This results in the truss station acceleration decaying to zero, but an *actuator/instrumentation instability* arises. This causes the RMA proof mass to violently swing back and fourth, even when the steady state truss acceleration is zero. A problem thought to be similar to this was noticed by Miller and Crawley in their experiments with RMAs [15].

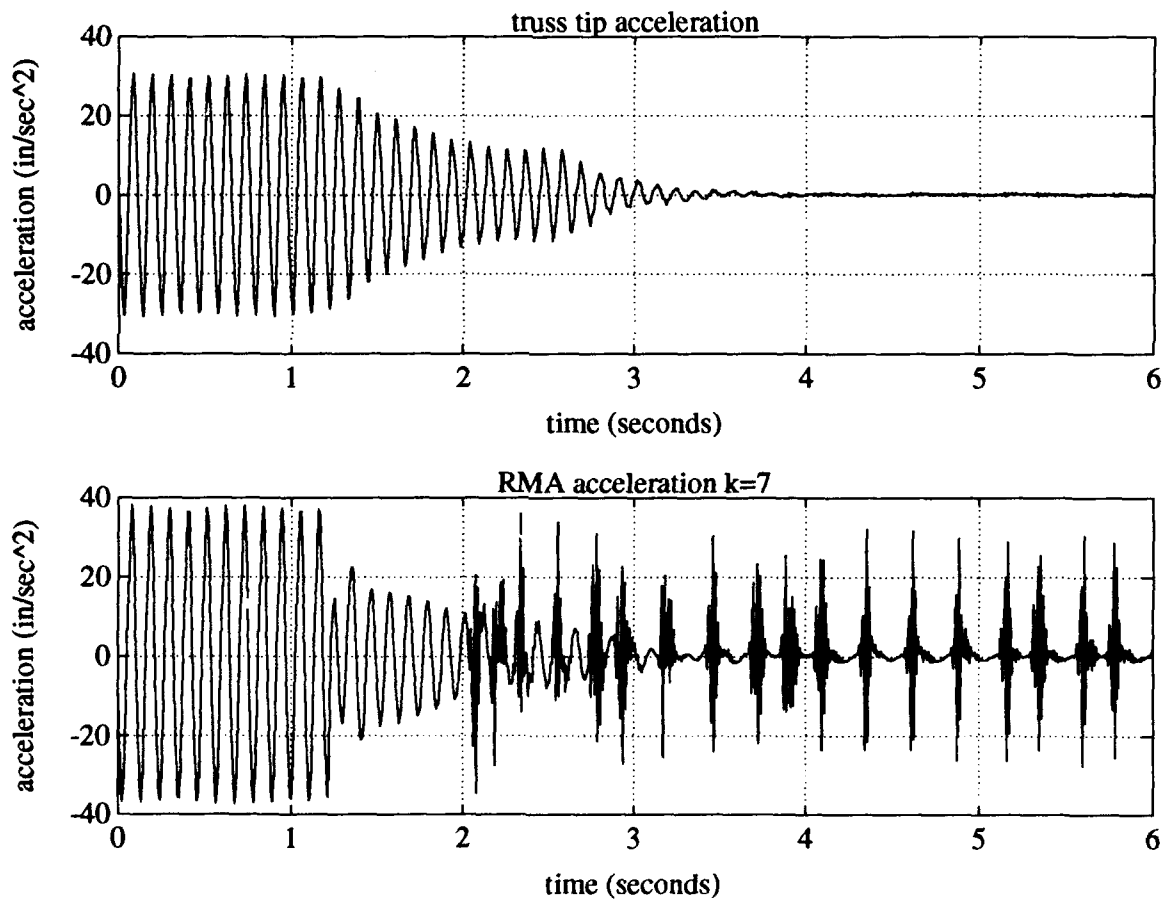


Figure 3.15: RMA actuator/instrumentation instability

Because the actuator/instrumentation instability limited the gain adjustments possible, the RMA controller for experimental implementation was chosen to be the velocity feedback controller for mode-2 suppression presented in section 3.3.3. The tip

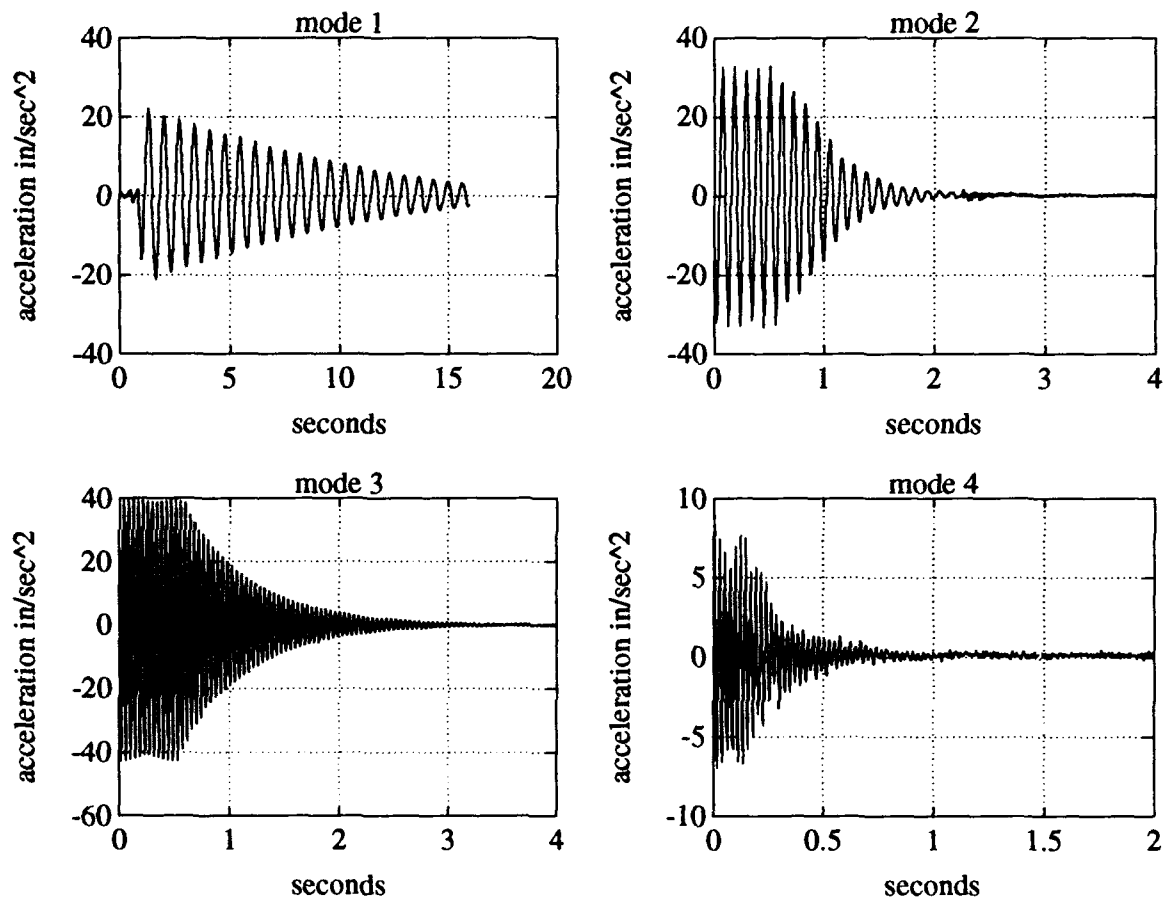


Figure 3.16: Experimental RMA-relative velocity feedback only-time responses

and midpoint amplifier gains were set to values of 3.5 for best experimental results for mode-2 damping.

The time responses of the experimental RMA controlled truss system are presented in figure 3.16. The time responses show the RMAs working effectively to actively suppress second bending mode vibrations. The damping ratios were calculated and are presented in table 3.12. The first mode was nearly unchanged from the open loop RMA-augmented truss system in section 3.5.1. The third and fourth modes both have their damping increased compared to the open loop RMA-augmented truss as was predicted in section 3.3.3. The second mode damping is most noticeably increased, as was indicated by the modal time responses in figure 3.16.

Table 3.12: Experimental closed loop modal data: relative velocity feedback to RMAs

	frequency (rad/sec)	damping ratio	$\log \left[\frac{\zeta}{\zeta_{openloop}} \right]$
mode 1	9.18	0.0128	0.275
mode 2	54.24	0.0308	0.865
mode 3	145.72	0.0140	0.192
mode 4	259.82	0.0155	-0.014

3.5.3 Experimental Hybrid Control

Implementation of the experimental hybrid control system involved using the AJT controller as reported in section 3.2.3 and the RMA controller as reported in section 3.5.2. A schematic of the controller is presented in figure 3.18. The dc offset to the approximate integrators was necessary to counter slight bias in the accelerometer signals resulting from the measurement of a small component of gravity.

Time responses were obtained by driving the truss at the respective modal frequencies and then switching both the RMA control circuits and the AJT control circuits on at the same time. The modal time responses are shown in figure 3.17. As predicted by the non-linear simulation reported in section 3.4 and by the research performed by Hallauer on the USAFA truss [8], the damping of the first, second, and third bending modes is increased. The AJTs and RMAs work particularly well at damping mode-2 vibration. The AJT still misfires during mode-4 excitation, but the RMAs seemed to have kept the AJTs from misfiring during mode-3 vibration suppression. The RMAs thus appear to assist the AJTs at the higher modes. The fourth mode appears to be positively affected by the addition of the RMAs to the control scheme as well compared to the AJTs acting alone. Also, the mode-1 damping appears cleaner when compared to the AJT-only control in figure 3.5. The RMAs probably damp out the high frequency noise caused by the bang-bang control of the AJTs. The damping ratios are shown in figure 3.13.

The damping ratios were higher than the levels of damping achieved by either controller acting independently except for the fourth mode which is adversely affected

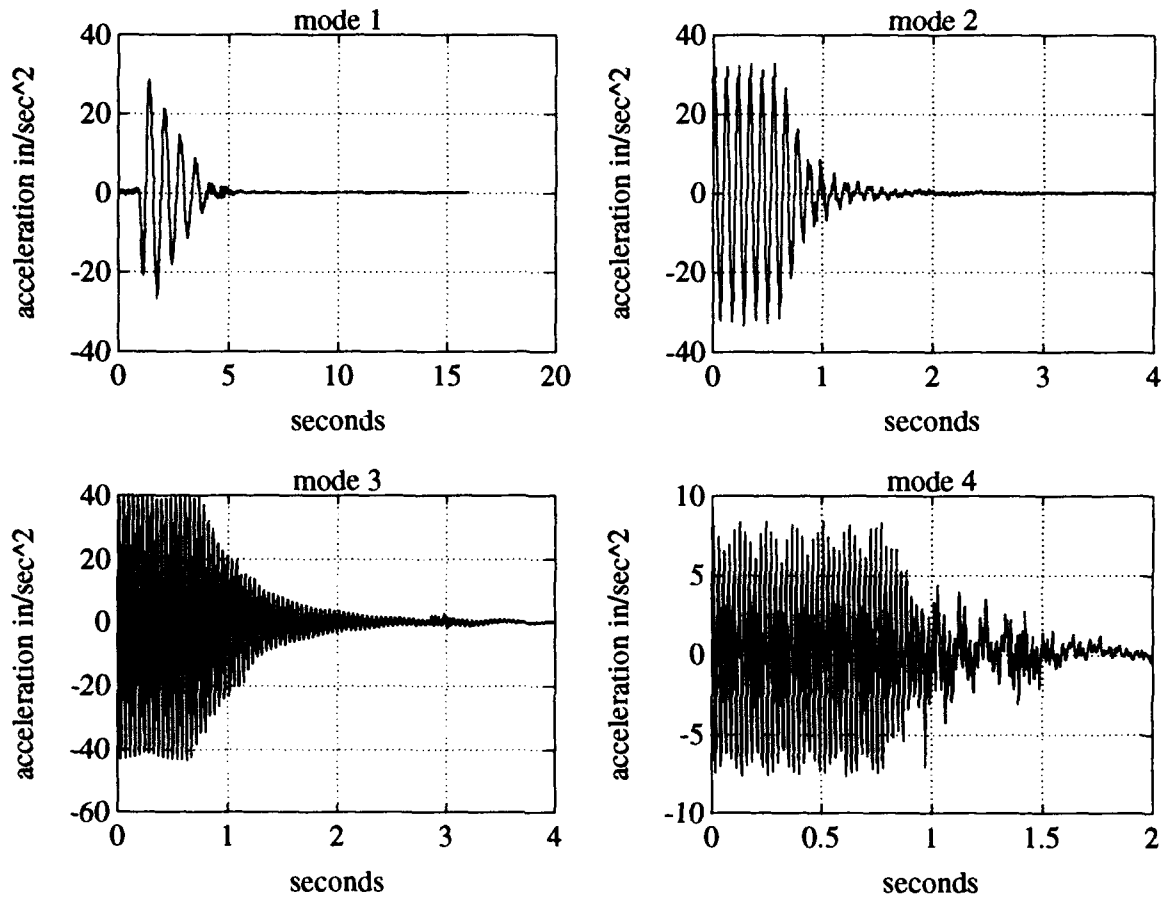


Figure 3.17: Experimental hybrid control truss tip time responses

by misfirings of the AJTs.

3.6 Classical Control Summary

The use of classical control techniques is effective for vibration suppression of the planar bending modes of the UWAA truss. The levels of damping achieved using the techniques presented in this study fall short of achieving the goal of 10% of modal damping desired in large space structures, but still increased the damping of mode-1 by nearly a factor of 10, the mode-2 damping by more than a factor of ten, and quadruples the level of damping of the third mode.

Furthermore, the results of this chapter show the validity of the modeling of chapter

Table 3.13: Experimental closed loop modal data: hybrid actuation

	frequency (rad/sec)	damping ratio	$\log \left[\frac{\zeta}{\zeta_{openloop}} \right]$
mode 1	9.18	0.0555	0.912
mode 2	54.24	0.0900	1.33
mode 3	145.72	0.0327	0.560
mode 4	259.82	AJT misfires	na

two. The non-linear simulation was at all times consistent with the hardware with two exceptions: the failure to predict the actuator/instrumentation instability in the RMAs and the misfiring of the AJTs when controlling the third and fourth modes of the truss. The performance of the simulation was in general slightly better than the experimental results. This may be attributed to non-linearities not accounted for in the modeling of the truss and the actuators and ignoring the effects of noise in the system.

It appears that the goal of 10% modal damping is within the reach of given actuators using classical control techniques for the first, second, and third modes. Tuning of the natural frequencies of the RMAs, addition of filters to the AJT control circuit, and the choice of actuator location could make the 10% damping goal a reality.

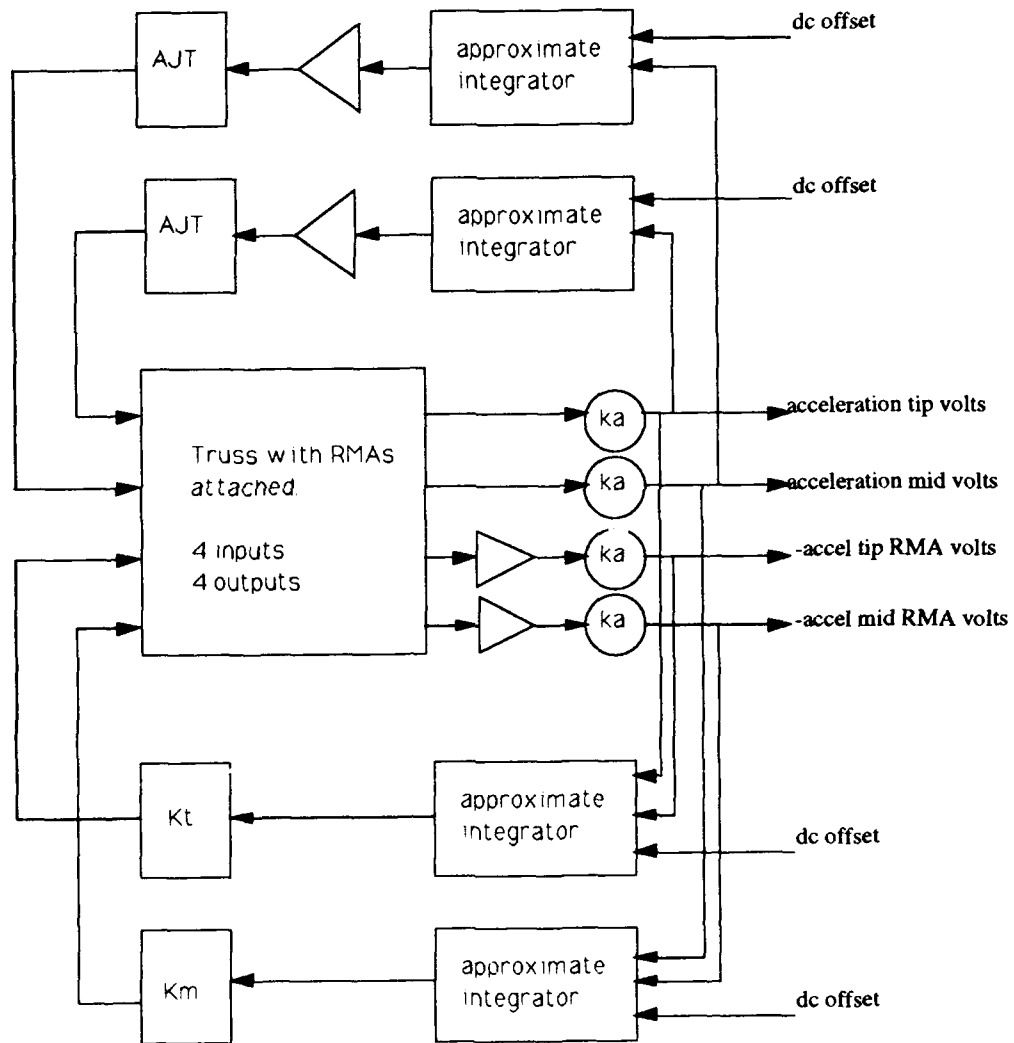


Figure 3.18: Hardware block diagram for hybrid actuation

Chapter 4

OPTIMAL CONTROL STRATEGIES

4.1 Overview

Chapter three reported the design and testing of a classical multiple-input, multiple-output hybrid actuation controller which delivered appreciable increases in damping of the lateral bending modes of the UWAA planar truss. In this chapter the application of linear quadratic Gaussian techniques to design a full state feedback controller for the reaction mass actuators is discussed, along with the non-linear simulation of a state feedback RMA controller working together with the air jet thruster's velocity controller previously discussed in chapter three.

4.2 LQG Design Problem

The solution of the linear quadratic Gaussian problem is well understood[13]. Given the plant model in state-space form:

$$\begin{aligned}\dot{x} &= Ax + Bu + \Gamma w \\ y &= Cx + v\end{aligned}\tag{4.1}$$

where w and v are zero-mean Gaussian stochastic processes (commonly referred to as white noises) assumed to be uncorrelated such that:

$$E\{wv^T\} = 0\tag{4.2}$$

The problem is then to form a feedback control law which minimizes the cost function [13]:

$$J = \frac{1}{2} \lim_{t \rightarrow \infty} E\left\{ \int_0^t (z^T Q z + u^T R u) dt \right\}\tag{4.3}$$

and z is a combination of the states given by:

$$z = Mx \quad (4.4)$$

Q is a positive semi-definite weighting (penalty) matrix on the linear combinations of the state variables and R is a positive definite weighting matrix on the control inputs. The problem at this point breaks down into two sub-problems: estimating the state using Kalman-filter theory and finding the control signal which minimizes the cost of equation 4.3. Here is where some assumptions are made to simplify the design and simulation for the UWAA planar truss reaction mass actuator controllers.

4.2.1 Optimal Controller Design

For the application of the optimal control design techniques to the UWAA planar truss RMA controller, several assumptions were made. First, the design is to be tested only in simulation as the applicable hardware is not available at this time to implement a controller with its own dynamics. Since the design is to be tested only in simulation, it was assumed that all the states were available for feedback thus eliminating the need for an estimator design. In practice, this could be accomplished with two more accelerometers mounted at the truss 3/4 point and 1/4 point and the use of integrating circuits, but would probably prove to be impractical. However, the goal of the research in this chapter is just to indicate the degree of performance one may expect from the added complexity of an optimal controller; future implementation problems will need to be solved later.

The second assumption is to ignore noise of the accelerometer sensors and reaction mass actuators. Although noise problems crept up in the experimental application of control laws in chapter three, in the simulation no provisions are made for noise injection to the sensors and actuators. Thus, we may measure performance gains in eigenvalue damping but lack some of the reality noise effects bring to the simulation. Without the inclusion of noise the LQG/Loop Transfer Recovery technique is likewise not available as a design tool. Future designs for an optimal controller will have to include noise.

Thus, we are left with the same twelfth order plant model developed in section 2.3.1:

$$\dot{x} = A_{12}x + B_{12}u \quad (4.5)$$

where the states are defined as

$$x = \begin{pmatrix} x_1 \\ x_2 \\ x_3 \\ x_4 \\ x_5 \\ x_6 \\ x_7 \\ x_8 \\ x_9 \\ x_{10} \\ x_{11} \\ x_{12} \end{pmatrix} = \begin{pmatrix} \dot{q}_{tip} \\ \dot{q}_{3/4} \\ \dot{q}_{mid} \\ \dot{q}_{1/4} \\ \dot{q}_{ta} \\ \dot{q}_{ma} \\ q_{tip} \\ q_{3/4} \\ q_{mid} \\ q_{1/4} \\ q_{ta} \\ q_{ma} \end{pmatrix} \quad (4.6)$$

The control inputs are likewise given to be:

$$u = \begin{pmatrix} u_1 \\ u_2 \end{pmatrix} = \begin{pmatrix} f_{b(tip)} \\ f_{b(mid)} \end{pmatrix} \quad (4.7)$$

The control signal will be given by the feedback law:

$$u = -K_c x \quad (4.8)$$

where K_c is the state-feedback matrix [13] and satisfies the deterministic cost function [12]:

$$J = \frac{1}{2} \int_0^{\infty} (z^T Q z + u^T R u) dt \quad (4.9)$$

or

$$J = \frac{1}{2} \int_0^{\infty} \left[\sum_{i=1}^p Q_{ii} z_i^2 + \sum_{i=1}^m R_{ii} u_i^2 \right] dt \quad (4.10)$$

To solve for K_c it is recognized that equation 4.8 may be rewritten as [13]:

$$u = -R^{-1} B^T P_c x \quad (4.11)$$

where $K_c = R^{-1}B^T P_c$ and P_c satisfies the algebraic Riccati equation [13]

$$A^T P_c + P_c A - P_c B R^{-1} B^T P_c + M^T Q M = 0 \quad (4.12)$$

The closed loop system is guaranteed to be asymptotically stable for a stabilizable through u and detectable through z system. Furthermore, as the control penalty weight R is reduced to zero, perfect regulation with infinite control is achieved for our minimum phase system [12]. The problem of design rests only with choosing the proper values for the Q and R weighting matrices. To help make a logical choice for the weighting matrices Bryson's rules were applied as follows [12].

Bryson's rules for selecting the diagonal elements Q_{ii} and R_{ii} are

$$Q_{ii} = \frac{1}{z_{imax}^2} \quad (4.13)$$

and

$$R_{ii} = \frac{1}{u_{imax}^2} \quad (4.14)$$

where z_{imax} and u_{imax} are the maximum allowable excursions in z_i and u_i [12]. The transformation matrix M in equation 4.4 was chosen to be equal to an eighth order identity matrix, thus equating z with the states x . The penalty weights are thus associated with exactly one state each¹. The weighting values were chosen by choosing the maximum excursions for truss velocity states to be 0.1 in/sec and to be 0.01 inches for the truss displacement states. The reaction mass actuator velocity states were chosen to have limits of 1.0 in/sec and limits on the displacement states equal to

¹ Another scheme was successfully chosen to pick the transformation matrix z which put penalties on the truss accelerations at the four truss locations and on the two RMA displacement states. The transformation matrix had the form

$$M = \begin{bmatrix} a_{11} & a_{12} & \cdots & a_{1,11} & a_{1,12} \\ a_{21} & a_{22} & \cdots & a_{2,11} & a_{2,12} \\ a_{31} & a_{32} & \cdots & a_{3,11} & a_{3,12} \\ a_{41} & a_{42} & \cdots & a_{4,11} & a_{4,12} \\ 0 & 0 & \cdots & 1 & 0 \\ 0 & 0 & \cdots & 0 & 1 \end{bmatrix} \quad (4.15)$$

The results obtained were similar to those obtained using the states as the penalized variables for gain matrices of similar magnitude.

the maximum throw of the actuators at 0.1 inches of travel as given in section 2.3.1. The resulting diagonal elements of the penalty matrix are shown in table 4.1.

Table 4.1: Penalty weights on the states

state	Q_{ii}	z_{imax}	$\frac{1}{z_{imax}^2}$	state	Q_{ii}	z_{imax}	$\frac{1}{z_{imax}^2}$
q_{tip}	Q_{11}	0.1	100	q_{tip}	Q_{77}	0.01	10000
$q_{3/4}$	Q_{22}	0.1	100	$q_{3/4}$	Q_{88}	0.01	10000
q_{mid}	Q_{33}	0.1	100	q_{mid}	Q_{99}	0.01	10000
$q_{1/4}$	Q_{44}	0.1	100	$q_{1/4}$	$Q_{10,10}$	0.01	10000
q_{ta}	Q_{55}	1.0	1	q_{tip}	$Q_{11,11}$	0.1	100
q_{tm}	Q_{66}	1.0	1	q_{tip}	$Q_{12,12}$	0.1	100

The penalties on the control inputs were chosen initially using Bryson's rules to limit the input signal to the amplifier (set at unity gain) to maximum excursion of one. This selection of a penalty resulted in an abnormally high values in the state feedback gain matrix K_c . After some trial and error to limit the magnitudes of the individual feedback gains to under ten, the penalties in the R matrix were chosen to be the values presented in table 4.2 Solving the algebraic Ricatti equation given by equation 4.12

Table 4.2: Penalty weights on the control inputs

input	R_{ii}	u_{imax}	$\frac{1}{u_{imax}^2}$
$f_{b(tip)}$	R_{11}	0.0632	250
$f_{b(mid)}$	R_{11}	0.0632	250

results in the gain matrix K_c , the numerical values of which are given in appendix B.1. The magnitude of the largest gain is less than ten, which when the accelerometer scale factor is introduced, is under 100. This was seen as a reasonable limit for implementation. The problem with the instrumentation instability of section 3.5.2 would be avoided as the gains assume unity gain for the amplifier, well below the instability threshold of amplifier gain observed at gains of seven or greater.

4.3 Performance of the Linear Optimal RMA Controller through Simulation

4.3.1 Linear Frequency Response

The RMA-optimal controller was tested using the linear simulation of the AJT forced RMA-controlled truss model. The frequency response in figure 4.1 shows the amount of vibration suppression that the optimal RMA controller introduced to the system. Mode-1 suppression was 8.67 dB, mode-2 suppression was 11.14 dB, and mode-3 suppression was 4.09 dB. There was no appreciable suppression of the the fourth mode vibrations indicated by the frequency response plot.

4.3.2 Non-linear Simulation of Modal Time Responses

Modal time responses of the truss model equipped with the RMA optimal controller were generated using non-linear simulation of the system by driving the RMA-augmented truss model with the AJTs at the natural frequencies. The optimal controller was switched on. When the level of modal excitation was approximately the same level as that used in section 3.5, the AJTs were switched off and the linear simulation decay of the individual modes was recorded. The eigenvalues of the linear system are reported in table 4.3.

Table 4.3: Linear model modal data: optimal RMA controller

	frequency (rad/sec)	damping ratio	$\Delta\zeta$ vs. open loop
mode 1	9.19	0.0193	0.453
mode 2	58.387	0.0837	1.299
mode 3	145.56	0.0158	0.245
mode 4	260.27	0.0187	0.067
RMA	40.41	0.10487	0.146
RMA	43.19	0.12170	0.195

Compared to the classically designed RMA controller of section 3.3.4, the damping of the first, second, and third modes were increased by a greater amount. Mode-4 damping, however, was greater for the classically designed controller. The optimal

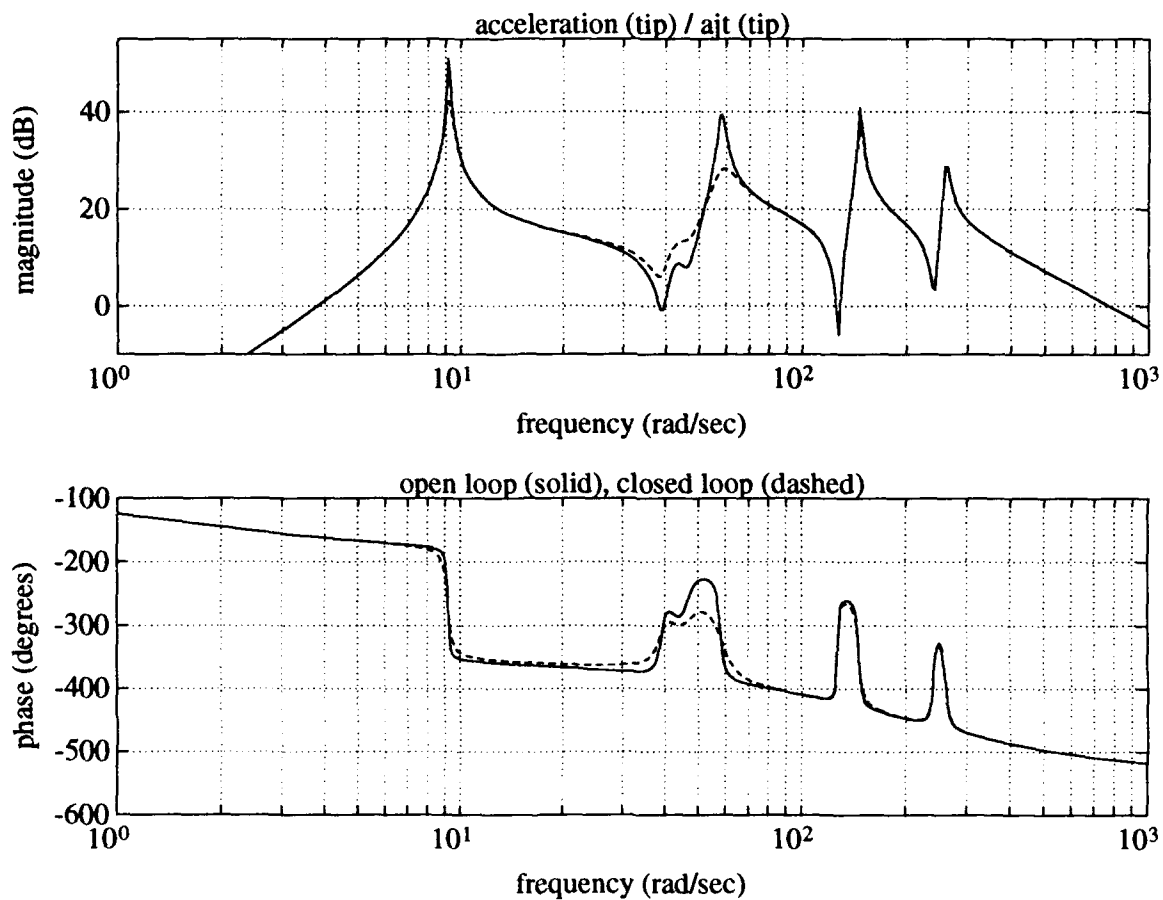


Figure 4.1: Linear simulation of the optimal-RMA controller for vibration suppression

controller does not decrease the damping in any of the modes as was the case with the classical controller. However, this was not noticed as a problem for the classical controller once hybrid actuation was introduced.

4.4 Non-Linear Simulation of the Hybrid Classical-AJT/Optimal-RMA Controller

Hybrid actuation was used with success for the classically designed systems of chapter three which all employed velocity feedback without any crossfeeds. The 'piggy-back' approach running the AJT controllers on top of the RMA controlled system was

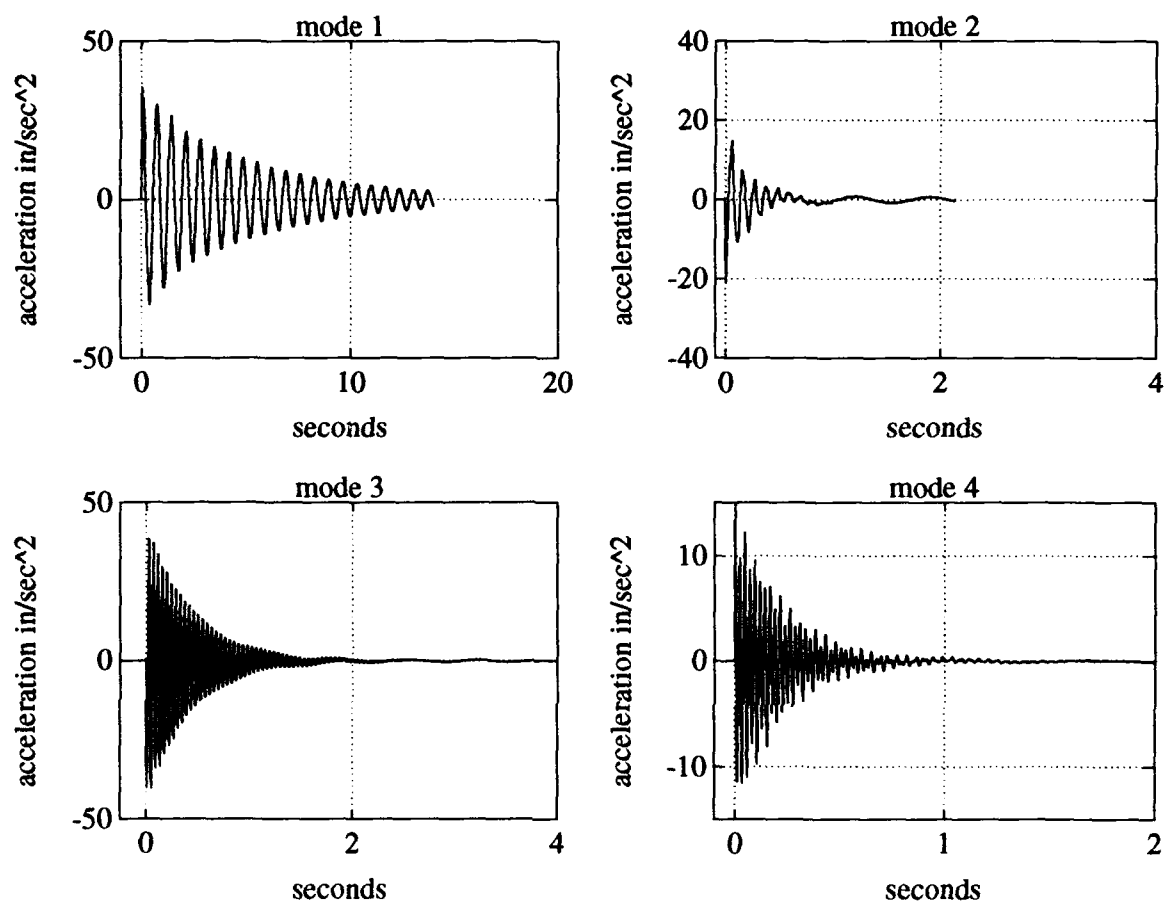


Figure 4.2: Non-linear simulation modal time responses: RMA optimal controller

accepted as a valid approach for control. The question remaining was if hybrid 'piggy back' control would work for a true MIMO system with crossfeed terms.

The non-linear simulation was performed in the manner common to this thesis by exciting the truss model with the AJTs at each mode with the RMA-optimal controllers already switched on. For hybrid control, the AJTs were switched from exciting the truss to the control velocity feedback circuit discussed in section 3.2.3 while the RMA-optimal controller was left on switched on. The modal time responses are presented in figure 4.3.

The mode-1 time response shows a significant gain over the independent RMA-optimal controller system in section 4.3.2. The three remaining modes show little

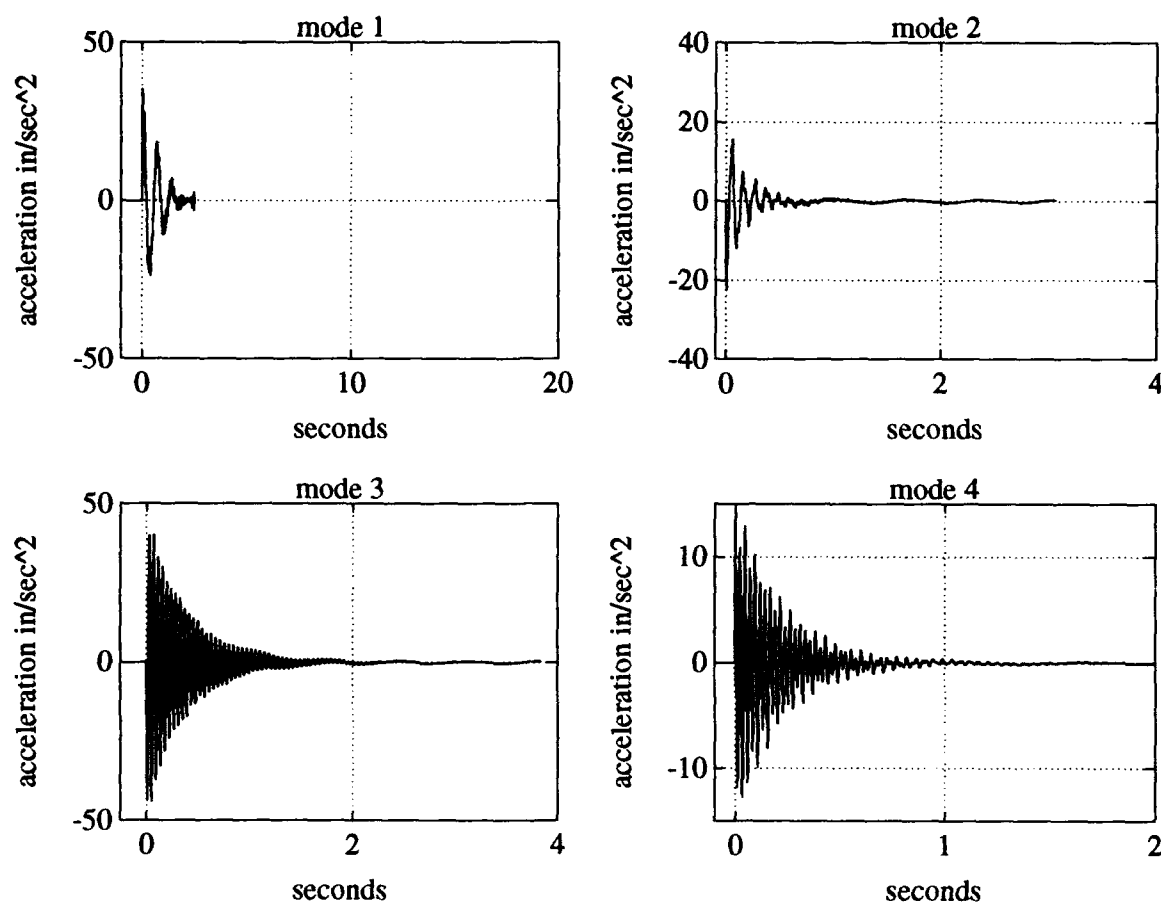


Figure 4.3: Modal time responses hybrid classical-AJT/optimal-RMA controller

change. The damping ratios were calculated and are presented in table 4.4. The damping ratios do indicate that the hybrid controller only significantly effects the first mode. The mode-1 damping ratio is 0.1280, well above the elusive 10% goal for large space structures. Although the simulation generally proved to have better performance than the actual experimental systems in chapter three, there is significant room for a decrease in performance should the optimal controller be experimentally implemented.

Table 4.4: Closed loop modal data: hybrid classical-AJT/optimal-RMA controller

	frequency (rad/sec)	damping ratio	$\Delta\zeta$ vs. open loop
mode 1	9.19	0.1280	1.275
mode 2	58.387	0.0823	1.292
mode 3	145.56	0.0147	0.213
mode 4	260.27	0.0136	-0.070

4.5 Optimal Control Conclusions

Optimal control design for the RMAs yields a system which does not sacrifice mode-1 damping when damping the higher modes is the main benefit apparent for the optimal controller of this chapter. The feedback gains in this section are larger than the gains in the classical system, but in experimental application would be applied in the computer hardware, not at the amplifier, so instrumentation/actuator instability should not occur. For experimental application, an estimator design and the inclusion of sensor and actuator noise should be included in the LQG design process.

The piggy-back approach is again a valid technique for application of hybrid actuation using velocity feedback AJT controllers on board the optimally designed RMA-controlled planar truss for vibration suppression. The failure of the hybrid controller to change the damping of the second, third, and fourth modes over the optimally controlled system is disappointing. Another approach might be applied in lieu of the piggy-back approach which provides for non-linear optimization of the AJTs in conjunction with the RMAs.

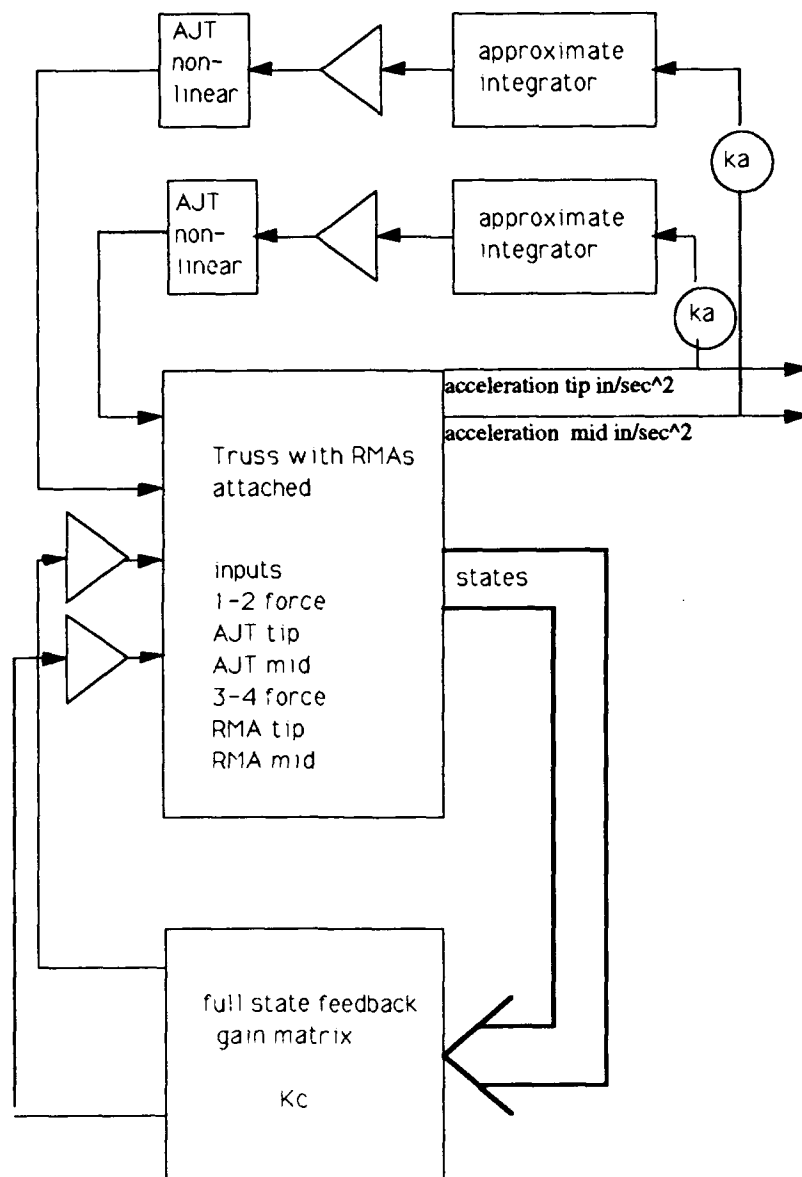


Figure 4.4: Non-linear block diagram for hybrid classical-AJT/optimal-RMA Controller (state model of truss in section A.2)

Chapter 5

CONCLUSIONS AND RECOMMENDATIONS

5.1 Overview

In this paper the set up, modeling, and control of the UWAA planar truss testbed is described. This chapter lists the conclusions made based upon the work performed for this study. Recommendations for future research on the UWAA planar truss testbed are also included.

5.2 Conclusions

The purpose of this paper has been to report the investigation of different control laws for vibration suppression of the UWAA planar truss via the available means of actuation, the air jet thrusters and the reaction mass actuators. The following tasks have been accomplished.

- Accurate linear and non-linear models of the two forms of space realizable actuation, the RMAs and the AJTs, have been formed and validated.
- The existing open loop truss model has been validated, and the augmentation of the truss model with the RMAs defined. Comparison with the USAF Academy truss, upon which the UWAA truss is based, is also reported.
- An array of classical control techniques applied to the vibration suppression problem was investigated. The goal of 10% structural damping is nearly reached via hybrid control, the use of the two means of actuation together.
- The optimal controller design problem has been formulated. Although satisfactory simulation results were obtained using optimal-LQG controlled RMAs in conjunction with classically controlled AJTs, there exists the need to account

for the non-linearities in the optimization problem. The optimal-control solution of this paper does not provide for much higher levels of damping than the classically designed hybrid controller.

- The set up of the working truss hardware is explained and the modeling/hardware validation will serve as a baseline for future studies. Computer non-linear simulation is shown to accurately reflect the results achieved using the hardware in experimental application. The computer work files are available on line in the truss directory at the University of Washington [21].

5.3 Recommendations For Future Research on the UWAA Planar Truss

The next step for future study should be the implementation of the control laws reported in this thesis through the use of a digital controller such as LABVIEW or other I/O capable software/hardware packages. The use of a digital controller allows for flexibility in implementing several different control laws quickly and accurately, and later would allow for the implementation of high order optimal linear control laws or non-linear control laws.

The UWAA truss would serve as an ideal platform to test other finite element model codes. Modeling of the non-linear joints of truss structures along with the incorporation of both viscous and coulomb damping terms in the finite element code was performed by W. Keith Belvin of Langley Research Center [3]. The joints are reported to have a dead band (different from the AJT dead band of this thesis) within which a joint may be made to move with nearly zero applied force. This modeling of the truss indicated that joints lower the overall stiffness of the truss and introduce additional damping terms, substantially affecting the low frequency vibrational response. A non-linear model for the truss would be an ideal intermediate step when progressing from the testing of controllers on linear models to actual experimental implementation.

A parametric study testing the effectiveness of other actuator and sensor locations rather than the truss tip and midpoint would be valuable. Noting that it is time consuming to reconfigure the hardware, most of the study could be performed via simulation, the results of which could then be validated through the use of the

hardware.

Another RMA might be built and should incorporate such features as user variable stiffness and damping terms through the use of electronic feedback instead of the present preset flexible structure. A detailed study might be performed where the specifications for the RMA to include the throw, proof mass, range of required damping and stiffness, and location (probably tip for one RMA) are all identified *before* the construction of the actuator is approved. This would rectify many of the limitations of the current RMAs.

The optimal control problem for the RMA-augmented truss could be performed in a parametric study. LQ techniques which include the state-estimator design, H_2/H_{inf} methodology, and SANDY design all need to be explored. Once the digital controller is operational, all of these controllers would be easy to experimentally implement in the truss hardware.

A difficult problem would be to develop an optimized solution for the non-linear AJTs. An easier first step might be to design and construct an AJT with linear characteristics and to develop the optimal control problem from there. True optimal hybrid control would thus be achieved.

The existing truss and actuator models, hardware, and simulation should serve as a baseline for studies in advanced hybrid actuation techniques as well as multi-input multi-output control law studies. The truss hardware allows for the incorporation of active truss members in place of the ordinary structural members. Current research at NASA's Jet Propulsion Laboratory in Pasadena [4] is being conducted utilizing active structural members with *piezoelectric actuators and colocated force and vibrational-velocity sensors*. The control laws are designed to control the mechanical impedance of the truss members. The mechanical impedance is defined as the Laplace transform of the ratio between the axial force applied to the member and the difference between the velocities of its ends and is analogous to electrical output impedance. Ideally, creating the complex conjugate of the entire structure's impedance with the active members through the use of control laws dissipates the energy at a maximum rate and hence provides for the greatest level of damping. If the UWAA planar truss could be made to shed energy in this way, the next step would be to incorporate hybrid control by including the AJTs in the analysis. Further research as to the optimum placement of active structural members could also be performed.

Large space structures will have an additional constraint besides lightweight as the cost of shuttle flights increase, that is to minimize astronaut extra-vehicular activity (EVA) time. Research ideas which involve leading edge technologies are hypothesized here to meet the constraint of limited EVA time. Trainable alloys which change shape when a small current is applied might be introduced to the truss structure. Lightweight and simple, trainable alloys might replace the current structural member actuators used today. A move towards embedded sensors in the structure to replace accelerometers mounted externally would again simplify construction of a structure in space and decrease weight. Lightweight fiber optic relay systems would increase reliability of sensor signals.

Finally, an intelligent control system which could learn characteristics of various truss configurations and generate controllers would replace the need for current gain scheduling routines of different truss configurations. The UWAA planar truss hardware is fully modular so that appendages could easily be added to test adaptive control schemes.

BIBLIOGRAPHY

- [1] Adams, R.J. Controller Design for a Laser Steering Mirror on a Flexible Structure. M.S. thesis, University of Washington, 1990.
- [2] Barker, K.J. Toward the Robust Control of High Bandwidth High Precision Flexible Optical Systems. Ph D thesis, University of Washington, 1991.
- [3] Belvin, W.K. Dynamic Analyses Including Joints of Truss Structures. *NASA Tech Briefs*. Dec. 1991, p.62.
- [4] Chen, G.S., Garba, J.A., Wada, B.K. Two Techniques for Suppressing Vibrations in Structures. *NASA Tech Briefs*. Dec. 1991, p.61-62.
- [5] Frederick, D.K. and Rimer, M. Benchmark Problems for CACSD Packages. *Abstracts of the Second Symposium on Computer-Aided Control System Design of the IEEE Control System Society*. Santa Barbara, CA, March 1985.
- [6] Fuller, D.C., Shepherd, M.J. and Zeigler, M.L. Parametric Study of Passively Damped Diagonals in a Large Space Structure, Flight Dynamics Laboratory, Wright Research and Development Center, WPAFB, OH, WRDC-TM-89-192-FIBG, September 1989.
- [7] Gross, H.N., Lechgar, E.H. and Skeen, M.E. Development of a Laser Pointing and Tracking System. AAS 90-021, *13th Annual AAS Guidance and Control Conference, Keystone, CO*, February 3-7, 1990.
- [8] Hallauer, W.L. Jr. and Lamberson, S.E. Experimental Active Vibration Damping of a Plane Truss Using Hybrid Actuation. AIAA Paper 89-1169, *30th Structures, Structural Dynamics and Materials Conference, Mobile, AL*, April 3-5, 1989.

- [9] Hughes, R.O. Conceptual Design of Pointing Control Systems for Space Station Gimbaled Payloads. AIAA Paper 86-1986, August, 1986.
- [10] Inman, D. J. Control/Structure Interaction: Effects of Actuator Dynamics. *Mechanics and Control of Large Flexible Structures*. ed Junkins, J.L., AIAA Inc, vol 129, 1990.
- [11] Juang, J.N. Optimal Design of a Passive Vibration Absorber for a Truss Beam. *Journal of Guidance, Control, and Dynamics* Vol.7, No.6, Nov.-Dec.1984,pp 733-739.
- [12] Ly, U.L. Lecture Notes / 518. Spring 1991. University of Washington, Seattle.
- [13] Maciejowski, J.M. *Multivariable Feedback Design*. Addison-Wesley Publishing Co., Wokingham, England. 1989.
- [14] Meirovitch, L. *Analytical Methods in Vibrations*. Macmillan Publishing Co., Inc. New York. 1967.
- [15] Miller, D.W. and Crawley, E.F. Theoretical and Experimental Investigation of Space-Realizable Inertial Actuation for Passive and Active Structural Control. *Journal of Guidance, Control, and Dynamics*. Vol.33, No.5, Sept.-Oct.1988,pp 449-457.
- [16] Ogata, K. *Modern Control Engineering*. Prentice-Hall, Inc., Englewood Cliffs, N.J. 1970.
- [17] Schulthess, M.R. Controller Design for a Laser Steering Mirror on a Flexible Studies in Dynamic Characterization and Control of a Flexible Structure and Optical Beampath. M.S. thesis, University of Washington, 1991.
- [18] Shepherd, M.J. Damping Characteristics of the 20-Bay Truss. Senior Paper, EM499, U.S. Air Force Academy, 1990.
- [19] SIMULAB/MATLAB version 3.5e MathWorks, Inc. Natick, Massachusetts. 24 July 91.

- [20] Thompson, W.T. *Theory of Vibration with Applications*. Prentice-Hall, Inc., Englewood Cliffs, N.J. 1988.
- [21] Unix Simulab Work Files. University of Washington Computer Account, controls@aa.washington.edu. 1991.
- [22] Wong, E. Rathbun, D. and Smith, K. *A Pointing System Design Concept for Space Station Attached Payloads*. AIAA 89-3513, 1989.
- [23] Zimmerman, D.C., Horner, G.C., and Inman, D.J. Microprocessor Controlled Force Actuator, *Journal of Guidance, Control, and Dynamics* Vol.11, No 3, May-June 1988, pp. 230-236.

Appendix A

TRUSS LINEAR STATE SPACE MODELS

This appendix contains the numerical values for the two truss models used in this thesis. The models are an eighth order model for the truss without actuators attached and a twelfth order model for the truss with RMAs attached to the truss midpoint and truss tip.

A.1 Open Loop Truss Model Without Actuators Attached

The open loop model for the truss dynamics is written as

$$\dot{x} = A_8x + B_8u \quad (\text{A.1})$$

The states are the truss station inertial velocities in inches per second and inertial displacements in inches. The state vector is

$$x = \begin{pmatrix} x_1 \\ x_2 \\ x_3 \\ x_4 \\ x_5 \\ x_6 \\ x_7 \\ x_8 \end{pmatrix} = \begin{pmatrix} \dot{q}_{tip} \\ \dot{q}_{3/4} \\ \dot{q}_{mid} \\ \dot{q}_{1/4} \\ q_{tip} \\ q_{3/4} \\ q_{mid} \\ q_{1/4} \end{pmatrix} \quad (\text{A.2})$$

Only the force inputs for the truss tip and truss midpoint are retained since that is where the AJTs were located. The input vector is scaled in lbf. and is written as

$$u = \begin{pmatrix} u_1 \\ u_2 \end{pmatrix} = \begin{pmatrix} f_{tip} \\ f_{mid} \end{pmatrix} \quad (\text{A.3})$$

The outputs were chosen based on what was available from the truss hardware. For the accelerometers mounted at the tip and midpoint measuring the lateral accelerations at those two locations the output state space equations may take on the form:

$$y = \begin{bmatrix} a_{11} & a_{12} & \cdots & a_{18} \\ a_{31} & a_{32} & \cdots & a_{38} \end{bmatrix} x + \begin{bmatrix} 0 & 0 \\ 0 & 0 \end{bmatrix} u \quad (\text{A.4})$$

The numerical values which comprise the A and B state matrices are:

$A_8 =$

$$\begin{bmatrix} -1.4731 & 3.2908 & -2.7590 & 1.1269 & -11,358 & 27,361 & -22,563 & 9095.9 \\ 1.1450 & -3.1484 & 2.8300 & -1.2085 & 9551.3 & -25,162 & 23,264 & -9693.1 \\ -0.69798 & 2.4674 & -3.5871 & 2.4496 & -5689.0 & 20,316 & -28,721 & 20,166 \\ 0.18168 & -1.0198 & 2.4646 & -3.3488 & 1408.8 & -8189.2 & 20,306 & -27,067 \\ 1 & 0 & 0 & 0 & 0 & 0 & 0 & 0 \\ 0 & 1 & 0 & 0 & 0 & 0 & 0 & 0 \\ 0 & 0 & 1 & 0 & 0 & 0 & 0 & 0 \\ 0 & 0 & 0 & 1 & 0 & 0 & 0 & 0 \end{bmatrix}$$

$B_8 =$

$$\begin{bmatrix} 15.0207 & 0.75580 \\ -2.0949 & -0.18716 \\ 0.75580 & 6.3577 \\ -0.29383 & 0.04895 \\ 0 & 0 \\ 0 & 0 \\ 0 & 0 \\ 0 & 0 \end{bmatrix}$$

A.2 Open Loop Truss Model with RMAs Attached at Midpoint and Tip

The open loop model for the truss dynamics with the RMAs attached at the truss tip and truss midpoint is written as

$$\dot{x} = A_{12}x + B_{12}u \quad (\text{A.5})$$

The state vector is

$$x = \begin{pmatrix} x_1 \\ x_2 \\ x_3 \\ x_4 \\ x_5 \\ x_6 \\ x_7 \\ x_8 \\ x_9 \\ x_{10} \\ x_{11} \\ x_{12} \end{pmatrix} = \begin{pmatrix} \dot{q}_{tip} \\ \dot{q}_{3/4} \\ \dot{q}_{mid} \\ \dot{q}_{1/4} \\ \dot{q}_{ta} \\ \dot{q}_{ma} \\ q_{tip} \\ q_{3/4} \\ q_{mid} \\ q_{1/4} \\ \dot{q}_{ta} \\ \dot{q}_{ma} \end{pmatrix} \quad (\text{A.6})$$

The truss stations' velocities and displacements have the same variable labels as in section A.1. The two new variables, q_{ta} and q_{ma} are the relative displacements at the truss tip and truss midpoint between the tip and midpoint proof mass positions and the corresponding truss stations. The displacements are in inches. The velocities are in inches per second.

The first two force inputs for the truss tip and truss midpoint are retained since that is where the AJTs were located. Inputs three and four are the forces applied to both the truss station and the proof mass at each of the respective stations. The input vector is scaled in lbf. and is written as

$$u = \begin{pmatrix} u_1 \\ u_2 \\ u_3 \\ u_4 \end{pmatrix} = \begin{pmatrix} f_{tip} \\ f_{mid} \\ f_{b(tip)} \\ f_{b(mid)} \end{pmatrix} \quad (\text{A.7})$$

The outputs were chosen based on what was available from the truss hardware similar to what is reported in section A.1. For full state feedback an identity matrix was used for C and a zero matrix for D in the modeling.

The numerical values which comprise the A and B state matrices are:

$A_{12} =$
columns 1 through 6

$$\begin{bmatrix} -1.4731 & 3.2908 & -2.7590 & 1.1269 & 0.912440 & 0.049127 \\ 1.1450 & -3.1484 & 2.8300 & -1.2085 & -0.12569 & -0.012165 \\ -0.69798 & 2.4674 & -3.5871 & 2.4496 & 0.045348 & 0.41325 \\ 0.18168 & -1.0198 & 2.4646 & -3.3488 & -0.017630 & 0.0031818 \\ 1.4731 & -3.2908 & 2.7590 & -1.1369 & -7.0818 & -0.049127 \\ 6.9798 & -2.4674 & 3.5871 & -2.4496 & -0.045348 & -7.08032 \\ 1 & 0 & 0 & 0 & 0 & 0 \\ 0 & 1 & 0 & 0 & 0 & 0 \\ 0 & 0 & 1 & 0 & 0 & 0 \\ 0 & 0 & 0 & 1 & 0 & 0 \\ 0 & 0 & 0 & 0 & 1 & 0 \\ 0 & 0 & 0 & 0 & 0 & 1 \end{bmatrix}$$

Appendix B

FULL STATE FEEDBACK GAIN

B.1 Optimal Control Gain K_c

$$K_c^T = \begin{bmatrix} 1.5523e-1 & 2.0046e-1 \\ 6.9095e-1 & 1.8848e-1 \\ 4.1918e-1 & -1.8663e-1 \\ 3.6230e-2 & -2.9339e-2 \\ 1.0046e-1 & -4.4728e-3 \\ -3.9297e-3 & 5.5639e-2 \\ -4.6436e-00 & 3.6697e-00 \\ 1.7244e-00 & -5.1648e-1 \\ 7.7796e-2 & -8.6408e-00 \\ 7.4760e-2 & -2.6993e-00 \\ 1.2032e-2 & -5.3007e-2 \\ 5.7819e-2 & 1.1015e-2 \end{bmatrix} \quad (\text{B.1})$$

Appendix C

EQUIPMENT LIST

This appendix contains a partial listing of the equipment used in the research reported in this thesis. The list is by no means all-inclusive but gives a good idea as to what hardware is required to set up the planar truss experiment. Manufacturer information are included in boldface for applicable items.

C.1 Truss Hardware

- Meroform 522117 tube-m 0.353 22M12 alum E6-CO (61)

MERO Structures, Inc.
N112 W1880 Mequon Road
Germantown, WI 53022
phone: (414)255-6553

- Meroform 522218 tube 0.500-m 22M12 alum E6-CO (20)
- Meroform 510018 std. node M12 Chrome (42)
- 3/8 in-dia steel ball bearings (40+6 for RMAs)
- Level table 4'x8' top (3)

C.2 Custom Fabricated Truss Hardware

- Steel table for cantilever support
- Cantilever mounting point (box beam)
- Steel battens (20)

- 1 7/8 x 4 in stainless steel type 301 sheets (40+)
- Accelerometer housings

C.3 Air Jet Thruster Hardware

- Solenoid valve MAC:113B551BAAA (4)

Fiero Fluid Power Inc.

10515 East 40th Ave.

Denver, CO 80239

phone: (303) 373 - 2600

- Polyvinyl tubing 1/4 in-inner dia 3/8 in-outer dia (80 feet)
- Brass nozzle (hose barb) 1/4 in i.d. x 1/4 in in. MIP (12)
- 65-psig regulated compressed air supply

C.4 Custom Fabricated Air Jet Thruster Hardware

- Manifold (for delivery of compressed air to individual AJTs)

C.5 Reaction Mass Actuator Hardware

- LDS V102 vibration generator (2)

Ling Dynamic Systems, Inc.

60 Church Street

Yalesville, CT 06492

phone: (203) 265 - 7966

- Swivel linkage (stinger) (2)

C.6 Custom Fabricated Reaction Mass Actuator Hardware

- Aluminum calibration/test jig
- Aluminum proof mass
- Aluminum cradle and grooved track
- Numerous adaptors for motor/stinger/node/test jig attachments

C.7 Instrumentation and Electronics

- Comdyna GP-6 Analog Computer (2)

Comdyna, Inc.

305 Devonshire Road, Barrington

IL 60010

phone: (708) 381 - 7560

- Hewlett Packard HP35665A Dynamic Signal Analyzer
- MDB-5 load cell and TM-2 amplifier

Transducer Techniques

43178 Bussiness Park Drive B-101

Rancho Temecula, CA 92390

phone:(714)676-1200

- Sundstrand QA-700 accelerometer (4)
- Control circuit hardware (misc. see also Schulthess [17])

- PA11503 ELECTRO-MIKE position sensor

ELECTRO Corp.

1845 57th Street

Sarasota, FL 33580